

# **Hydrographical and biogeochemical characterization of the Beibu Gulf, South China Sea**

**Dissertation**

zur

Erlangung des akademischen Grades  
doctor rerum naturalium (Dr. rer. nat.)  
der Mathematisch-Naturwissenschaftlichen Fakultät  
der Universität Rostock

vorgelegt von

Andrea Bauer

geb. am 08.03.1985 in Jena

Rostock, den 30. August 2012

## **Gutachter**

PD Dr. habil. Joanna J. Waniek  
Leibniz-Institut für Ostseeforschung Warnemünde

Prof. Dr. Detlef E. Schulz-Bull  
Leibniz-Institut für Ostseeforschung Warnemünde

Prof. Dr. Venugopalan Ittekkot  
Zentrum für Marine Tropenökologie

**Datum der öffentlichen Verteidigung:** 21.01.2013

# Contents

<b>Abstract</b>	<b>IV</b>
<b>Zusammenfassung</b>	<b>VI</b>
<b>1 Introduction</b>	<b>1</b>
1.1 Global importance of shelf seas . . . . .	1
1.2 The Beibu Gulf . . . . .	8
1.3 Thesis outline . . . . .	11
<b>2 Material and Methods</b>	<b>13</b>
2.1 Sampling and <i>in-situ</i> data processing . . . . .	13
2.2 Current measurements . . . . .	13
2.3 Coupled physical-biological model . . . . .	16
2.4 Additional data sets . . . . .	19
<b>3 Regional differences of hydrographical and sedimentological properties in the Beibu Gulf, South China Sea</b>	<b>20</b>
3.1 Introduction . . . . .	21
3.2 Material and Methods . . . . .	24
3.2.1 Study area . . . . .	24
3.2.2 Water samples . . . . .	25
3.2.3 Geological samples . . . . .	26
3.2.4 Geochemical samples . . . . .	27
3.2.5 Additional data sets . . . . .	28
3.3 Results . . . . .	29
3.3.1 Beibu Gulf Coastal Zone . . . . .	32
3.3.2 Qiongzhou Strait Zone . . . . .	38

3.3.3	Beibu Gulf Central Zone . . . . .	40
3.3.4	Southern Beibu Gulf Zone . . . . .	42
3.4	Discussion . . . . .	44
3.4.1	Hydrographical and biogeochemical differences between the zones . . . . .	44
3.4.2	Differences of sediment characteristics and geochemical prop- erties between the zones . . . . .	51
3.5	Conclusions . . . . .	58
<b>4</b>	<b>Factors affecting the chlorophyll <i>a</i> concentration in the central Beibu Gulf, South China Sea</b>	<b>59</b>
4.1	Introduction . . . . .	60
4.2	Material and Methods . . . . .	63
4.2.1	Study area . . . . .	63
4.2.2	In situ data for model validation . . . . .	64
4.2.3	Simple 1D coupled physical-biological model . . . . .	65
4.2.4	Meteorological and comparative satellite data . . . . .	69
4.3	Results . . . . .	69
4.3.1	Mean annual cycle . . . . .	71
4.3.2	Annual cycle 2009 . . . . .	75
4.3.3	Effects of strong wind events . . . . .	77
4.3.4	Effects of tides . . . . .	78
4.3.5	Interannual variability . . . . .	81
4.4	Discussion . . . . .	86
4.5	Conclusions . . . . .	92
<b>5</b>	<b>Sediment resuspension patterns and the diffusive boundary layer in the Beibu Gulf, South China Sea</b>	<b>97</b>
5.1	Introduction . . . . .	97
5.2	Material and methods . . . . .	100
5.2.1	Current records and their analysis . . . . .	100
5.2.2	Water and sediment sampling . . . . .	102
5.2.3	Tidal model . . . . .	102

5.3	Results and discussion . . . . .	105
5.3.1	Tidal cycle . . . . .	105
5.3.2	Sedimentation patterns . . . . .	108
5.3.3	Diffusive Boundary Layer . . . . .	113
5.4	Conclusions . . . . .	118
<b>Conclusions</b>		<b>120</b>
<b>References</b>		<b>124</b>
<b>List of Figures</b>		<b>137</b>
<b>List of Tables</b>		<b>139</b>
<b>List of Abbreviations</b>		<b>140</b>
<b>Specific contributions to the manuscripts</b>		<b>142</b>
<b>Danksagung</b>		<b>144</b>
<b>Eidesstattliche Erklärung</b>		<b>146</b>

## Abstract

As a transition zone between the highly populated Chinese and Vietnamese land masses, providing a great river discharge, and the South China Sea, the Beibu Gulf plays an important role for near-costal input of terrestrial, naturally and anthropogenically induced, matter and material as well as energy fluxes into the South China Sea northwestern areas. Therefore, the Beibu Gulf is a significant region for biogeochemical cycling, degradation of organic matter and hence induced element fluxes as well as sediment accumulation.

Influenced by the Asian monsoon system, strong tidal currents and occasionally typhoon crossings, affecting circulation patterns and the water mass exchange with the South China Sea, hydrographical conditions, water column biogeochemistry and sedimentation processes are highly variable in this shallow shelf sea. On this account, the Beibu Gulf is an interesting region for deepening the understanding of meteorological and tidal forcing on hydrography, biogeochemical properties as well as sedimentation patterns and processes regulating the benthic-pelagic material and energy fluxes.

To characterize the Beibu Gulf hydrographically and biogeochemically, this thesis combines investigations on physical and biogeochemical conditions of the water column, current and sedimentation patterns as well as geochemical properties of the sediments. The analyses are based on *in-situ* measurements (temperature, salinity,  $\sigma_t$ , currents, chlorophyll, nutrients, suspended particulate matter, grain size, sediment pore water properties, foraminifera and plant pigment contents in surface sediments) carried out during two German-Chinese cruises with the RV FENDOU 5 in September/October 2009 and RV SONNE in December 2011, model work and satellite derived sea surface temperature and surface chlorophyll concentrations.

For the understanding of the system "Beibu Gulf", its hydrodynamics, sedimentological and geochemical variability, different zones are distinguished in the study area for the sampling period in September/October 2009, extending from the coastal areas in the north and east across the central region to the southern part of the gulf. These zones are

mainly influenced by tidal mixing and riverine input in the coastal regions, water mass transport from the South China coastal regions through the Qiongzhou Strait in the east and South China Sea waters in the south, due to circulation patterns driven by monsoon winds and tides. The regional hydrographic peculiarities are mirrored in the biogeochemical properties of the water column and sediment characteristics like grain size, plant pigment contents and foraminifera in the surface sediments as well as geochemical properties, which follow the hydrodynamically controlled sedimentation conditions and reflect distinctions in primary production within the water column.

The physical structure of the water column mainly driven by monsoonal forcing is reflected in the seasonal cycle of primary production, with a low-productive period in summer due to water column stratification and a phytoplankton bloom in winter initiated by vertical mixing and related nutrient supply. Along with the semi-annual wind system change, occasionally strong wind events (typhoons) play an important role in primary production and the associated biogeochemical cycling in the Beibu Gulf.

While wind forcing influences the water column from top-down the tidal forcing is the main mechanism driving sedimentation patterns and influencing geochemical processes within the sediments. For all zones and tidal phases (ebb, flood, slack water) current velocities contribute to sediment deposition, transport and resuspension during the sampling period in September/October 2009. The, in general, strong currents during most of the tidal cycle prevent the establishment of a diffusive boundary layer and hence allow an exchange of compounds, nutrients and gases across the sediment-water interface, which indicates an existing benthic-pelagic coupling in the Beibu Gulf.

## Zusammenfassung

Der Beibu Golf bildet eine Übergangszone zwischen dem stark bevölkerten chinesischen/vietnamesischen Festland und dem Südchinesischen Meer. Aus diesem Grund spielt er eine bedeutende Rolle für den küstennahen, natürlichen und anthropogenen, Stoffeintrag sowie für Material- und Energieflüsse in die nordwestlichen Regionen des Südchinesischen Meeres. Diese Region ist wichtig für biogeochemische Kreisläufe, den Abbau von organischem Material und damit einhergehenden Elementflüssen sowie für sedimentäre Ablagerungsprozesse.

Die physikalischen und biogeochemischen Eigenschaften der Wassersäule sowie Sedimentationsprozesse im Golf unterliegen starken Schwankungen, da Zirkulationsmuster und der Wassermassenaustausch mit dem Südchinesischen Meer stark durch wechselnde Monsunwinde, Gezeitenströmungen und gelegentlich vorüber ziehende Taifune beeinflusst werden. Daher ist der Beibu Golf eine interessante Region um das Verständnis für den Einfluss von meteorologischen und Gezeitenkräften auf die Wassersäuleneigenschaften sowie auf Sedimentationsmuster zu vertiefen.

Um den Beibu Golf hydrographisch und biogeochemisch zu charakterisieren, werden in dieser Arbeit Untersuchungen der physikalischen und biogeochemischen Bedingungen der Wassersäule mit Strömungs- und Sedimentationsmustern sowie geochemischen Parametern der Sedimente kombiniert. Hierzu wurden *in-situ* Messungen (Temperatur, Salzgehalt,  $\sigma_t$ , Strömungen, Chlorophyll, Nährstoffe, suspendiertes partikuläres Material, Korngröße, Porenwassereigenschaften der Sedimente und Foraminiferen sowie Pflanzenpigmentkonzentrationen in den Oberflächensedimenten) zweier deutsch-chinesischer Expeditionen, mit den Forschungsschiffen FENDOU 5 im September/Okttober 2009 und SONNE im Dezember 2011, ausgewertet sowie Modellierungsarbeiten in Verbindung mit von Satellitendaten abgeleiteten Meeresoberflächentemperaturen und -chlorophyllkonzentrationen durchgeführt.

Um die hydrodynamische, sedimentologische und geochemische Variabilität des Systems "Beibu Golf" zu verstehen, wurden, in einem ersten Schritt, verschiedene Zonen



für das Untersuchungsgebiet und den Untersuchungszeitraum September/Okttober 2009 definiert. Diese Zonen erstrecken sich von den Küstenregionen im Norden und Osten über den zentralen bis hin zum südlichen Teil des Golfes. Sie sind hauptsächlich beeinflusst durch gezeitengetriebene Durchmischung und Flusseinträge in den küstennahen Regionen, Transport von Wassermassen der Südchinesischen Küstenregionen durch die Qiongzhou Straße im Osten und Wassermassen des Südchinesischen Meeres im Süden des Golfes. Dabei wird der jeweilige Einfluss der Wassermassen auf die Zonen durch die golfweite Zirkulation, angetrieben durch Monsunwinde und Gezeiten, bestimmt. Die regionalen Besonderheiten der Hydrographie spiegeln sich in den biogeochemischen Eigenschaften der Wassersäule und in denen der Sedimente, wie Korngröße, Pflanzepigmentkonzentrationen und Foraminiferen in den Oberflächensedimenten sowie geochemischen Parametern, wider. Die Sedimenteigenschaften folgen dabei den hydrodynamisch kontrollierten Sedimentationsbedingungen und reflektieren gleichzeitig Unterschiede in der Primärproduktionsrate der Wassersäule.

Die physikalische Struktur der Wassersäule, beeinflusst durch die Monsunwinde, wird von der Primärproduktion reflektiert, mit einer Phase geringer Produktion im Sommer durch Schichtung der Wassersäule und einer Phytoplankton Blüte im Winter, ausgelöst durch vertikale Durchmischung und damit zusammenhängender Verfügbarkeit von Nährstoffen. Zusammen mit dem halbjährlichen Wechsel des Windsystems, tragen auch zeitweise auftretende starke Stürme (Taifune) erheblich zur Primärproduktion und den damit in Zusammenhang stehenden biogeochemischen Kreisläufen bei.

Während der Wind die Wassersäule an der Oberfläche beeinflusst, sind Gezeiten die treibenden Kräfte für Ablagerungsbedingungen und bestimmen gleichzeitig auch geochemische Eigenschaften der Sedimente. Für den Beprobungszeitraum im September/Okttober 2009 tragen Strömungsgeschwindigkeiten in allen Zonen und zu allen Gezeitenphasen (Ebbe, Flut, Stillwasser) zu Ablagerung, Transport und Resuspension der Sedimente bei. Die im Allgemeinen während eines Gezeitenzyklus sehr starken Strömungen verhindern die Entstehung einer diffusiven, bodennahen Grenzschicht und erlauben dadurch einen Austausch von Verbindungen, Nährstoffen und Gasen zwischen Sediment und Wassersäule. Das weist auf eine benthisch-pelagische Kopplung im Beibu Golf hin.

# 1 Introduction

## 1.1 Global importance of shelf seas

Continental shelves reach in their spatial extent from the coastline to the continental slope and form a margin around continents variant in width. With a depth up to 200 m, shelves provide only a mere of 7% of the oceans surface and less than 0.5% of the oceans volume [Chen *et al.*, 2003] compared to the around 4000 m mean depth of the open ocean (Fig. 1.1a). A clear definition of strict boundaries between the open ocean and shelf seas is difficult as water masses of oceanic and neritic provinces blend into each other in most cases. However, in general, the continental slope is the area where hydrographic conditions change between both provinces [Postma and Zijlstra, 1988].

The global importance of shelf areas is primarily caused by the immediate proximity to the land masses. As regions connecting the mainland with the open oceans, shelf seas are important regions for transferring energy and material, controlling anthropogenic and terrestrial fluxes and fates of chemicals, pollutants and primary production to and from the open ocean [Mantoura *et al.*, 1991]. In shelf and deltaic regions over 90% of the riverine particulates and associated carbon, trace metals and pollutants are trapped [Mantoura *et al.*, 1991]. Anthropogenic perturbations are mainly caused by land use, land reclamation and sand mining, industry and aquaculture/mariculture which affect mobilization, input and deposition of metals, anthropogenic organic compounds, toxic substances and nutrients leading to eutrophication, which may influence marine ecosystems and the composition of biological communities, especially in coastal regions [O’Kane *et al.*, 1991; Doney *et al.*, 2003]. Further direct and indirect human impacts are, for example, due to waste disposal, tourism, coastal engineering, freshwater management and changes in river flows, habitat destruction like cutting of mangrove forests, draining of marshes with associated effects on sediment dynamics as well as diminishing fishery resources which may lead to a shift in species dominance [Sharp, 1988;

*O’Kane et al.*, 1991]. Shelf regions respond very quickly to environmental changes and are important regions for biogeochemical fluxes, with a carbon turnover time from days to weeks [*Ross*, 2004], for instance.

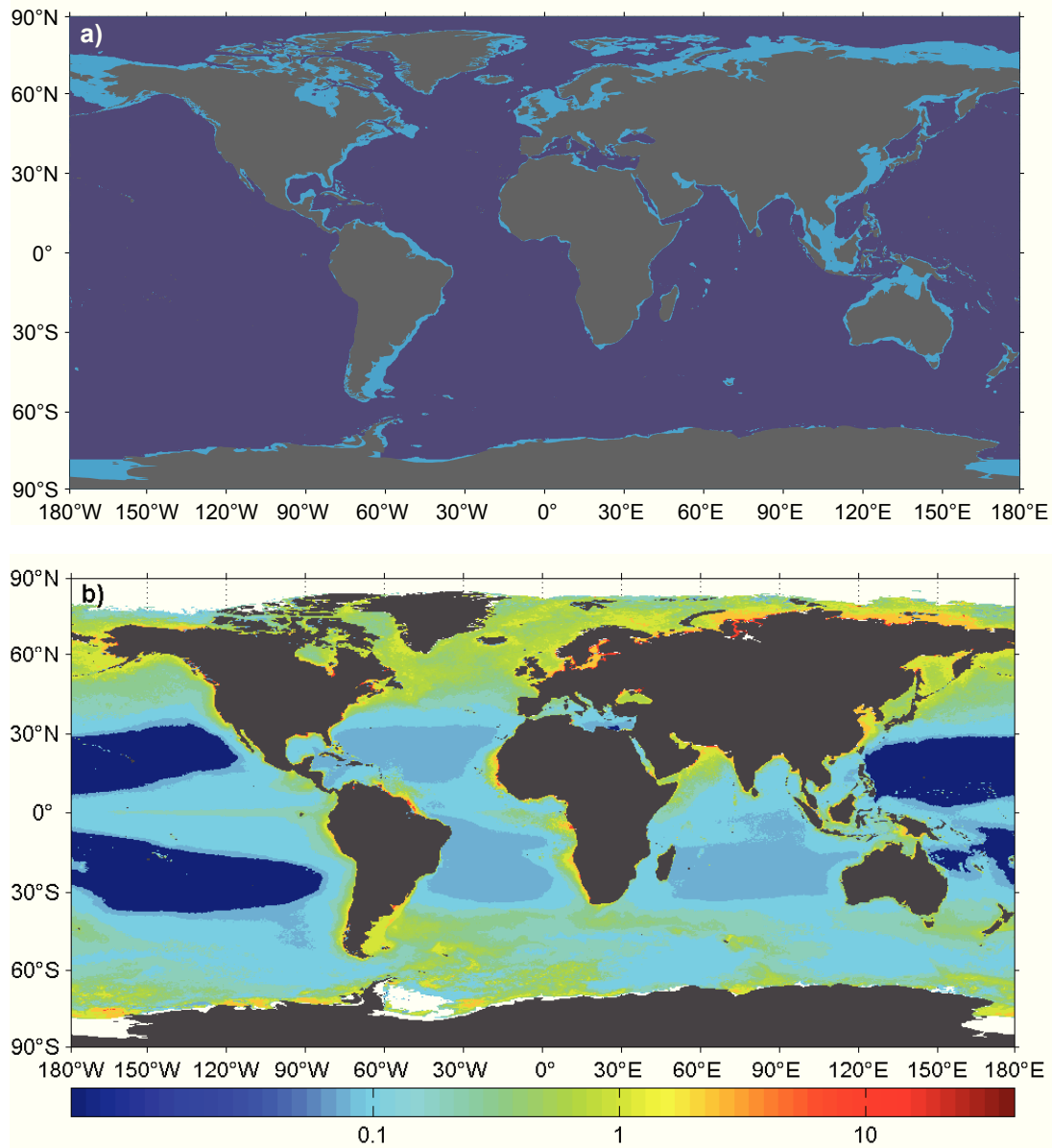


**Figure 1.1:** Global a) shelf areas (depth up to 200 m) marked in light blue and b) mean surface chlorophyll-*a* concentrations in  $\text{mg l}^{-1}$  (indicated in the colorbar) from MODIS (average 2003-2011, 9 km resolution).

Furthermore, shelves are highly productive regions, accounting for around 14% of total global ocean production, along with 80-90% of the new production [Chen *et al.*, 2003] (Fig. 1.1b). This is the result of a high nutrient supply in these regions, due to riverine input and upwelling.

During photosynthesis, phytoplankton converts inorganic material, such as nitrate and phosphate, into organic compounds, and thereby initiates the oceanic food chain reaching through all trophic levels [Ross, 2004]. As one of the main global fixers of carbon dioxide, phytoplankton is crucial for oceanic carbon fixation which in turn has an impact on the atmospheric carbon dioxide content [e.g. Mantoura *et al.*, 1991; Chen *et al.*, 2003; Ross, 2004] and is hence fundamentally important for the functioning of marine ecosystems [e.g. Waniek and Holliday, 2006]. An amount of 40-50% of the total  $10^{11}$  tonnes of carbon fixed each year globally by all marine and terrestrial plants, are estimated to be fixed by marine primary producers [Ross, 2004]. Further on, depending on the region, the amount of organic matter reaching the bottom and hence its burial is higher in shelf seas compared to the open ocean [Postma and Zijlstra, 1988] and important for sedimentary chemical redox reactions (e.g. denitrification, trace metal reduction) with implications for the carbon, nitrogen, phosphorous and iron cycles [Doney *et al.*, 2003].

The shelf, providing a high number of different ecosystems (e.g. mangroves, seaweed meadows) and ecological niches, is a biologically highly diverse area. Many marine species live on the shelf, others spend a part of their lifecycle in these regions, mainly because of the high food supply. Especially for rearing the offspring and juvenile developmental stages (e.g. larval fish) estuaries, bays and lagoons on the land-side boundary of the shelf, are favoured places, and of course allure predators of higher trophic levels. Thus it is not surprising that around 90% of the global fish landings are yielded on the world's shelf regions [Postma and Zijlstra, 1988].

But why are shelves that productive regions?

The significantly higher rates of organic productivity in shelf seas are caused by a rapid nutrient turnover and a higher supply of nutrients due to riverine input, wind-driven coastal upwelling [Chen *et al.*, 2003] and tidal mixing.

Different shelf areas show different hydrographical characteristics. Considering that,

the shaping of the shelf region is of consequence, which means width, bathymetry, nature of the coastline itself [Longhurst, 2007] and the shape of the connection to the adjacent ocean, its latitudinal position, which determines the solar irradiance and hence the seasonal temperature cycle [Walsh, 1981], and the wind regime. Especially the width, which is very variable between 0 and 1500 km [Postma, 1988], the bathymetry, the connection to the open ocean and the strength of the tidal forcing are responsible for the residence time of the shelf water bodies which is important for material deposition in the shelf sea itself or rapid transport via currents into the open ocean, biogeochemical cycles and hence the water quality. The faster water exchanges, phytoplankton cells may be transported away from the shelf and hence away from optimal living conditions related to nutrients, light availability and stratification. In general, planktonic algae tend to be larger in shelves because of the reduced vertical stability in these regions and the occasional presence of upwelling [Postma and Zijlstra, 1988]. In addition, organic matter can only be deposited to a minor degree which influences especially biogeochemical cycles within the sediments, burial of organic matter and benthic communities.

The residence times for shelf seas can mostly be measured rather in months than in years [Postma and Zijlstra, 1988]. An exception is, for example, the Baltic Sea, having only a narrow connection to the Atlantic through Skagerrak/Kattegat, which leads to an only sporadically water exchange and a residence time of about 30 years. The wind regime contributes to the water residence time as well, as it introduces specific circulation patterns, best documented for the changing monsoon winds in Asian regions, for instance, the Arabian Sea and the South China Sea (SCS).

As a land-ocean interface shelf seas are influenced by riverine freshwater discharge, which may bring nutrients into the system and lead to coastal near water masses determined by lower salinities and higher buoyancy, on the one hand and high saline waters from the open ocean which intrudes into the shelf regions on the other hand. These different water masses may lead to the formation of shelf break fronts, which occur almost everywhere due to the density gradient between the shelf and the oceanic water [Longhurst, 2007], and can be taken as boundaries for the shelf region. Associated with the fronts nutrient upwelling from deeper nutrient-rich waters can occur and enhance primary production within the frontal region.

The most important characteristic of shelf seas, responsible for most of the distinct differences to the open ocean, is their shallowness. This feature leads to a faster warm-

ing and cooling of water bodies compared to the open ocean and causes a seasonal stratification. During periods of highest solar irradiance, in the northern hemisphere in spring and summer, its influence overcomes the capacity of tidal mixing to maintain a vertically well-mixed water column and the water column stratifies thermally [Sharpley, 2008]. The seasonal thermocline is a physical barrier separating the wind-mixed surface layer from the tidally-mixed deeper water layer [Ross and Sharpley, 2007]. It further inhibits properties transfer, such as oxygen, nutrients and algal cells [e.g. Klein and Coste, 1984; Sharpley et al., 2001]. Above, the light environment promotes photosynthesis but the water layer is impoverished of nutrients in most cases, due to their only limited availability, fast consumption and prevented replenishment from deeper waters. Below the thermocline, enough nutrients are available but the poor light conditions prevent primary production. A net production through photosynthesis, compensating destruction processes by respiration, can only occur, when algal cells are trapped near the surface and nutrients as well as light are sufficiently available [Sverdrup, 1953; Ward and Waniek, 2007].

Many stratified regions show oligotrophic conditions during the period of vertical stratification [Varela et al., 1992]. A result of the poor nutrient supply in these regions, is a low primary production which is common for the outer shelf regions. In those regions a deep chlorophyll maximum (DCM) is commonly observed within the thermocline. This feature is promoted by pulses in the strength of mixing processes, such as tidally-induced motion, wind events and surface breaking waves [Lauria et al., 1999] bringing nutrients into the thermocline [Klein and Coste, 1984; Sharpley and Tett, 1994]. The oscillation of the thermocline induced by these pulses supports also a nutrient flux into the surface layer. For the western North Pacific Ocean almost 55% of the total chlorophyll in the entire water column has been found within 50 m depth around the DCM layer [Takahashi and Hori, 1984].

In autumn the stratification breaks down due to sea surface cooling and eroding of the thermocline by wind and tides and leads to a deep mixing. The nutrient supply in the euphotic zone increases, which triggers a winter phytoplankton bloom especially in subtropical waters where the solar irradiance during winter still supports primary production [Yoder et al., 1993]. By contrast, in temperate to polar/subpolar latitudes the phytoplankton biomass cycle is dominated by a spring bloom, which occurs in response to the stratification and increasing solar irradiance during spring and summer [Yoder

*et al.*, 1993]. Depending on the depth of the oceanic region, phytoplankton may be vertically transported below the euphotic depth during periods of deep mixing and can not conduct photosynthesis anymore [Lauria *et al.*, 1999] although enough nutrients are provided. In shallow coastal areas, without stratification periods, nutrients are almost permanently available resulting in eutrophic conditions with high primary production rates.

Due to the high nutrient uptake during a phytoplankton bloom, different input of nutrients through atmospheric wet (rainfall) and dry (dust) deposition, river discharge and vertical fluxes [Longhurst, 2007] mainly during periods of stratification, lead to a change in the availability of dissolved nutrients. As a consequence of either nitrate or phosphate limitation in the surface waters, the shifts in nutrient supply induce changes in the stoichiometry of nutrient uptake (Redfield ratio) and consequently may limit phytoplankton growth [Boyd and Doney, 2003]. Further, such changes may affect the species composition and species succession as well. For example, the essential uptake of silicate by diatoms may lead to a silicate limitation. If no silicate will further be induced into the system, hence, the diatom bloom terminates.

Tidal forces, inducing currents and undulation everywhere in the marine environment, are only fully effective in shallow regions [e.g. Li *et al.*, 2004]. Tides on shelves are co-oscillating tides because they are mainly generated by incoming tidal waves from the adjacent ocean [Postma, 1988]. While in the deep oceans tidal waves only lead to a slight forward and backward movement of the water, in the shelf regions they can trigger strong mixing processes. As a result of the decreasing depth, the tidal energy, which could spread vertically over the entire depth of several 1000 m in the deep ocean basins, is forced to spread over a depth of only 200 m and less when it comes upon the shelf break. Consequently, the tidal wave is modified in height and direction by morphology, bottom friction, Coriolis force and reflection against the coast which may increase or decrease the tidal amplitude, depending on the relative importance of the influencing factors, and leads to high tidal currents which increase, in general, from the shelf edge towards the shore [Postma, 1988]. Tidal effects do not show the same intensity in all shelf regions. At an open, wide shelf region with a gradual bathymetric slope, tidal forcing is of little importance compared to semi-closed shelf regions, with a sharply rising bathymetry.

The with tides associated turbulence causes vertical and horizontal mixing. At the

seabed, frictional effects of the water movement lead to a shear stress eroding and resuspending sediments into the water column. Resuspended sediments may then be transported with currents and deposited elsewhere. In addition, coupled with the sediments also pollutants, dissolved substances, like nutrients, stored in sediment pore waters and benthic communities (e.g. benthic foraminifera) will be mixed, resuspended and transported [Jago *et al.*, 2002]. This benthic-pelagic exchange is of high importance and especially over continental shelves, because of the shallow depth, strongly coupled [Longhurst, 2007]. As stated before, depending on the strength of the tides, the tidal turbulence leads to an oscillation of the thermocline which may bring nutrients through the thermocline into the surface water layer. A further biological effect of the resuspension lies in the enhanced turbidity, which could diminish the light environment and hence reduce photosynthesis rate of phytoplankton.

As an opponent to the tides, the wind acting on the surface affects vertical mixing and motion of the water column [Walsh, 1981; Dickey, 1988]. Depending on its strength and the water depth, wind induced turbulence may contribute to the formation of the DCM [Klein and Coste, 1984; Sharples and Tett, 1994] or reach to the bottom and hence could lead to sediment resuspension including deposited compounds. While tidal forcing may constantly erodes the thermocline from below, surface wind stress induces turbulent erosion of the thermocline from above [Klein and Coste, 1984], if it is strong enough and therefore it could also supply nutrients into the surface water layers. Furthermore, this forcing may induce surface currents and could be important for upwelling processes. Caused by a wind stress acting on the sea surface over an extended period of time, a surface water movement  $45^\circ$  to the main wind direction occurs, called Ekman Drift. Due to frictional processes between the water layers, this effect can be transferred to the Ekman depth with a further deflection of the water movement resulting in a mean water transport rectangular to the wind direction at the surface. This process is important for shallow as well as deep oceanic regions as it affects circulation processes. For instance, the SCS shows an anticyclonic circulation during summer due to the southwest monsoon but an cyclonic circulation during winter due to the stronger northeast monsoon [e.g. Huang *et al.*, 1994; Shi *et al.*, 2002; Su, 2004; Gan *et al.*, 2006], which affects upwelling mechanisms and hence primary production in this region. Coastal upwelling is a lateral Ekman Transport affecting a zone of 10-20 km from the coast [Walsh, 1981]. Induced by wind stress at the sea surface parallel to the coastline [Chen and Tang, 2011] nutrient-



rich deeper waters originating from offshore are brought to the surface and probably enhance primary production.

Another feature, especially important for subtropical/tropical regions, are hurricanes or typhoons. These short but strong wind events are able to break down the seasonal stratification and mix the water column completely, particularly important in shelf regions, which leads to a nutrient supply in the surface water layer and may induce a phytoplankton bloom [e.g. *Zheng and Tang*, 2007]. Hence, the cyclone events made the shelf more active in producing particulate and dissolved organic matter [*Shiah et al.*, 2000]. The effect of such an event depends on the wind's intensity, the transit time and the ocean's precondition, which means the depth of the nutrient-rich water body [*Lin*, 2012]. Typhoon Kai-Tak, for instance, passed the SCS in July 2000 and accounted for 2-4% of the annual new production in the oligotrophic SCS [*Lin et al.*, 2003].

The combination of all processes acting on shelf regions provide a highly turbulent environment for primary producers which always have to cope with the limitation of nutrients in a stratified and the vertical attenuation of light in a well-mixed regime. Although shelf sea areas represent only a comparatively small part of the world oceans surface they are highly productive regions representing a major carbon sink affecting intensely the global carbon mass balance [*Walsh*, 1981; *Mantoura et al.*, 1991; *de Haas et al.*, 2002; *Chen et al.*, 2003], and hence the global climate.

## 1.2 The Beibu Gulf

The semi-enclosed Beibu Gulf, also called Gulf of Tonkin, is a marginal sea of the SCS (Fig. 1.2a) and located on the well developed shelf area of the SCS occupying about 47% of the total SCS area [*Wang and Li*, 2009] and belonging to the "Sunda-Arafura Shelves Province" with a depth less than 100 m [*Longhurst*, 2007].

This, on average not more than 45 m deep shelf sea, has an individual tongue-shaped bathymetry that deepens gradually from the north to the southeast where the gulf reaches its maximum depth of 100 m [*Manh and Yanagi*, 1997; *Wu et al.*, 2008]. Bounded in the north and west by South China and Vietnam as well as in the east by the Leizhou Peninsula and the Hainan Island, the Beibu Gulf is connected to the northwestern SCS through the Qiongzhou Strait in the east and a wide opening in the south (Fig. 1.2b). As typical for shelf seas, the Beibu Gulf is affected by water masses from the SCS on the

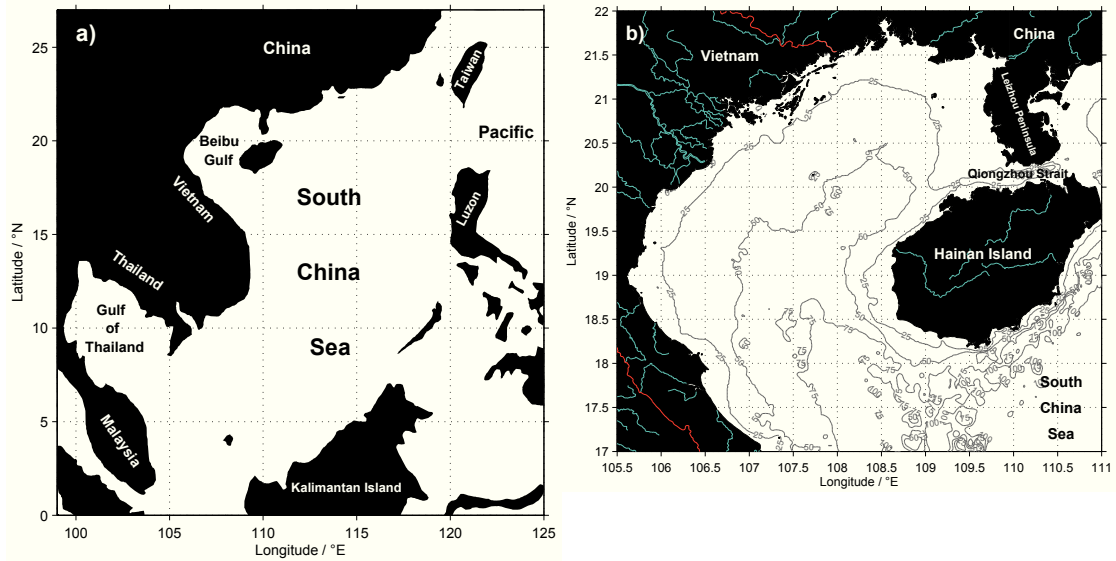


**Figure 1.2:** a) The South China Sea and b) the Beibu Gulf. Bathymetry is based on ETOPO1 (<http://www.ngdc.noaa.gov>).

one hand and river discharge along the shore on the other hand. Especially the Red River water discharge of about  $123 \text{ km}^3 \text{ yr}^{-1}$  [Milliman and Meade, 1983; Wong *et al.*, 2007] along with rivers at the northern coast influence Beibu Gulf waters, generating a low salinity zone in the northwestern part [Chen *et al.*, 2009] particularly during the rainy season in summer [Dai *et al.*, 2011]. In addition to the water transport, the Red River, for instance, also transports on average  $160 \times 10^6 \text{ t yr}^{-1}$  suspended load which may reach the SCS [Milliman, 1991]. The connections to the SCS lead to a water mass exchange from the SCS to the Beibu Gulf and vice versa, transporting, for example, chlorophyll and suspended sediments. Water masses transported through Qiongzhou Strait originate mainly from the South China coastal areas, probably including discharge from the Pearl River [e.g. Su and Weng, 1994; Tang *et al.*, 2003]. Hence, the Beibu Gulf plays an important role for the understanding of material and energy fluxes in the north-western coastal regions of the SCS.

The Beibu Gulf is influenced by tidal waves entering the gulf through the connections to the SCS and, due to the gulfs shape, induce a diurnal tidal regime [Manh and Yanagi, 1997; Shi *et al.*, 2002; Wu *et al.*, 2008] with strongest currents of about  $60 \text{ m s}^{-1}$  [Manh

and Yanagi, 1997]. The propagation of tidal waves into the gulf from the south drives mainly the southern marine influence and currents important for the gulf's circulation [Cai *et al.*, 2003]. The circulation pattern in the Beibu Gulf, driven by monsoon winds, tidal currents and currents outside the gulf [Chen *et al.*, 2009], is hardly discussed. Former studies demonstrated that the surface circulation reverses monsoonal driven from a cyclonic pattern in winter to an anticyclonic one in summer [e.g. Manh and Yanagi, 1997, 2000]. Such a changing circulation pattern is already known from the SCS main basin generated by the winter northeast monsoon and the southwest monsoon occurring during summer [e.g. Huang *et al.*, 1994; Shi *et al.*, 2002; Su, 2004; Gan *et al.*, 2006]. In contrast, most recent results show that the circulation in the Beibu Gulf is cyclonic throughout the entire year [Shi *et al.*, 2002; Wu *et al.*, 2008] mainly driven by a tide-induced westward transport through the Qiongzhou Strait in all seasons [Shi *et al.*, 2002] a surface southward flow along the Vietnamese coast and a compensating northern directed return flow in the interior and along Hainan Island's west coast [Wu *et al.*, 2008].

The surface water temperatures in the Beibu Gulf are relatively uniform, between 27.5 and 29.5°C in summer and 20 to 24°C during winter [Manh and Yanagi, 2000]. The annual cycle of phytoplankton biomass is typical for subtropical/tropical regions with a main productive season in winter with higher chlorophyll concentrations in the northeast and lower in the southwest part [Hu *et al.*, 2003; Tang *et al.*, 2003]. During summer surface chlorophyll concentrations are relatively low [Hu *et al.*, 2003] and uniform in the entire gulf, due to stratification, but with a narrow zone of high concentrations along the coasts [Tang *et al.*, 2003] caused by riverine nutrient input. The reversal monsoon winds and concomitant changes of the water conditions cause the seasonality of primary production [Tang *et al.*, 2003].

On average, 24 typhoons occur at the northwestern Pacific and the SCS every year [Shiah *et al.*, 2000] and an annual average of 5 typhoons passes Hainan Island [Chen and Tang, 2011]. Hence, for the Beibu Gulf typhoons are a common feature affecting this area intensely and may initiate or intensify phytoplankton blooms in the entire gulf during their passing.

### 1.3 Thesis outline

This thesis "*Hydrographical and biogeochemical characterization of the Beibu Gulf, South China Sea*" is embedded in the German-Chinese bilateral research project "*Status der marinen Umwelt des Beibu Golfs, Südchinesisches Meer, und Entwicklung während des Holozäns im Wechselfeld natürlicher und anthropogener Einflüsse - Holocene environmental evolution and anthropogenic impact of Beibu Gulf, South China Sea*" funded by the German Federal Ministry of Education and Research. General aim of the project is to investigate meso- to large scale energy and material fluxes in the Beibu Gulf as an answer to natural and anthropogenic forces.

As a marginal sea of the SCS influenced by a great river discharge, the Beibu Gulf plays an major role as a connecting link between the highly populated Vietnamese/Chinese land masses and the SCS. It is hence a region important for the understanding of natural and anthropogenic inputs, energy fluxes and biogeochemical cycling in the SCS northwestern region. So far, only limited knowledge exists about the oceanic, biological and sediment processes acting in this hydrodynamically highly variable sea area, influenced by the Asian monsoon system, strong tidal currents and occasional typhoon passing.

Aim of the present thesis is to characterize the hydrographical and biogeochemical conditions in the Beibu Gulf. Therefore, the three studies in the chapters 3 to 5 address several aspects of the Beibu Gulf's naturally caused hydrographical, biogeochemical and sedimentological features.

In the introduction (**chapter 1**) the general global importance of continental shelves is outlined including important characteristics of those regions, influencing their crucial role in biogeochemical cycling compared to the open ocean. Further, the Beibu Gulf is introduced.

**Chapter 2** summarizes all used material and methods. Repetitions concerning the respective subchapters within the single studies are unavoidable as those studies are already accepted (chapter 3) or manuscripts under revision (chapter 4).

**Chapter 3** presents an interdisciplinary study elucidating regional differences in hydrography during the sampling period in September/October 2009. It is shown that these

differences affect biological properties in the water column and are further mirrored in sediment deposition patterns and its geochemical and biological characteristics [*Bauer et al.*, in press].

In **chapter 4** a 1D coupled physical-biological model is used to simulate the seasonal cycle of primary production in the central Beibu Gulf. For an 11 year period, important factors generating interannual variability in the timing of stratification and the phytoplankton bloom are demonstrated. Furthermore, effects of the spring-neap tidal cycle and strong wind events on the primary production are shown [*Bauer and Waniek*, 2013].

In **chapter 5** the bottom currents and associated sediment resuspension patterns as well as the establishment of a diffusive boundary layer in relation to the different tidal stages, during the sampling period in September/October 2009, and regions defined in chapter 3 are investigated. It is demonstrated that within the Beibu Gulf, the different current patterns influence sedimentological and geochemical processes substantially.

Finally, in **chapter 6** the main outcomes of the thesis are summarized and some further, yet unanswered questions as well as future perspectives are outlined.

All references are listed in the "References" section at the end of this thesis.

## 2 Material and Methods

In this section all materials and methods used in this work are only summarized. A detailed description of the methods (including all calculations) used for the respective studies is given in each of the following chapters.

### 2.1 Sampling and *in-situ* data processing

*In-situ* data were collected during two German-Chinese expeditions with the Chinese RV FENDOU 5 in September/October 2009 and the German RV SONNE in December 2011 (Fig. 2.1). During the FENDOU 5 cruise depth profiles (temperature, conductivity, oxygen, chlorophyll-fluorescence) were recorded and water samples were taken at 25 stations (Fig. 2.1a) using a IOW mini PUMP CTD system based on *Strady et al.* [2008] including a YSI probe (6600 V2-4). For a detailed description please read section 3.2.

A Seabird CTD with a Niskin bottle rosette sampler system was used during SONNE cruise for hydrographical profiling and water sampling at 14 stations analyzed in this work (Fig. 2.1b). For analysis of chlorophyll, nutrients ( $\text{NO}_2$ ,  $\text{NO}_3$ ,  $\text{PO}_4$  and  $\text{SiO}_4$ ) and suspended particulate matter (SPM) concentrations water samples were taken at all stations from different depths during the upcast. Treatments of water samples according to the respective parameters are described in detail in sections 3.2, 4.2 and 5.2.

### 2.2 Current measurements

U- and v-component (zonal and meridional) of currents were recorded during transects using an Acoustic Doppler Profiler (ADP) (Fig. 2.1a) and used for analyzing the bottom current field during the FENDOU 5 cruise after pre-processing (chapter 5). A simple tidal model has been developed to identify the tidal stages of all stations and ADP lines by using tidal heights predicted by the WXTide32 software (explained in section 5.2).

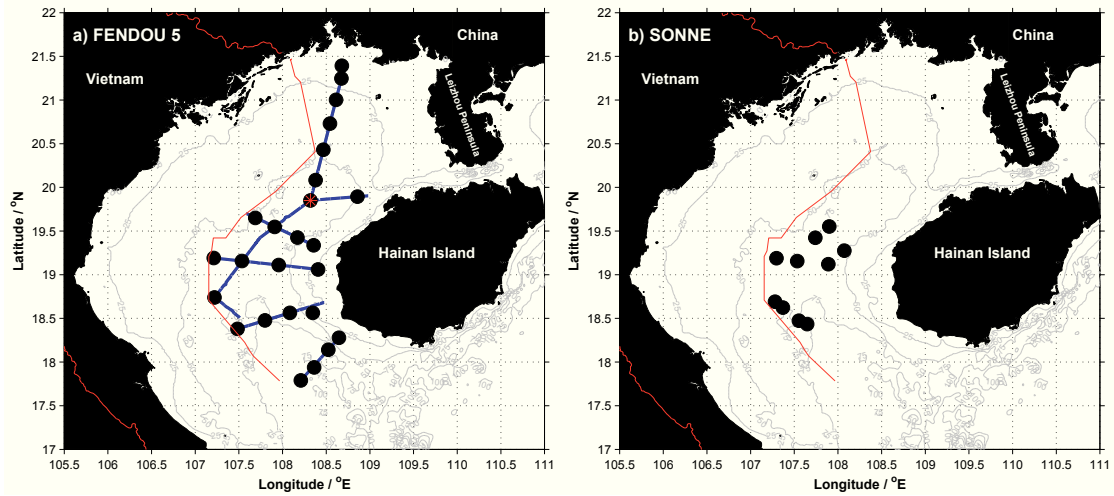


**Figure 2.1:** Sampling stations (black) of a) FENDOU 5 and b) SONNE cruise used in this work. The blue lines indicate ADP measurements and the red star indicates a station where 25 h current measurements were carried out.

To validate the model results two 25 h Aanderaa Recording Current meter (RCM 7) measurements in 10 and 50 m depth with a temporal resolution of one minute as well as stationary ADP records with temporal resolutions of one minute or 30 seconds were carried out at one station (Fig. 2.1a, red star) during the FENDOU 5 cruise. The results of the harmonic analysis were used to validate the tidal model.

### ***Harmonic analysis***

The harmonic analysis is a method of signal demodulation in which the user specifies frequencies to be examined using least-squares technique [Emery and Thomson, 2001]. This method is useful for analysis of tidal heights and currents as these signals are superpositions of basic waves.

Tides can be extracted from local tidal observations as harmonic tidal constituents whose amplitudes determine the type of tide (diurnal, semidiurnal and mixed). Harmonic analysis estimates amplitude and phase for a set of given tidal constituents or partial tides representing the astronomical tide [Boon, 2004] which can then be used for long-term tidal prediction [Emery and Thomson, 2001]. Partial tides are a collection of

sinusoidal waves, each corresponding to a type of lunar or solar tractive forcing and, in sum, constituting the observed tide. Each partial tide in this mixture is identified by a distinctive period of oscillation.

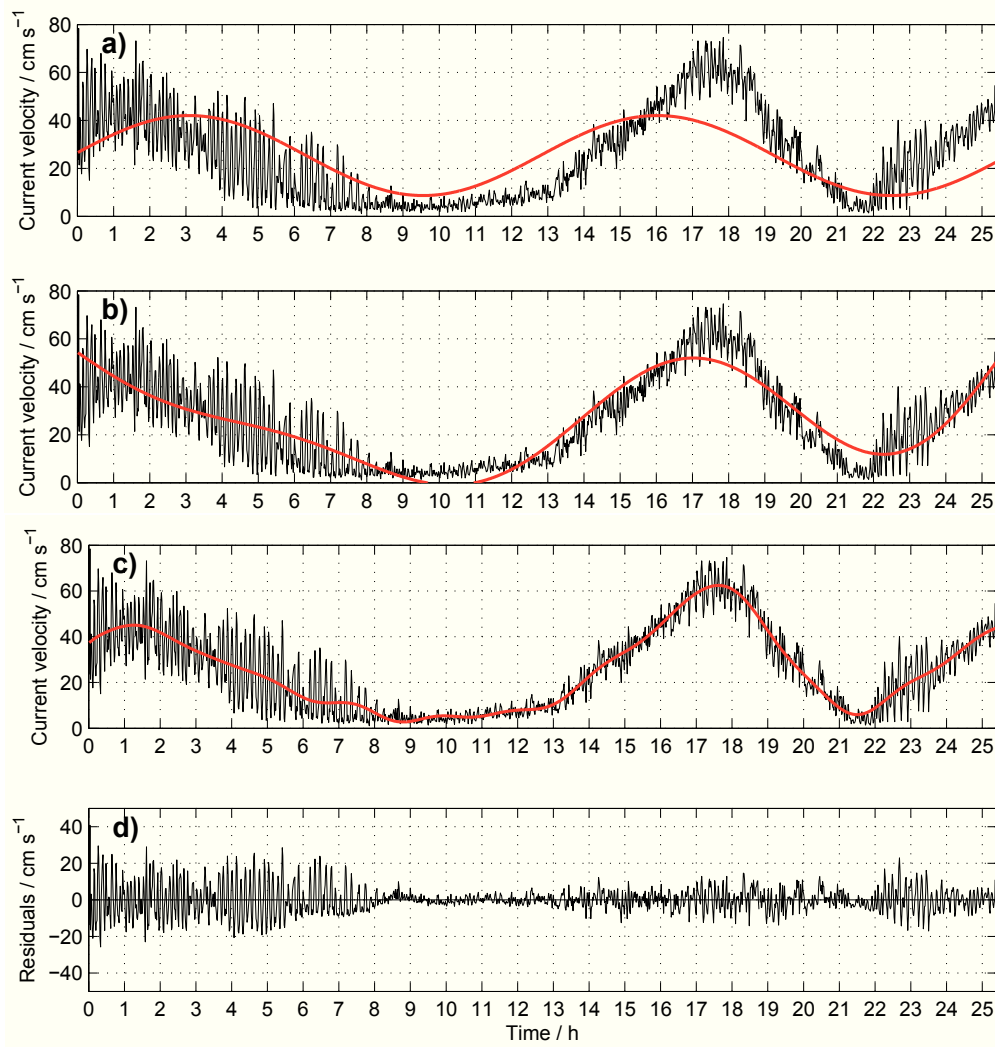


**Figure 2.2:** Absolute current velocity from a 25 h RCM measurement in 10 m depth during the FENDOU 5 cruise as well as the curves (red lines) resulting from the harmonic analysis by using a) only the M<sub>2</sub> tidal constituent, b) M<sub>2</sub>, S<sub>2</sub> and K<sub>1</sub> constituents and c) all constituents given in Tab. 2.1. The black line in d) shows the residuals of the harmonic analysis of c).

For demodulation of the 25 h current signal recorded during the FENDOU 5 cruise, first, the signal has been examined only for the M<sub>2</sub> tidal constituent (Fig. 2.2a), as de-



scribed by *Emery and Thomson* [2001]. The resulting curve does not fit with the measured current signal (Fig. 2.2a). In the next step, the  $M_2$ ,  $K_1$  and  $S_2$  tidal constituents has been applied simultaneously, which resulting curve corresponds better with the raw signal (Fig. 2.2b). The original time series can be reconstructed once the tidal constituents defining the current signal have been determined (Tab. 2.1, Fig. 2.2c).

In the Beibu Gulf, besides the astronomically dominated main constituents for marginal seas, additional periods occur (Tab. 2.1) generated by friction processes [*van Maren et al.*, 2004]. These are tides with periods shorter than semidiurnal tides, arising in shallow water areas, also called shallow water tides or overtides which are multiples of fundamental frequencies. The differences between observed and predicted tide, the so-called residual components (Fig. 2.2d), are tidal and non-tidal variations (e.g. meteorological causes) not captured by harmonic analysis [*Emery and Thomson*, 2001; *Boon*, 2004].

In this work results of the harmonically analyzed current measurements has been used to calculate the  $S_2$  tidal amplitude as a fraction of  $M_2$  needed for the modeling study in chapter 4 and for the already mentioned validation of a tidal model essential for current analysis in chapter 5.

## **2.3 Coupled physical-biological model**

As *in-situ* data are rare for biogeochemical investigations within longer time scales ( $>1$  year) a 1-dimensional physical-biological coupled model was used established by *Sharples* [1999]. The model has been particularly developed for shelf seas and simulates daily vertical profiles of currents, temperature, turbulent mixing, photosynthetic active radiation (PAR), chlorophyll and dissolved inorganic nitrogen (DIN). Using this model the linkage between meteorological forcing (daily mean wind u- and v-components, daily mean dewpoint temperature and daily mean solar irradiance), physical properties of the water column (temperature distribution), especially stratification and mixing, and primary production (chlorophyll distribution) in the central Beibu Gulf has been studied.

The vertical model grid is split into a series of grid cells [*Sharples*, 1999] which are coupled among each other through vertical turbulent mixing (Fig. 2.3) controlled by a 2.2b turbulence closure scheme [*Simpson et al.*, 1996] in the physical module. Quadratic stress boundary conditions are applied at the surface by wind to transmit wind-driven

**Table 2.1:** Harmonic constituents acting in the Beibu Gulf.

Tidal type	Tidal constituent	Period [h]	Origin	Source
Diurnal	K <sub>1</sub>	23.93	lunisolar	<i>Boon</i> [2004]
	P <sub>1</sub>	24.07	solar	<i>Boon</i> [2004]
	S <sub>1</sub>	24.00	solar	<i>Boon</i> [2004]
	O <sub>1</sub>	25.82	lunar	<i>Boon</i> [2004]
Semidiurnal	K <sub>2</sub>	11.97	lunisolar	<i>Boon</i> [2004]
	M <sub>2</sub>	12.42	lunar	<i>Boon</i> [2004]
	S <sub>2</sub>	12.00	solar	<i>Boon</i> [2004]
	N <sub>2</sub>	12.66	lunar	<i>Boon</i> [2004]
Shallow water	M <sub>4</sub>	6.21	lunar	<i>Boon</i> [2004]
	S <sub>4</sub>	6	solar	<i>Boon</i> [2004]
	M <sub>6</sub>	4.14	lunar	<i>Boon</i> [2004]
	M <sub>8</sub>	3.105	lunar	Calculated (4M2)
	M <sub>10</sub>	2.484	lunar	Calculated (5M2)
	M <sub>12</sub>	2.07	lunar	Calculated (6M2)
	M <sub>14</sub>	1.77	lunar	Calculated (7M2)

momentum into the water column and at the seabed by friction inducing bottom-near turbulence introducing remineralized nutrients into the water column by resuspension. Incident solar radiation attenuates by 55% within the top depth cell to simulate the rapid attenuation of the infra-red light portion and further distributes exponentially through the water column as well as PAR, as an user-defined fraction of solar radiation (between 0.4 and 0.5) [*Sharples*, 1999]. Related to wind speed and dewpoint temperature, including evaporation, also a cooling of the warm sea surface is modeled by a longwave radiation loss term applied to the surface grid cell. Tidal currents are driven by the oscillating sea-surface slope containing M<sub>2</sub> and S<sub>2</sub> tidal constituent for simulating the spring-neap tidal cycle.

The biological module is a cell quota, threshold limitation model with one or two taxa/species of phytoplankton growing [*Sharples* 1999]. Nutrients, modeled as DIN, are assimilated by the algal cells (representative of a diatom) having an internal nutrient concentration (IN). Growth of phytoplankton biomass, modeled as chlorophyll concen-

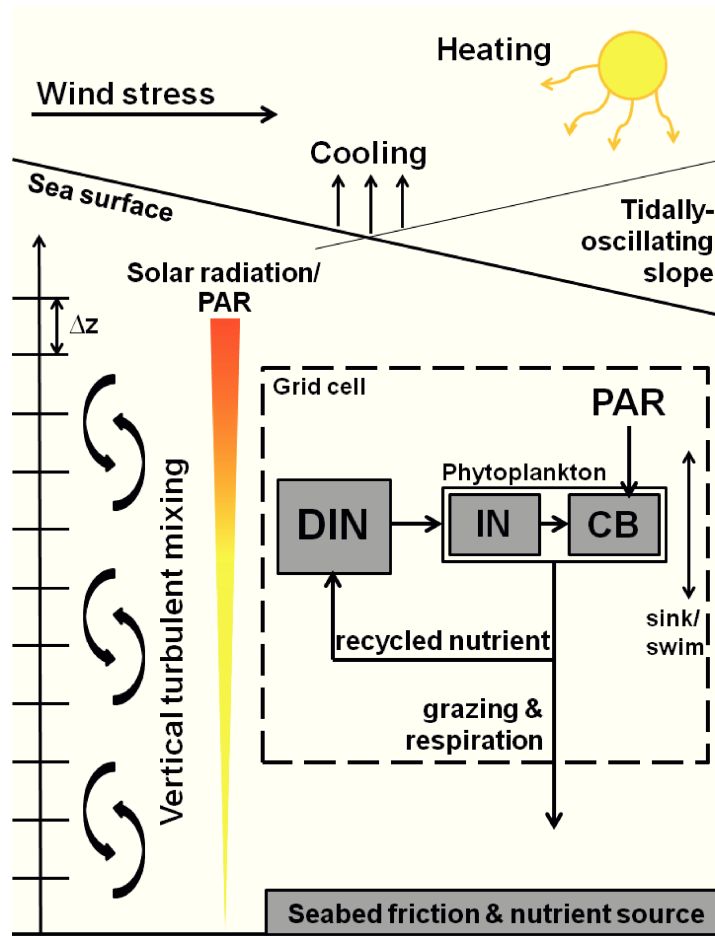


**Figure 2.3:** Schema of the coupled physical-biological model, modified after *Sharpley* [1999]. PAR is the photosynthetic active radiation, DIN is dissolved inorganic nitrogen, IN stands for algal internal nutrients and CB is the algal chlorophyll biomass.

tration (CB), occurs depending on the availability of PAR and DIN. The cells start to respire if the light or internal nutrient concentration is insufficient for growth. Furthermore, a fixed grazing rate acts on the phytoplankton biomass which leads, together with respiration, partially to nutrient recycling and nutrient loss. Phytoplankton cells are neutrally buoyant and can be set to have the ability moving vertically. Biomass and DIN are vertically mixed by turbulence calculated by the physical module.

A detailed description of the model, of all used parameters and settings as well as processing of comparative data can be found in section 4.2.

## **2.4 Additional data sets**

To identify the monsoonal phase during the FENDOU 5 expedition, daily surface wind fields for the Beibu Gulf region were obtained from the National Centers for Environmental Prediction (NCEP/NCAR, <http://www.esrl.noaa.gov>; *Kalnay et al.* [1996]). To calculate the Ekman depth (chapter 3) during the passing of typhoon KETSANA (23.-30.09.2009) regional daily wind speeds were obtained from weather stations in Haikou, Dongfang and Sanya ([www.cmabbs.com](http://www.cmabbs.com)). Daily wind speeds from the NCEP/NCAR Reanalysis database were used to calculate Ekman depth in chapter 5. For the modeling necessary meteorological parameters (wind components, downward longwave radiation flux as well as air temperature and relative humidity for calculating dewpoint temperature) were taken as well from the NCEP/NCAR Reanalysis database for 11 years (2000-2010). For model validation, satellite data for daily sea surface temperature (SST) were taken from <http://www.remss.com> (Tropical Rainfall Measuring Mission Microwave Imager (TMI), resolution  $0.25^{\circ} \times 0.25^{\circ}$ ) and monthly SeaWiFS (2000-2010) as well as MODIS (07/2002-2010) surface chlorophyll concentrations from <http://gdata1.sci.gsfc.nasa.gov> were used. All remotely measured data for the modeling study, used in a meteorological data file as well as comparative satellite data, were averaged for the central Beibu Gulf (explained in section 4.2.4).

For sediment sampling, box corer, multi corer and gravity corer were used during FENDOU 5 cruise. Sediment cores were described macroscopically and sliced for further investigations. Samples were taken for grain size, geochemical (water contents, particulate major and trace elements, organic and inorganic carbon, total nitrogen) as well as surface sediment foraminifera and plant pigment analysis. Furthermore, pore water samples were taken with rhizons [e.g. *Seeberg-Elverfeldt et al.*, 2005] on board of FENDOU 5. The sampling of geological and geochemical parameters is described in detail in sections 3.2.3, 3.2.4 and 5.2.2.

### 3 Regional differences of hydrographical and sedimentological properties in the Beibu Gulf, South China Sea

*Bauer et al. (in press), Journal of Coastal Research: Special Issue 66*

#### Abstract

Analyzing the Beibu Gulf's hydrography and sediment properties is crucial for the understanding of naturally and anthropogenically induced matter and energy fluxes in the SCS's northwestern coastal regions. For this reason, the present study combines hydrographical (T, S,  $\sigma_t$ ), chlorophyll, nutrients, SPM) and sedimentological (grain size, pore water properties, phosphate speciation, foraminifera, plant pigment contents) investigations.

On the basis of hydrographical profiles (temperature, salinity and  $\sigma_t$ ) taken at 25 stations, four ecological zones are identified in the study area for the sampling period in September/October 2009. These zones are mainly influenced by riverine input and tidal mixing, water mass transport through the Qiongzhou Strait which also affects the gulf's circulation, and SCS waters in the southern Beibu Gulf. The zonation extends from the coastal areas in the northern Beibu Gulf and west of Hainan Island across the central regions to the southern part of the gulf.

The study demonstrates that the hydrographical peculiarities of the different zones influence not only the biogeochemical features (chlorophyll, nutrients, SPM) of the water column but also the deposition of sediments and their biological (plant pigment contents and foraminifera) and geochemical (pore water properties) characteristics. Both, the near-shore area and the zone in the vicinity of the Qiongzhou Strait show relatively high chlorophyll concentrations and therefore give evidence of enhanced primary production

in the entire water column. Whereas the grain size and the foraminifera in the surface sediments follow the hydrodynamically controlled sedimentation conditions, plant pigment contents in the surface sediments additionally follow the productivity pattern in the water column. Depending on the depositional environments with their respective sedimentology and organic matter contents, the geochemical sediment properties reflect the primary production within the water column as well.

### **3.1 Introduction**

The SCS is one of the largest and for the regional climate most important sea of the Southeast Asian Waters [Liu *et al.*, 2002]. Bathymetrically, about 47% of the total area of the SCS consist of a well developed shelf area [Wang and Li, 2009]. This broad shelf with a depth less than 100 m belongs to the so-called "Sunda-Arafura Shelves Province", a large continental shelf area extending from Burma and South China down to the northern coast of Australia [Longhurst, 2007].

The Beibu Gulf, also known as the Gulf of Tonkin, is one of the SCS major embayments. It is located in the northwestern part of the SCS, bounded by South China and Vietnam in the north and west and by Leizhou Peninsula and Hainan Island in the east, connected to the northwestern shelf of the SCS through the Qiongzhou Strait, and has a broad opening to the western SCS in the south. As a shallow shelf sea area the Beibu Gulf has an average depth of about 45 m and a bathymetry that deepens gradually to the south where the gulf reaches its maximum depth of about 100 m [Manh and Yanagi, 1997; Wu *et al.*, 2008].

The circulation in the Beibu Gulf is mainly governed by wind, tidal currents and currents outside the gulf [Chen *et al.*, 2009]. In the traditional view the surface circulation in the Beibu Gulf reverses from a winter cyclonic to a summer anticyclonic circulation due to the change from northeast to southwest monsoon [e.g. Manh and Yanagi, 1997, 2000], equally to the circulation in the SCS main basin [e.g. Huang *et al.*, 1994]. However, most recent modeling results and observational data reveal that the circulation is cyclonic throughout the entire year [Shi *et al.*, 2002; Wu *et al.*, 2008]. A broad southward flow in the upper layer along the Vietnamese coast is compensated by a northward return flow in the interior and along the west coast of Hainan Island which results in a gulf-wide cyclonic gyre [Wu *et al.*, 2008] (Fig. 3.1a). The tide-induced westward

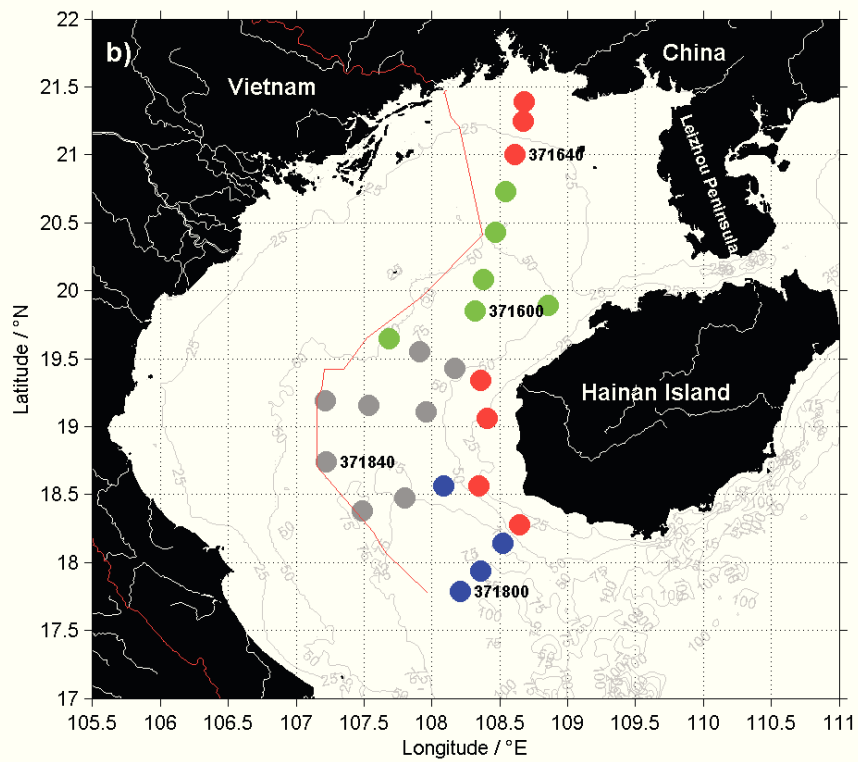
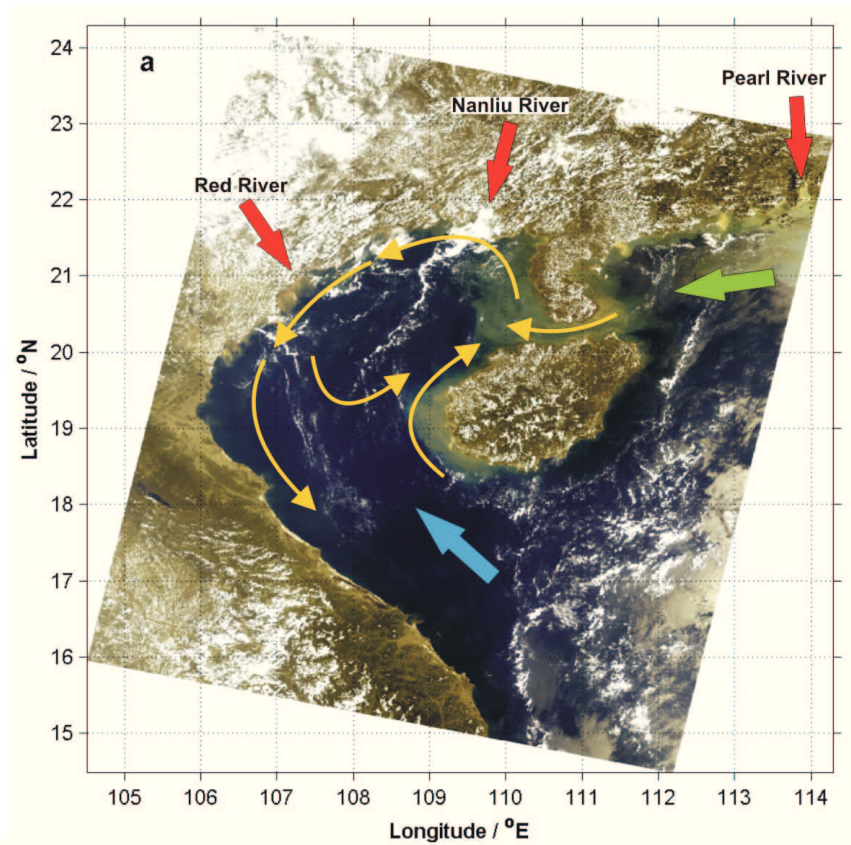
mean transport of about 0.1-0.2 Sv through Qiongzhou Strait into the Gulf of Beibu in all seasons [Shi *et al.*, 2002] (Fig. 3.1a) is the key factor for the cyclonic circulation, especially in summer when the southwestern monsoonal forcing tends to drive an anticyclonic one [Wu *et al.*, 2008]. Many rivers with a mean annual discharge of about  $14 \times 10^{10} \text{ m}^3$  influence the Beibu Gulf [Chen *et al.*, 2009]. Rivers play a major role in the transport of material from land to the sea and thereby significantly influence the biogeochemical processes in coastal waters [Gago *et al.*, 2005]. River loads from the Red River and some smaller rivers in the northern coastal area [Tang *et al.*, 2003] are transported southward through the Beibu Gulf into the SCS (Fig. 3.1a). Furthermore, the semi-enclosed Beibu Gulf interacts with the surrounding SCS through water mass exchanges [Wu *et al.*, 2008]. Different water masses originating from the coastal areas off South China in the northern SCS can be transported through Qiongzhou Strait and therefore influence the region [e.g. Su and Weng, 1994]. Also discharge from the Pearl River located 400 km away to the northeast may reach the gulf through the Qiongzhou Strait [Tang *et al.*, 2003] (Fig. 3.1a).

The marine influence from the south is mainly driven by tidal waves propagating into the Beibu Gulf through the wide opening with a current velocity of about  $40 \text{ cm s}^{-1}$  at the surface [Manh and Yanagi, 1997] (Fig. 3.1a). Model experiments by Cai *et al.* [2003] showed that tidally driven currents play a significant role in the formation of a cyclonic circulation in the Beibu Gulf, especially in summer.

This study presents first results of the German/Chinese bilateral research project BEIBU which focusses on the Beibu Gulf. Shelf areas like the Beibu Gulf are hot spots for biogeochemical fluxes and respond very quickly to environmental changes, e.g. the carbon turnover time is in order of days to weeks [Ross, 2004]. Therefore, they are im-

---

**Figure 3.1 (following page):** a) Satellite image of the Beibu Gulf region from ESA ENVISAT MERIS (18. September 2009) showing the general cyclonic circulation pattern (yellow arrows, after Shi *et al.* [2002] and Wu *et al.* [2008], riverine (red arrow), coastal parallel (green arrow) and marine input (blue arrow). b) FENDOU 5 cruise track in September/October 2009. The different zones as defined in this study are color-coded (red dots: BGCoZ, Beibu Gulf Coastal Zone, green dots: Qiongzhou Strait Zone, QSZ, grey dots: Beibu Gulf Central Zone, BGCoZ and blue dots: Southern Beibu Gulf Zone, SBGZ). The stations representing the zones are labelled.





portant for the understanding of changes in the balance of river input and coastal erosion, near-surface degradation of organic material and hence induced element fluxes as well as changes in the conditions of recent sediment accumulation. As a large marginal sea of the SCS the Beibu Gulf plays an important role for the understanding of naturally and anthropogenically induced matter and energy fluxes in the SCS northwestern coastal regions. So far, less is known about the biogeochemical element cycles in the Beibu Gulf, which is nowadays an important region for the industrial production of P-bearing fertilizers [Yan, 2006]. Element and material transport via benthic-pelagic coupling towards surface waters, for example, may be an important factor driving primary production in this region.

The aim of this study is to elucidate regional differences in hydrography influencing not only biological properties in the water column but also deposition and coupled geochemical and biological characteristics of the sediments. Until now, no interdisciplinary study on the Beibu Gulf which combines water column and sediment properties has been presented or published.

## 3.2 Material and Methods

### 3.2.1 Study area

The study area is situated in the northern and eastern part of the Beibu Gulf in the territorial waters of P. R. China (Fig. 3.1b).

During summer, the surface water temperature is high, ranging from 27.5°C in the north of the gulf to 29.5°C in the south [Manh and Yanagi, 2000]. Because of the high fresh water discharge in summer in the northwestern area, a low salinity zone and a cold water mass exists in the center of the gulf [Chen *et al.*, 2009]. In winter, the water column is vertically well mixed and surface water temperatures increase from 20°C in the north to 24°C in the south [Manh and Yanagi, 2000].

The Beibu Gulf contains tropical mesotrophic waters [Tang *et al.*, 2003]. A vertical stratification develops in summer with rapidly decreasing water temperatures from about 29.5°C at the surface, to 19°C at depth [Manh and Yanagi, 2000] and a relative uniform SST in the entire gulf. This stratification, caused by sea surface heating, limits entrainment of nutrients and phytoplankton growth [Tang *et al.*, 2003]. Therefore, in

summer the chlorophyll *a* content is relatively low and uniform in the entire gulf [Tang *et al.*, 2003]. In a narrow band along the coasts, tidal mixing induces upwelling of nutrients to the euphotic zone which leads to a higher chlorophyll *a* concentration and a higher primary production [Tang *et al.*, 2003]. In contrast, during winter the chlorophyll *a* concentrations increase in the entire gulf, with higher chlorophyll *a* concentrations in the northeastern and lower in the southwestern part [Tang *et al.*, 2003].

Geologically, the depositional center of the gulf and local depressions are filled with fine-grained sediments, substituted by sandy deposits closer to the coasts [Su and Wang, 1994]. The near-surface sediment layers are complex and include siliciclastic deposits with variable carbonate-organogenic components [Su and Wang, 1994]. The accumulation rate varies between  $1.2 \text{ mm yr}^{-1}$  for the deltas [Liu *et al.*, 1992] and  $0.25 \text{ mm yr}^{-1}$  in local lagoons [Li *et al.*, 1996]. It has to be mentioned that in earlier stages during the Holocene the accumulation rates reached in delta areas more than  $3 \text{ mm yr}^{-1}$  [Tanabe *et al.*, 2003a,b].

### **3.2.2 Water samples**

During a cruise with the Chinese RV FENDOU 5 in September/October 2009 depth profiles (temperature, conductivity, oxygen, chlorophyll-fluorescence) were recorded as well as water, pore water and sediment samples were taken at 25 stations (Fig. 3.1b). Hydrographic profiling and water sampling was done by using an IOW mini PUMP CTD system based on Strady *et al.* [2008]. The instrument consists of a YSI probe (6600 V2-4) including sensors for pressure, temperature, conductivity, oxygen, fluorescence and turbidity in a frame additionally equipped with an extra underwater high pressure pump. This pump produces a water flow from the CTD through a 150 m long tube with a rate of about  $2 \text{ l min}^{-1}$  to the ship-board laboratory. The YSI is directly connected to a notebook on deck for continuous recording of the hydrographical parameters and calculating the depth during downcast.

Water samples were taken from different depths during upcast and stored in 5 l canisters. For chlorophyll and SPM analyses, 0.5 to 1 l water were low vacuum filtered through  $0.7 \mu\text{m}$  Whatman GF/F glass fibre filters. In addition, water samples for analysis of dissolved nutrients ( $\text{NO}_2$ ,  $\text{NO}_3$ ,  $\text{PO}_4$ ,  $\text{SiO}_4$ ) were taken. All filters were washed with deionized water before storage and frozen at around  $-20^\circ\text{C}$  until laboratory analy-

sis at Leibniz-Institute for Baltic Sea Research (IOW). The extracted chlorophyll samples were analyzed through a fluorometer (TURNER 10-AU) after *JGOFS* [1994] without correction for phaeopigments. Nutrient samples were processed using an autoanalyzer (EVOLUTION III, Alliance Instruments, (detection limits:  $\text{NO}_2$ : 0.02  $\mu\text{M}$ ,  $\text{NO}_3$ : 0.05  $\mu\text{M}$ ,  $\text{PO}_4$ : 0.02  $\mu\text{M}$ ,  $\text{SiO}_4$ : 0.1  $\mu\text{M}$ )) according to standard procedures [Hansen and Koroleff, 1999].

### 3.2.3 Geological samples

For sediment sampling box corer (BC), multi corer (MUC), and gravity corer (GC) were used. The MUC was equipped with 4 liners (60 cm long, inner diameter 10 cm), the GC was loaded with 4 m long plastic liners (diameter of 120 mm). After recovery, the GC cores were cut into sections of 1 m. At each station the first gravity core was used for macroscopic sediment description according to standard protocols, e.g. sediment color was determined using the rock-color chart [Rock Color Chart, 1991].

The MUC cores were sliced into 1 cm sections for the upper 20 cm and 2 cm sections for depths >20 cm. Cores taken by GC were cut into 2 cm slices. Every sample from the upper 50 cm and every second sample from the lower 50 cm of the GC core was analyzed in the laboratory later. Preparation, treatment and measurement of all sediment samples were carried out in the laboratory of Marine Geology Section, IOW and in the laboratory of the Guangzhou Marine Geological Survey (GMGS). The grain size was determined using a laser particle sizer analyzer (Cilas 1180L) with an ultrasonic pretreatment for 10 min to disperse the aggregates (T. Leipe, personal comment) at IOW (cores at stations 371800 and 371840) and a diffraction particle size analyzer (Mastersizer 2000) at GMGS (cores at stations 371600 and 371640). For further geological analysis sediment samples were freeze-dried and homogenized by mixing and grinding.

The sediment samples for plant pigment analyses were taken from the topmost 1 cm of cores recovered by BC and MUC. After thawing in the dark, four sediment portions per sample were placed in a fluorometric cuvette containing 7 ml 90% acetone in magnesium carbonate solution and left for extraction for 24 h in the dark at 4°C in the laboratory of the University of Szczecin, Poland. Pigment contents in the extracts were measured fluorometrically in a calibrated TURNER 10-AU fluorometer (Turner Designs, USA) before (chlorophyll *a*) and after (phaeopigments) acidification with 0.1 N

HCl. The extracted sediment was dried at 105°C and weighted. The fluorescence read-outs were converted to pigment content per 1 g dry sediment and the results of the 4 portions per sample were averaged.

For foraminiferal analysis, BC sediment samples, about 20 g each, were processed using standard techniques according to *Wei et al.* [2006]. First, the samples were washed in distilled water to remove adhering particles and then soaked in 10% NaOCl solution for 24 h to remove organic materials. The samples were pre-sieved on a 0.063 mm mesh size sieve and the residues >0.063 mm were separated into two fractions using a 0.15 mm mesh size copper sieve. Foraminifera from the >0.15 mm fraction were identified and counted without discrimination between living and dead individuals. Finally, the abundances of various species were standardized to 10 g sediment because of the low total abundance.

### 3.2.4 Geochemical samples

Particulate major and trace elements were analysed by ICP-OES (Thermo iCAP 6300-Duo). Precision ( $1\sigma$ ) and accuracy of all measurements were checked by parallel analysis of international and in-house reference materials (precision and accuracy were  $\leq 7.4\%$  and  $\leq 4.3\%$  for major elements and  $\leq 6.8\%$  and  $\leq 10.7\%$  for trace metals) according to *Dellwig et al.* [2010]. Samples for pore water analysis were taken with rhizons [e.g. *Seeberg-Elverfeldt et al.*, 2005] connected to syringes through holes in the core liners on board of the ship. Samples for dissolved elements were filtered through 0.45  $\mu\text{m}$  SFCA syringe filters and acidified to 1 vol%  $\text{HNO}_3$  in precleaned PE-bottles. All acids used were of suprapure quality.

Sediments were taken from sliced sections of sedimentary short (MUC) and long cores (GC) and analyzed for water contents (gravimetry), organic and inorganic carbon, and total nitrogen as described by *Leipe et al.* [2010]. For the depth correction of all gravity cores, an estimated top core loss of about 20 cm was assumed. Sedimentary phosphorous (P) fractions were extracted sequentially according to the scheme of van Beusekom (after *De Jonge and Engelkes* [1993]). Reactive iron was extracted from wet sediments using 0.5 M HCl for 1 h at room temperature [*Kostka and I.G.W.*, 1994; *Thamdrup et al.*, 1994]. A one hour extraction with HCl is selective for the amorphous or poorly crystallized Fe-ox(yhydrox)ide and carbonate phases, with minor contribu-

tion of silicates [e.g. *Haese et al.*, 1997]. The extracted P fractions (iron-bound (P-Fe), iron-aluminum-bound (P-FeAl) and Ca-apatite (P-Ap)) and extractable iron (Fe\*) were measured by spectrophotometry (Specord 40 spectrophotometer, Analytik Jena) according to *Koroleff and Kremling* [1999] and *Stookey* [1970], respectively.

### 3.2.5 Additional data sets

Daily surface wind fields for the Southeast Asian and the Beibu Gulf region during September/October 2009 were obtained from the QuikSCAT satellite ([www.remss.com](http://www.remss.com)) and from NCEP/NCAR Reanalysis database ([www.esrl.noaa.gov](http://www.esrl.noaa.gov); *Kalnay et al.* [1996]) to identify the mean wind direction and hence the monsoonal phase during the expedition. The mean daily wind velocity vectors for the Beibu Gulf indicate a northeastern wind direction during sampling period (Fig. 3.2). The high wind speeds between 27<sup>th</sup>

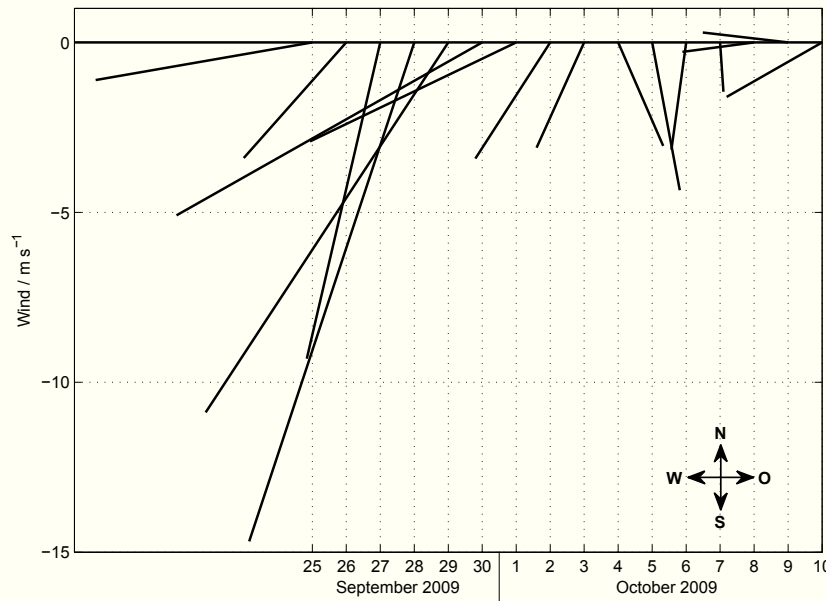


**Figure 3.2:** NCEP Reanalysis daily mean wind velocity vectors for the sampling period between September and October 2009 for the entire Beibu Gulf.

and 30<sup>th</sup> of September are generated by the typhoon KETSANA (23.-30. September 2009). In addition, regional daily wind speeds were received from weather stations in

Haikou, Dongfang and Sanya at Hainan Island (www.cmabbs.com) and used to estimate the Ekman depth which may be potentially reached during the passing of typhoon KETSANA. The Ekman depth (in m) is defined as

$$D_E = \frac{4.3 W}{\sqrt{\sin|\phi|}},$$

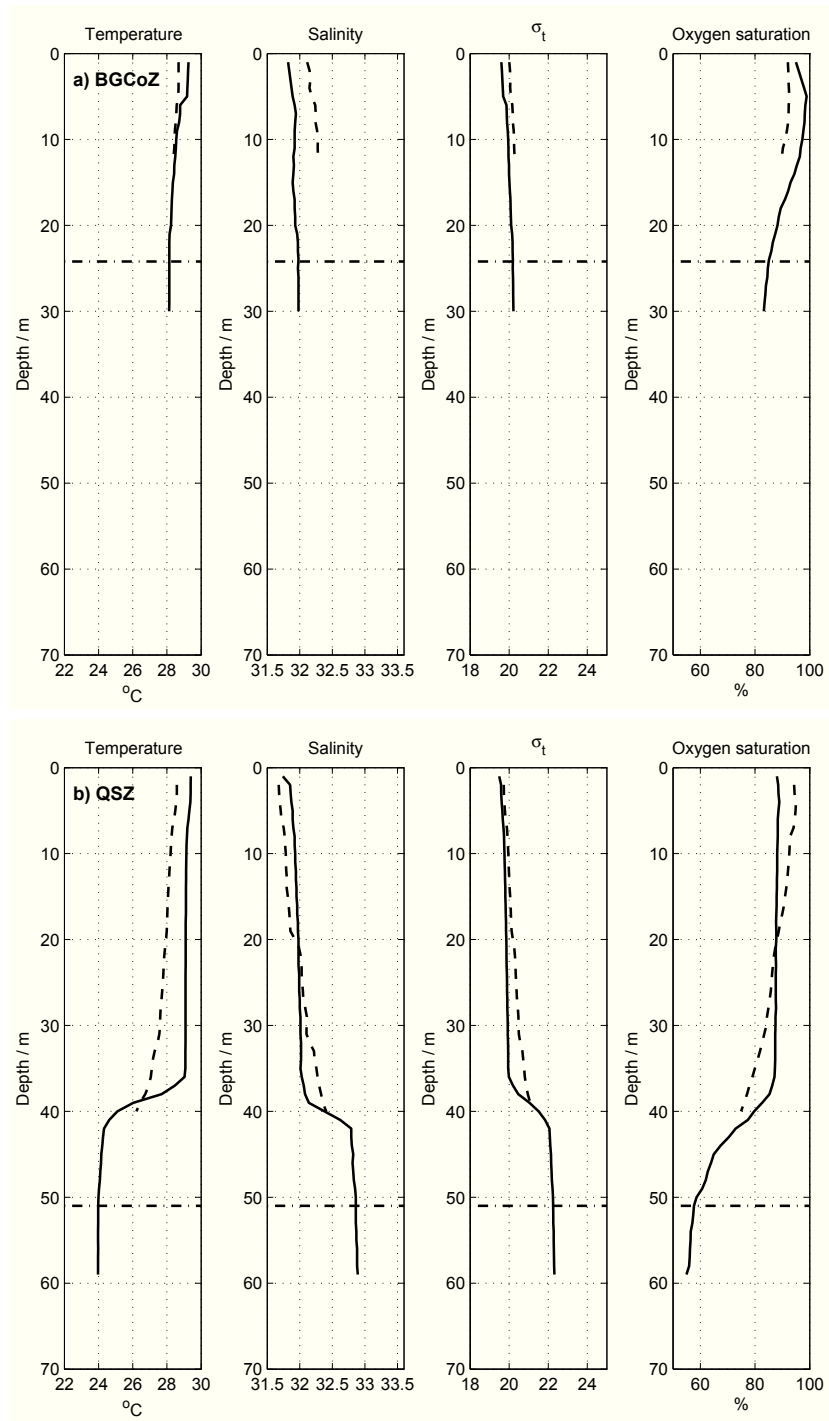
where  $W$  is the wind speed ( $\text{m s}^{-1}$ ) at latitude  $\phi$  [Pond and Pickard, 1983].

### 3.3 Results

Hydrographical profiles (temperature, salinity and  $\sigma_t$ , as the density of seawater -1000) from all stations are used to identify different zones in the study area analogous to *Holliday et al.* [2006]. Fig. 3.1b shows the locations of the stations color-coded according to the corresponding zones: Beibu Gulf Coastal Zone (BGCoZ), Qiongzhou Strait Zone (QSZ), Beibu Gulf Central Zone (BGCEZ) and Southern Beibu Gulf Zone (SBGZ).

Henceforth, each zone will be represented by one station (BGCoZ: 371640, QSZ: 371600, BGCEZ: 371840, SBGZ: 371800, Fig. 3.3, solid lines) and for the hydrographical and biological properties the mean profile is shown as well (Fig. 3.3, 3.4, dashed lines). As the stations within the different zones do not have the same depth the mean profile is as long as the shallowest station in each zone. The determined zones based on hydrographical data are also transferred to physical sediment parameters like grain size, plant pigments and foraminiferal distribution in surface sediments as well as downcore pore water characteristics.

**Figure 3.3 (following page):** Vertical temperature ( $^{\circ}\text{C}$ ), salinity,  $\sigma_t$  (Density of seawater -1000) and oxygen ( $\text{mg l}^{-1}$ , from left to right) distribution in each zone (a) BGCoZ, Beibu Gulf Coastal Zone, b) QSZ, Qiongzhou Strait Zone, c) BGCEZ, Beibu Gulf Central Zone, d) SBGZ, Southern Beibu Gulf Zone). Solid lines are profiles of the stations representing the different zones (a) station 371640, b) station 371600, c) station 371840, d) station 371800), dashed lines are mean profiles (same length as the shallowest station in one zone) and dash-dotted horizontal lines show the mean depths.



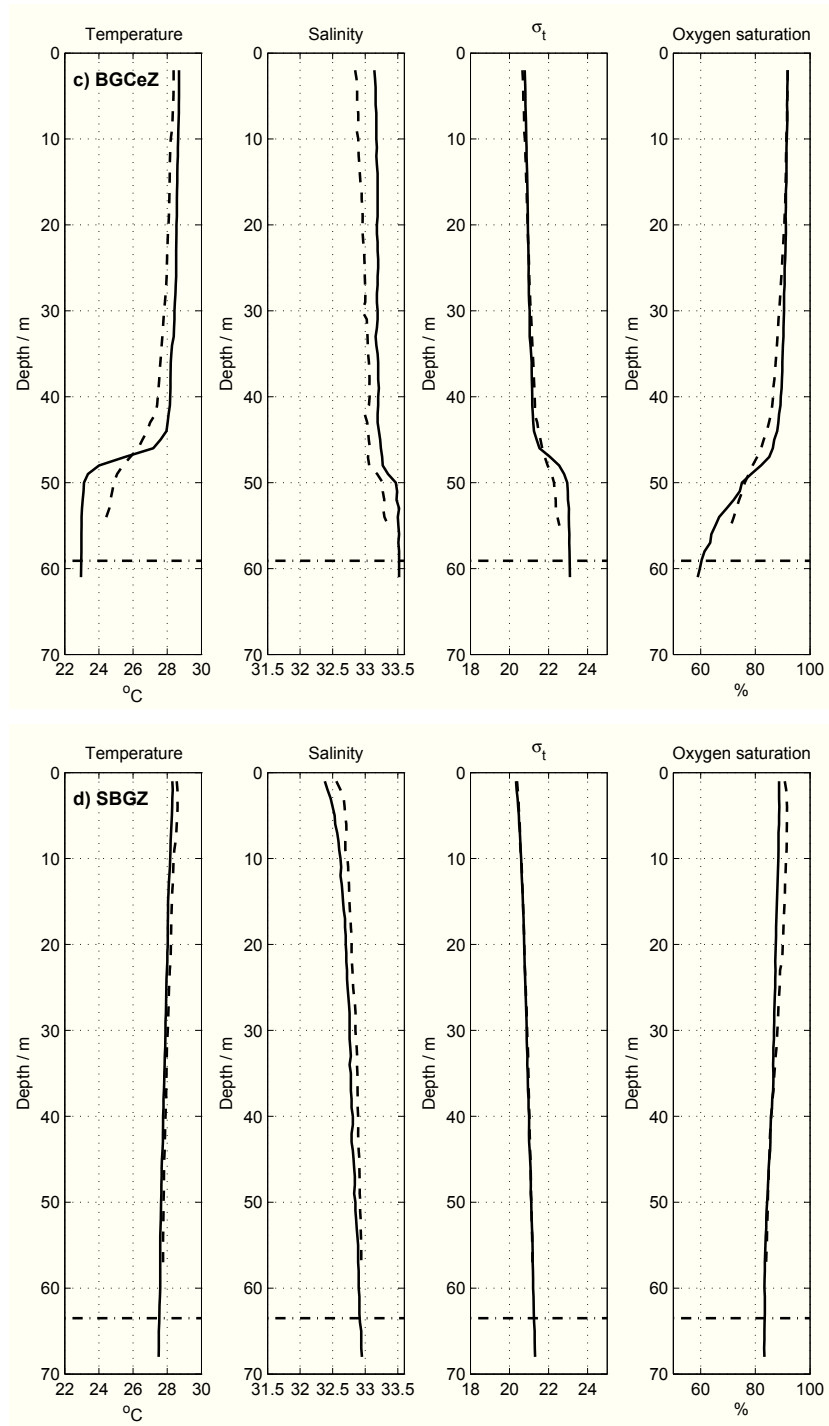


Figure 3.3: Continued.



### 3.3.1 Beibu Gulf Coastal Zone

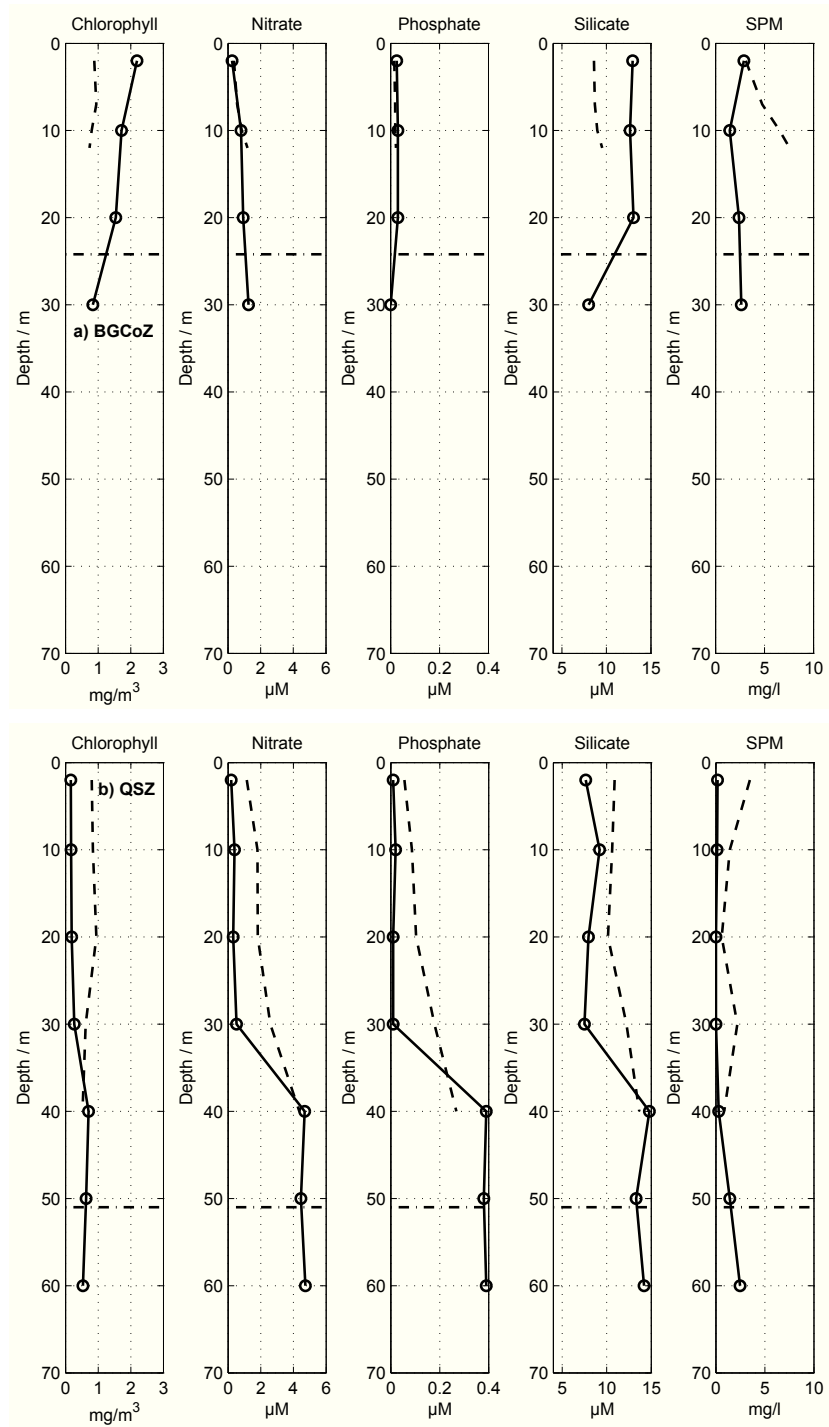
As only few stations are available the stations in the shallow coastal areas in the north and along Hainan Island west coast are combined into one zone, the Beibu Gulf Coastal Zone (BGCoZ) with a depth range from 12 to 43 m. The water column of the BGCoZ is characterized by similar values in temperature (28-29.5°C), salinity (31.8-32) and  $\sigma_t$  (around 20, Fig. 3.3a) from surface to the bottom. This shallow area shows no stratification as the water column is well mixed due to tide- and wind-induced forcing. On account of the intensive mixing the highest oxygen saturation level of 99% is measured at around 5 m depth with a rapidly decreasing saturation down to 83% at the bottom (Fig. 3.3a).

Fig. 3.4a-d show the chlorophyll, nutrients (nitrate, phosphate and silicate) and SPM profiles (from left to right) for all zones. The highest chlorophyll and silicate concentrations with  $2.3 \text{ mg m}^{-3}$  and  $13 \text{ }\mu\text{M}$ , respectively, are measured in the surface layer, followed by a steep decrease towards the bottom to the respective concentrations of  $0.9 \text{ mg m}^{-3}$  and  $8 \text{ }\mu\text{M}$  (Fig. 3.4a). Also phosphate decreases down to the bottom but with very low concentrations in the entire water column (up to  $0.03 \text{ }\mu\text{M}$ , Fig. 3.4a). Only nitrate shows an increase with depth reaching a maximum value of  $1.25 \text{ }\mu\text{M}$ . SPM concentrations of up to  $2.9 \text{ mg l}^{-1}$  at the surface and the bottom with a minimum of  $1.5 \text{ mg l}^{-1}$  at around 10 m depth point to a relatively low variability of SPM distribution down the water column in the BGCoZ (Fig. 3.4a).

BGCoZ sediments are light olive grey or dark greenish grey colored, are soft to plastic, homogeneous and calcareous with some bivalve and snail shell fragments. Sediment samples from BGCoZ are moderately sorted (1.4-1.8). The grain size ternary diagram for sediment classification (after Folk [1954]) shows that the silt fraction dominates with 65%-75%, followed by the clay fraction (22%-29%) and an only slight sand frac-

---

**Figure 3.4 (following page):** Vertical chlorophyll ( $\text{mg m}^{-3}$ ), nitrate ( $\mu\text{M}$ ), phosphate ( $\mu\text{M}$ ), silicate ( $\mu\text{M}$ ) and SPM ( $\text{mg l}^{-1}$ , from left to right) distribution in each zone (a) BGCoZ, b) QSZ, c) BGCEZ, d) SBGZ. Solid lines are profiles of the stations representing the different zones (a) station 371640, b) station 371600, c) station 371840, d) station 371800), dashed lines are mean profiles (as long as the shallowest station in one zone) and dash-dotted horizontal lines show the mean depths. Circles indicate sampling depths.



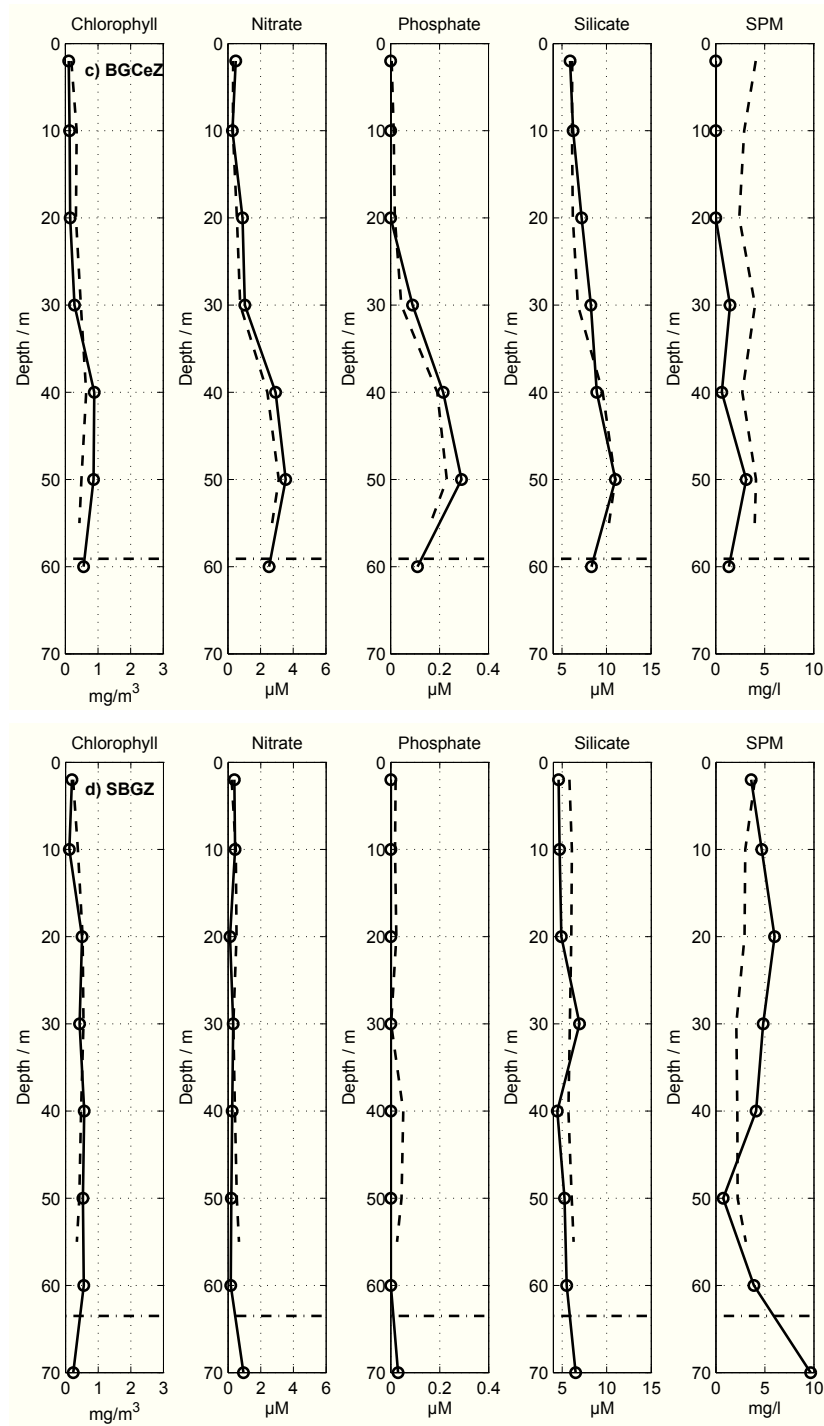
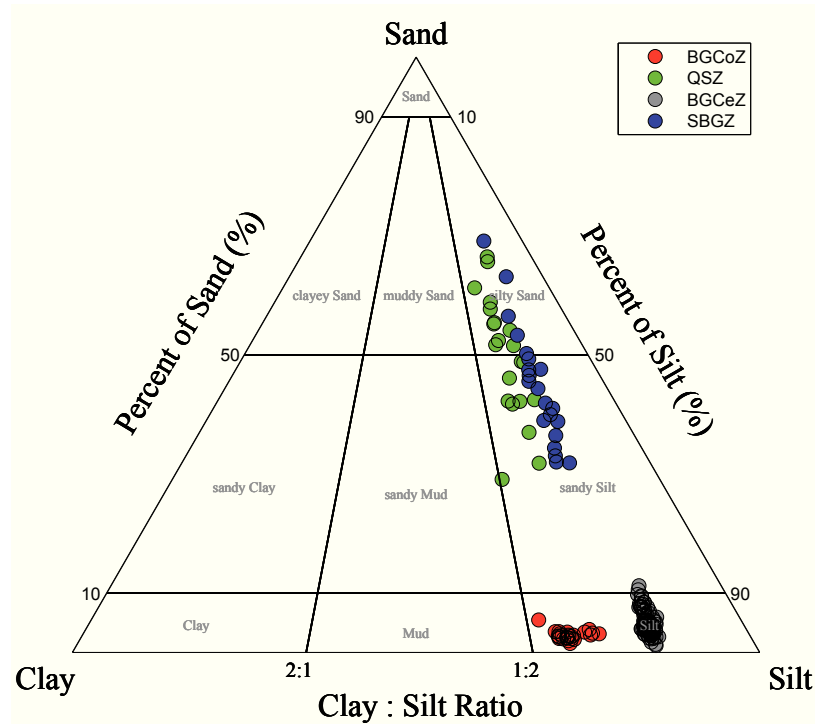


Figure 3.4: Continued.

tion (1%-5%, Fig. 3.5, red dots). The mean grain size ranges from 6.9 to 7.3  $\mu\text{m}$  for which reason the sediment can be generally considered as consisting of medium silt.



**Figure 3.5:** Grain size ternary diagram for sediment classification of the sediments from the different zones (red: BGC0Z, green: QSZ, grey: BGCEZ, blue: SBGZ).

In BGC0Z the zone averaged surface sediment plant pigment content (Fig. 3.6a), expressed as the so-called Chloroplastic Pigment Equivalents (CPE, sum of plant pigment contents) is about  $9.7 \mu\text{g g}^{-1}$  dry sediment (d.s.). The plant pigment pool consists of chlorophyll *a*, a signature of "fresh", not degraded phytal material, and phaeopigments, representing the "old", degraded material. The chlorophyll *a* and phaeopigment contents are about  $3.1 \mu\text{g g}^{-1}$  d.s. and  $6.6 \mu\text{g g}^{-1}$  d.s, respectively (Fig. 3.6a). The ratio between the chlorophyll *a* content and that of phaeopigments is a criterium of the freshness of the plant material in the sediments (Fig. 3.6b). In BGC0Z this ratio varies between 0.38 and 0.75.

The surface sediments contain no planktonic foraminifera (Fig. 3.7a) and altogether the overall foraminiferal abundance is very low (83 shells/10 g sediment). Agglutinated

benthic foraminifera and calcareous species contribute 1% and 99% to the total assemblage, respectively, therefore the latter can be regarded as the most important group in this zone. The dominant species are *Hanzawaia mantaensis* [e.g. Wang *et al.*, 1988; He and Hu, 2001] and *Florilus decorus* [Wang *et al.*, 1988]. *H. mantaensis* inhabits temperate-warm inner shelves [Murray, 2006] while *F. decorus* is typical for coastal regions and inner shelves up to a water depth of 50 m [Wang *et al.*, 1988].

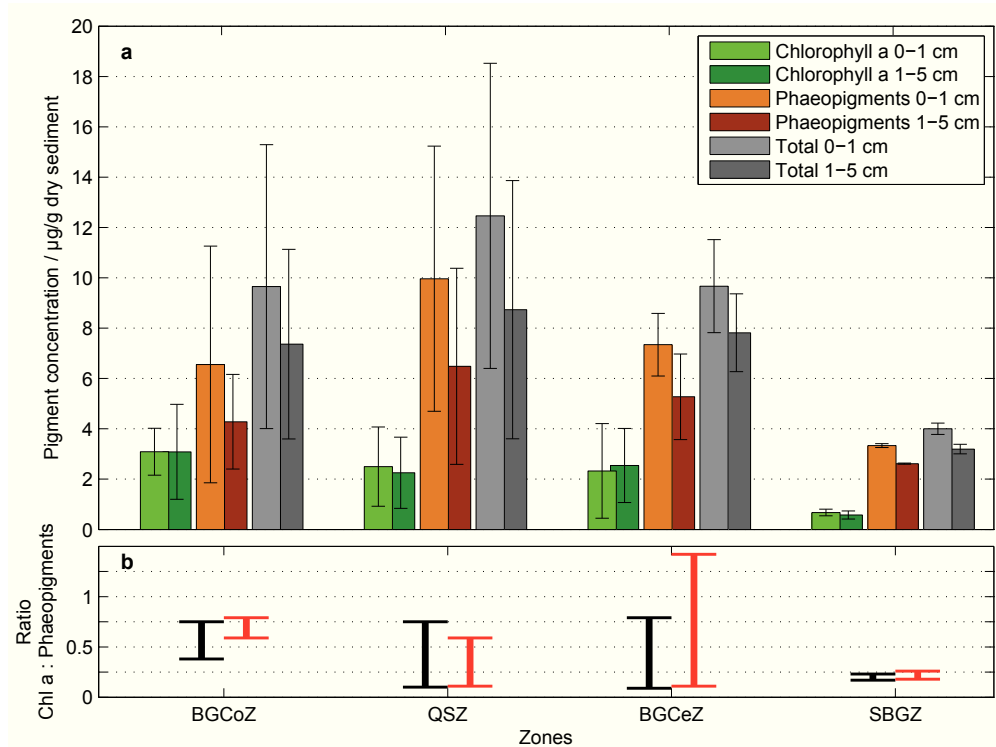


**Figure 3.6:** Surface (0-1 cm) and subsurface (1-5 cm) sediment pigment concentrations (a, in  $\mu\text{g g}^{-1}$  dry sediment) averaged over all stations within the corresponding zones and range of the chlorophyll *a* to phaeopigment ratio (b) for the zones and sediment layers (black: surface, red: subsurface). The standard deviations are represented by the vertical black lines.

Pore water profiles from BGCoZ of dissolved iron, manganese, phosphate, silica and sulphate (from left to right) are shown in Fig. 3.8a-e. Distinct near-surface maxima of dissolved manganese and iron are found in 3 and 4 cm depth, respectively (Fig. 3.8a, b). Concentrations of phosphate and silica increase with depth, reaching maxima between

8 and 10 cm sediment depth (Fig. 3.8c, d). The sulphate profile displays almost constant concentrations around 26 mM down to 15 cm depth (Fig. 3.8e).

TOC contents display only a slight variability in BGCoZ with values around 0.8% (Fig. 3.9a). Reactive iron shows highest contents of 0.3% at the surface (0.5 cm depth) and decreases with depth (Fig. 3.9b). The down-core variations of phosphorus-bearing fractions are shown in Fig. 3.9c-e. Apatite-bound phosphorus (P-Ap) contents decrease from 220  $\mu\text{mol g}^{-1}$  in the surface layer to 150  $\mu\text{mol g}^{-1}$  in 20 cm sediment depth (Fig. 3.9c). Iron- (P-Fe) and iron-aluminum-bound phosphorus (P-FeAl) show similar profiles, with highest contents (42 and 44  $\mu\text{mol g}^{-1}$ ) measured at the surface between (Fig. 3.9d, e). In 14 and 19 cm sediment depth, P-FeAl contents are almost equal to those in the surface sediment layer.

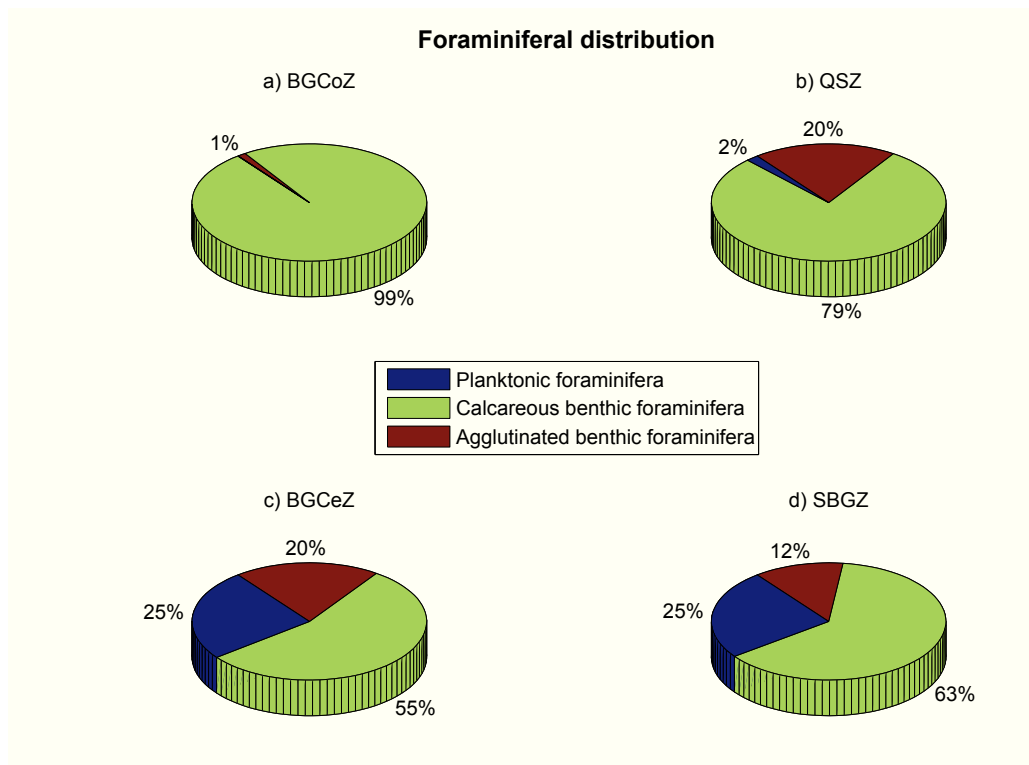


**Figure 3.7:** Foraminiferal distribution in the surface sediments representing the four regional zones as defined in this study.

### 3.3.2 Qiongzhou Strait Zone

The stations located in the vicinity of the Qiongzhou Strait represent the Qiongzhou Strait Zone (QSZ) with a maximum depth between 40 and 65 m. The QSZ water column shows a well-mixed surface layer and a strong thermo-, halo- and pycnocline between 40 m and 65 m depth (Fig. 3.3b). Two different water masses can be distinguished: a very warm ( $>29^{\circ}\text{C}$ ) and haline (31.7-32) upper water mass and a colder ( $24^{\circ}\text{C}$ ) bottom water mass with slightly higher salinity (up to 32.9). The oxygen profile shows a well mixed surface layer with a saturation of around 88% and a sudden and strong decrease to 55% from 40 m depth, below the thermocline, down to 59 m depth (Fig. 3.3b).

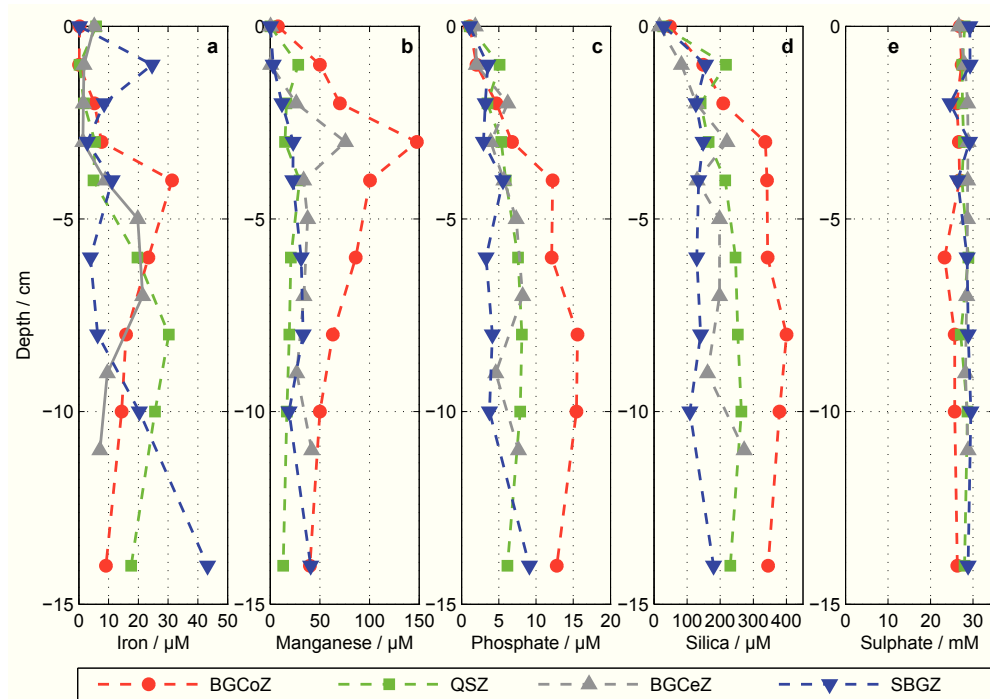


**Figure 3.8:** Pore water downcore profiles of iron (a,  $\mu\text{M}$ ), manganese (b,  $\mu\text{M}$ ), phosphate (c,  $\mu\text{M}$ ), silica (d,  $\mu\text{M}$ ) and sulphate (e, mM) in the four zones. Surface sediments were collected by MUC. Based on measured sodium concentrations, all data were corrected to the salinity of near bottom water.

At a water depth of about 40 m the maximum chlorophyll concentration of  $0.7 \text{ mg m}^{-3}$  is found (Fig. 3.4b). A similar distribution pattern can be seen in the nitrate, phosphate and silicate profiles (Fig. 3.4b). Their maximum concentrations of  $4.7 \mu\text{M}$ ,  $0.4 \mu\text{M}$  and

15  $\mu\text{M}$ , respectively, are located in 40 m depth, coincident with the thermo- and halocline. In the QSZ the vertical distribution of SPM is rather homogeneous in the water column down to 40 m depth (up to 0.3  $\text{mg l}^{-1}$ , Fig. 3.4b). Only in 50-60 m depth the SPM concentration increases slightly up to 2.5  $\text{mg l}^{-1}$  (Fig. 3.4b).

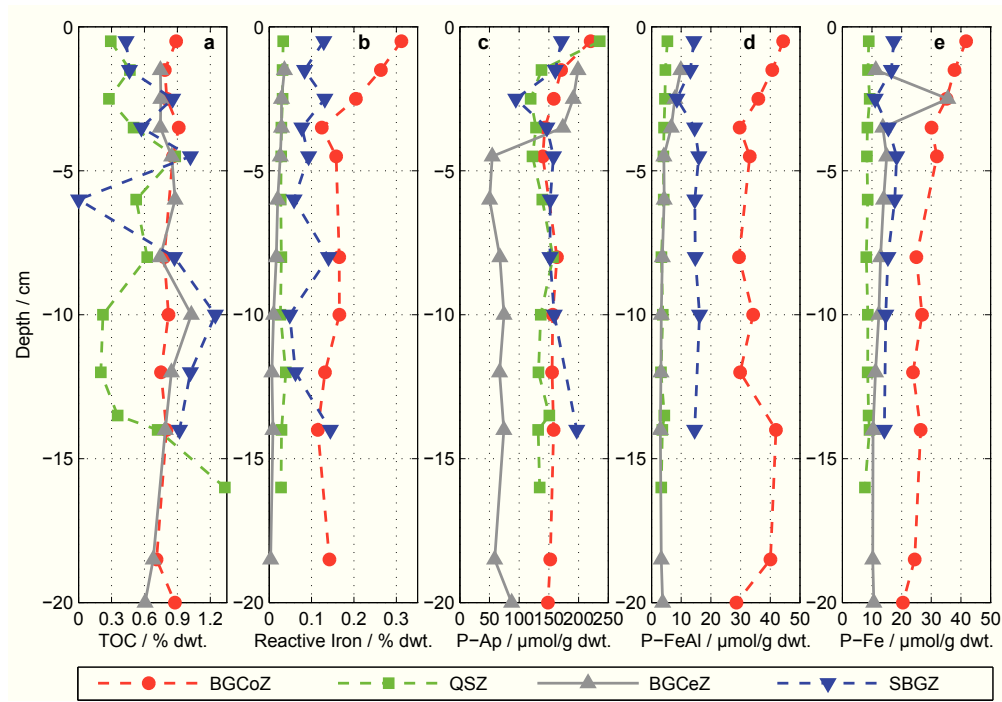


**Figure 3.9:** Down-core variations of total organic carbon (TOC in % dry weight (% dwt.), a), reactive iron (in % dwt., b) and phosphorous-bearing fractions in  $\mu\text{mol g}^{-1}$  dry weight: c) apatite-bound phosphorus (P-Ap), d) iron-aluminum-bound phosphorous (P-FeAl), e) iron-bound phosphorous (P-Fe) in the four zones. Surface sediments were collected by MUC, deeper sediments by GC. An estimated top core loss of about 20 cm was assumed for depth correction of all gravity cores.

The lower sediment layers (14-22 cm) in the QSZ are of dark greenish grey color, calcareous with volcanic debris, clasts of clay (dark yellowish brown), shell debris and foraminifera. These sediments consist of a clay fraction between 11% and 23%, a silt fraction of 34%-52% and a sand fraction of 29%-55% (Fig. 3.5, green dots). The sorting is very poor (4.8 to 5.5) and the mean grain size ranges from 14-85  $\mu\text{m}$  denoting the sediment as consisting primarily of coarse silt. The upper layer sediments (0-14 cm) have a light olive grey color, are not calcareous and include mainly quartz, volcanic



debris and clasts of shells. Sand provides the highest fraction (42%-66%), followed by silt (27%-66%) and clay (6%-15%, Fig. 3.5, green dots). With values between 3.4 and 6.1 the sorting in the upper sediments is very poor as well. The mean grain diameter is between 21 and 118  $\mu\text{m}$  denoting the sediment as fine sand. For the entire sediment core in the QSZ the averaged mean grain size is about 61  $\mu\text{m}$  showing the sediments to be dominated by coarse silt or fine sand.

In QSZ, the CPE amounts to 12.5  $\mu\text{g g}^{-1}$  d.s. with chlorophyll *a* and phaeopigment contents of 2.5  $\mu\text{g g}^{-1}$  d.s. and 10  $\mu\text{g g}^{-1}$  d.s., respectively (Fig. 3.6a). Here the ratio of chlorophyll *a* to phaeopigments ranges between 0.1 and 0.75 (Fig. 3.6b).

The foraminiferal abundance in the QSZ surface sediments is about 2760 shells/10 g sediment of which a proportion of 79% is provided by calcareous benthic foraminifera, the most abundant group in the surface sediment sample (Fig. 3.7b). The proportion of agglutinated foraminifera accounts for 20% of the total assemblage. The dominant species are *Pseudorotalia indopacifica* [Wang *et al.*, 1988], a marine species living in shallow waters from temperate to tropical conditions [Gallagher *et al.*, 2009], and *Eponides* spp. [He and Hu, 2001], an epifaunal species occurring from shelf to abyssal depths [Murray, 1991]. Planktonic foraminifera are sparsely represented with only 2%.

The pore waters of QSZ depict near-surface maxima of dissolved manganese and iron in around 4 and 8 cm sediment depth, respectively (Fig. 3.8a, b). Additionally, slight phosphate and silica maxima are visible in 8-10 cm depth (Fig. 3.8c, d), and sulphate shows almost constant values around 27 mM (Fig. 3.8e). The TOC profile displays strong variations with a minimum (0.2%) in around 12 cm depth and a maximum (1.3%) in 16 cm depth (Fig. 3.9a). In the surface sediments very low contents of reactive iron are measured (Fig. 3.9b). Apatite-bound phosphorus shows a strong near-surface decrease and remains constant at higher depths (Fig. 3.9c). The profiles of P-FeAl and P-Fe contents show nearly no vertical variability and are low, ranging between 3 and 5  $\mu\text{mol g}^{-1}$  and 7-9  $\mu\text{mol g}^{-1}$ , respectively (Fig. 3.9d, e).

### **3.3.3 Beibu Gulf Central Zone**

The Beibu Gulf Central Zone (BGCEZ) is identified by parameters determined at the stations located in the central part of the Beibu Gulf (maximum depth between 54 and 78 m). This zone is characterized by a strong thermo-, halo- and pycnocline in around

45-50 m water depth. With a salinity of about 33.2 at surface and 33.5 at the bottom the BGCEZ is the most haline zone in the Beibu Gulf (Fig. 3.3c). The oxygen saturation remains relatively constant down to 45 m depth with 85-92% followed by a strong decrease to 59% in around 60 m depth. With a concentration of  $0.9 \text{ mg m}^{-3}$ , the chlorophyll maximum is located slightly above the thermo- and halocline (Fig. 3.4c). Below, the chlorophyll concentration decreases to  $0.5 \text{ mg m}^{-3}$  in 60 m depth. The profiles of nitrate, phosphate and silicate show a similar pattern (Fig. 3.4c). Their maxima of  $4.7 \text{ }\mu\text{M}$ ,  $0.4 \text{ }\mu\text{M}$  and  $15 \text{ }\mu\text{M}$ , respectively, are measured at 50 m depth concurrent with the chlorophyll maximum. Beneath the maximum the nutrient concentrations decrease to  $3 \text{ }\mu\text{M}$ ,  $0.1 \text{ }\mu\text{M}$  and  $8 \text{ }\mu\text{M}$ , respectively, at a depth of 60 m. From the surface down to a depth of 20 m SPM concentrations below the detection limit are found (Fig. 3.4c). Furthermore, the SPM distribution shows concentrations ranging between  $0.6$  and  $3.1 \text{ mg l}^{-1}$  from 20 m depth down to the bottom (Fig. 3.4c).

The BGCEZ sediment properties were determined from the 386 cm long GC sediment core 371840. The sediments are of light olive grey or greyish green color, plastic, calcareous and homogeneous, and contain mainly fine to medium sand embeddings, quartz and shell debris. Foraminifera as well as bivalve and snail shells are found between 10 and 169 cm depth. The sediments show a high silt content (77%-84%), less clay (12%-15%) and a slight sand admixture of up to 11% (Fig. 3.5, grey dots). With sorting values of 2-3.2 sediment in the entire core is very poorly sorted. The medium grain size varies between  $6.7$  and  $11 \text{ }\mu\text{m}$  thus showing the sediment to consist, generally, of medium silt.

The CPE content in the BGCEZ surface sediments is about  $9.7 \text{ }\mu\text{g g}^{-1} \text{ d.s.}$  (Fig. 3.6a). The chlorophyll *a* and phaeopigment contents are  $2.3 \text{ }\mu\text{g g}^{-1} \text{ d.s.}$  and  $7.3 \text{ }\mu\text{g g}^{-1} \text{ d.s.}$ , respectively, and the chlorophyll *a* to phaeopigment ratio varies between 0.09 and 0.79 (Fig. 3.6a, b).

The foraminiferal abundance in the surface sediments of BGCEZ amounts to about 1852 shells/10 g sediment. Planktonic foraminifera account for 25% of the assemblage (Fig. 3.7c). As typical for subtropical/tropical regions most of the identified species are thermophilous: *Globigerinella aequilateralis*, *Globigerinoides quadrilobatus*, *Globigerinoides ruber*, *Globigerinoides sacculifer* and *Pulleniatina obliquiloculata*. Furthermore, the fraction of calcareous benthic foraminifera and the fraction of agglutinated foraminifera is about 55% and 20%, respectively. The benthic foraminiferal assemblage is dominated by *Pseudorotalia schroeteriana* [He and Hu, 2001], a neritic, euryhaline

species living in tropical and subtropical regions [Gallagher *et al.*, 2009].

The down-core pore water profile of dissolved iron from BGCEZ reveals a maximum in 7 cm sediment depth (Fig. 3.8a). Dissolved manganese shows highest concentration in 3 cm depth and constant concentrations below (Fig. 3.8b). The phosphate and silica profiles display down core increasing concentrations (Fig. 3.8c, d). Sulphate concentrations are relatively uniform (29 mM, Fig. 3.8e). The sediment TOC profile of BGCEZ evince relatively stable organic carbon contents of around 0.8% (Fig. 3.9a). A very low (about 0.03%) and relatively constant content of reactive iron is found throughout the entire core (Fig. 3.9b). The apatite-bound phosphorus shows a decrease in the upper 5 cm depth and remains uniform down to 20 cm depth (Fig. 3.9c). In case of P-FeAl the measured concentrations are relatively uniform in the entire core (Fig. 3.9d). The profile of P-Fe shows a maximum in 2.5 cm depth and also constant contents further down the core (Fig. 3.9e).

### **3.3.4 Southern Beibu Gulf Zone**

The Southern Beibu Gulf Zone (SBGZ) includes the stations located southwest of the Hainan Island in the transition zone between the Beibu Gulf and the SCS with a maximum depth ranging from 57 to 94 m. The water column in the SBGZ shows no thermocline but a gradually decreasing temperature profile with a difference of around 0.8°C from the surface (28.3°C) to the bottom (27.5°C). Temperature, salinity,  $\sigma_t$  and oxygen profiles are shown in Fig. 3.3d. The salinity distribution shows a gradual increase with depth from 32.4 at the surface to around 33 at the bottom. In case of oxygen saturation the water column is well mixed with a total difference in saturation between surface (89%) and bottom (83%) of only about 6%. In this zone the chlorophyll maximum is found between 40 and 60 m water depth with a concentration of about 0.6 mg m<sup>-3</sup> (Fig. 3.4d). Slightly lower concentrations are found above (0.1-0.5 mg m<sup>-3</sup>) and below (0.2 mg m<sup>-3</sup>) the chlorophyll maximum. Nitrate is sparsely available with values below 0.5 µM up to 70 m depth, then the concentration increases to 1.5 µM in 90 m depth. No phosphate is found down to 70 m depth (Fig. 3.4d). Below that water depth the concentration increases slightly to 0.03 µM. Silicate exhibits a maximum of around 7 µM in 30 m depth, 10 m below the first small chlorophyll peak of 0.5 mg m<sup>-3</sup>. In general, chlorophyll and silicate profiles show opposite patterns (Fig. 3.4d). In SBGZ the verti-

cal SPM distribution shows maximum concentrations of  $6 \text{ mg l}^{-1}$  in 20 m depth and of  $9.7 \text{ mg l}^{-1}$  in 70 m depth (Fig. 3.4d). Furthermore, a minimum of around  $0.7 \text{ mg l}^{-1}$  is found in 50 m depth (Fig. 3.4d).

The deeper sediment layers (7-22 cm) in SBGZ are olive grey, plastic, homogeneous and calcareous with quartz, volcanic debris, isolated shell fragments as well as snail and bivalve shells. Foraminifera and needles of echinoidea are found as well in depths between 10 and 43 cm. The lower sediment layers show a high sand fraction (32%-69%), a silt fraction of 25%-54% and an only slight clay fraction of 6%-14% (Fig. 3.5, blue dots). The sorting is very poor (2-4.6) and the mean grain size ranges between 20 and  $124 \mu\text{m}$  indicating silty sand as the prevalent sediment type. The upper sediment layers (0-7 cm) are light olive grey, soft, homogeneous and calcareous with some shell fragments. In the uppermost 7 cm the sand fraction is highest as well with 32%-63%, followed by silt (32%-56%) and an only slight clay fraction (5%-12%, Fig. 3.5, blue dots). The sorting is very poor (3.9-4.4) and the mean grain diameter ranges between 20 and  $56 \mu\text{m}$  indicating the prevalence of coarse silt. The mean grain size averaged for the entire core is about  $50 \mu\text{m}$  indicative of coarse silt as the predominant sediment type.

In SBGZ the sediment pigment contents are relatively low. The surface sediments show chlorophyll *a* and phaeopigment contents of about  $0.7 \mu\text{g g}^{-1}$  d.s. and  $3.3 \mu\text{g g}^{-1}$  d.s., respectively (Fig. 3.6a). In total the CPE is about  $4 \mu\text{g g}^{-1}$  d.s (Fig. 3.6a). The chlorophyll *a* to paeopigment ratio ranges between 0.17 and 0.23.

According to the foraminiferal analysis the SBGZ shows the highest species abundance with 5632 shells/10 g sediment gulf-wide (Fig. 3.7d). The planktonic foraminifera account for 25% of the assemblage whereas the proportion of agglutinated benthic foraminifera is only 12%. In SBGZ the planktonic species *Neogloboquadrina dutertrei* [Hemleben *et al.*, 1989], a species occurring abundantly in upwelling regions of the tropics [Huang *et al.*, 2003], is found. With a percentage of 63% of the assemblage calcareous benthic foraminifera provide the most abundant group. The dominant species are *Pseudorotalia schroeteriana* [He and Hu, 2001] and *Heterolepa praecineta* [He and Hu, 2001], species occurring from the shelf to the abyssal and preferring cold to temperate conditions [Murray, 2006]. The presence of *H. praecineta* indicates that the SBGZ is influenced by oceanic waters entering from SCS.

The SBGZ sediment pore water dissolved iron concentrations show a first peak in

1 cm depth and increase with depth to about 41  $\mu\text{M}$  (Fig. 3.8a). Also the pore water manganese concentration displays a maximum of about 43  $\mu\text{M}$  in a sediment depth of 14 cm (Fig. 3.8b). The profiles of phosphate and silica display a slight near-surface increase in 1 cm depth (Fig. 3.8c, d). The Phosphate concentrations increase slightly with depth up to 9  $\mu\text{M}$  in 14 cm sediment depth and the silica concentrations vary down-core between 110 and 180  $\mu\text{M}$ . The sulphate concentrations remain almost constant around 29 mM (Fig. 3.8e). The TOC profile displays a high variability with minimum concentrations at detection limit in around 6 cm sediment depth and a maximum in 10 cm depth (1.3%, Fig. 3.9a). Relatively high contents of reactive iron are found showing a high variability between 0.05 and 0.14% (Fig. 3.9b). P-Ap shows a minimum in 2.5 cm sediment depth (94  $\mu\text{mol g}^{-1}$ , Fig. 3.9c) and a subsequent increase up to 200  $\mu\text{mol g}^{-1}$  in 14 cm depth. A slight minimum of 8.5 and 11  $\mu\text{mol g}^{-1}$ , respectively, is also seen for P-FeAl and P-Fe at 2.5 cm depth (Fig. 3.9d, e). Further down the core the contents remain on the same level.

## 3.4 Discussion

### 3.4.1 Hydrographical and biogeochemical differences between the zones

In general, the mean profiles of hydrographical properties (Fig. 3.3a-d) as well as the mean values and standard deviations for temperature, salinity,  $\sigma_t$  and oxygen in the surface and the shallowest bottom layer (Tab. 3.1) point to a higher variability in the BGCoZ and the QSZ in contrast to BGCoZ and SBGZ. Although the surface temperatures show only little variability in all zones with values between 28 and 30°C the zones are affected by different water masses during the sampling period in September/October (Fig. 3.10). The water masses in BGCoZ are similar to the surface layer water mass of QSZ (Fig. 3.10). According to the general cyclonic circulation pattern acting in Beibu Gulf and being mostly driven by the tide-induced year-round westward mean flow through the Qiongzhou Strait [Shi *et al.*, 2002; Chen *et al.*, 2009] (Fig. 3.11) the two zones may be directly affected by water masses transported through the Qiongzhou Strait into the gulf. The reason can be the splitting of the westward current at the western entrance into two branches, especially during NE monsoon con-

ditions, which is indicated by the spatial distribution of model-predicted surface residual currents of *Shi et al.* [2002] and *Chen et al.* [2009] inside the Qiongzhou Strait. One branch passes northwestward and the other one is moving in western and southwestern directions (Fig. 3.11). This assumption is supported by the wind pattern during the cruise which was mainly from northeast to southwest over the Beibu Gulf region as shown by NCEP data (Fig. 3.2) and therefore promotes the westward current pattern. Between August and September the main wind direction changed from prevailing SW monsoon to wintery NE monsoon in northern SCS, thus the cruise took place during the inter-monsoon period with mainly northeasterly winds. The NE monsoon forces a generally southwestward current component across the shallow part of the shelf and thereby drives a sea-level elevation against Hainan Island [Su, 2004] which results in a

**Table 3.1:** Mean values and standard deviations for hydrographical properties in surface and bottom layers of the different zones. The bottom layer is defined as the depth of the shallowest station in one zone.

Zone	Stations	Depth range [m]	Layer	Temperature [°C]	Salinity	$\sigma_t$	Oxygen [mg l <sup>-1</sup> ]
BGCoZ	6	12-43	surface	28.7±0.4	32.1±1.1	20.0±0.8	6.1±0.2
			bottom	28.4±0.3	32.3±0.9	20.3±0.7	5.9±0.3
QSZ	6	40-65	surface	28.6±0.6	31.7±0.4	19.7±0.4	6.2±0.3
			bottom	26.2±1.1	32.4±0.3	21.2±0.5	5.1±0.7
BGCoZ	8	54-78	surface	28.4±0.3	32.9±0.2	20.7±0.2	6.1±0.1
			bottom	24.3±1.5	33.4±0.2	22.6±0.5	5.0±0.6
SBGZ	4	57-94	surface	28.6±0.3	32.6±0.2	20.4±0.2	6.0±0.1
			bottom	27.8±0.2	32.9±0.1	21.2±0.2	5.6±0.1

flow into the Beibu Gulf through the open boundaries. A closer look on the surface water mass of BGCoZ and QSZ during the sampling period in September/October allows to attribute it to water masses from the shelf in the northern SCS which are arranged in bands parallel to the South China coast following the work of *Su and Weng* [1994]. At the surface, BGCoZ and QSZ are influenced by the Coastal Mixed Water Mass, a shallow sea water mass type modified by Pearl River inflow through convectional and turbulent mixing, with temperatures between 28.9 and 30.3°C and salinities of 30.7-

32.9 in August (Fig. 3.11).

As mentioned in the introduction, the Pearl River discharge with a flow rate of about  $316 \text{ km}^3 \text{ yr}^{-1}$  [Wong *et al.*, 2007] can reach the Beibu Gulf through Qiongzhou Strait [Tang *et al.*, 2003]. Such strong freshwater discharges influencing shelf water masses through e.g. turbulent tidal mixing, can result in a lesser haline upper water mass which may be transported from the south and southeast China coastal area through Qiongzhou Strait mainly under favorable wind conditions (NE monsoon) and may influence the QSZ (Fig. 3.11). Hence, for the Beibu Gulf the Qiongzhou Strait provides a very important exchange passage of water masses from SCS northern coastal areas which intensively affect the northern gulf region.

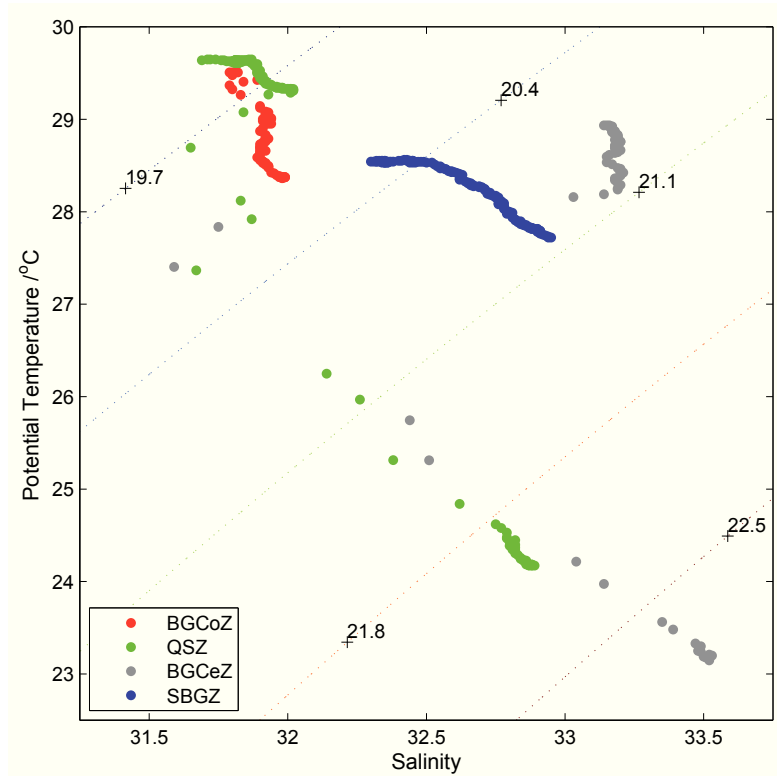


**Figure 3.10:** T/S diagram of the four stations (371640, 371600, 371840 and 371800) representing the zones as defined in this study.

The shallow BGC0Z is defined by high surface temperatures and, in comparison to the other zones, low salinities in the entire, through tides well-mixed water column.

This indicates an influence of terrestrial fresh water originating from rivers at the northern coast of the Beibu Gulf, e.g. Nanliu River with an average annual flow of  $166 \text{ m}^3 \text{ s}^{-1}$  [Dai *et al.*, 2011], and along the west coast of Hainan Island (Fig. 3.11). Such a low salinity zone is already known from the northwestern area of the gulf due to great fresh-water discharges [Chen *et al.*, 2009] from the Red River with a flow rate of  $123 \text{ km}^3 \text{ yr}^{-1}$  [Milliman and Meade, 1983; Wong *et al.*, 2007] (Fig. 3.11). Especially during the rainy season between May and September the riverine inflow is particularly high [Dai *et al.*, 2011].

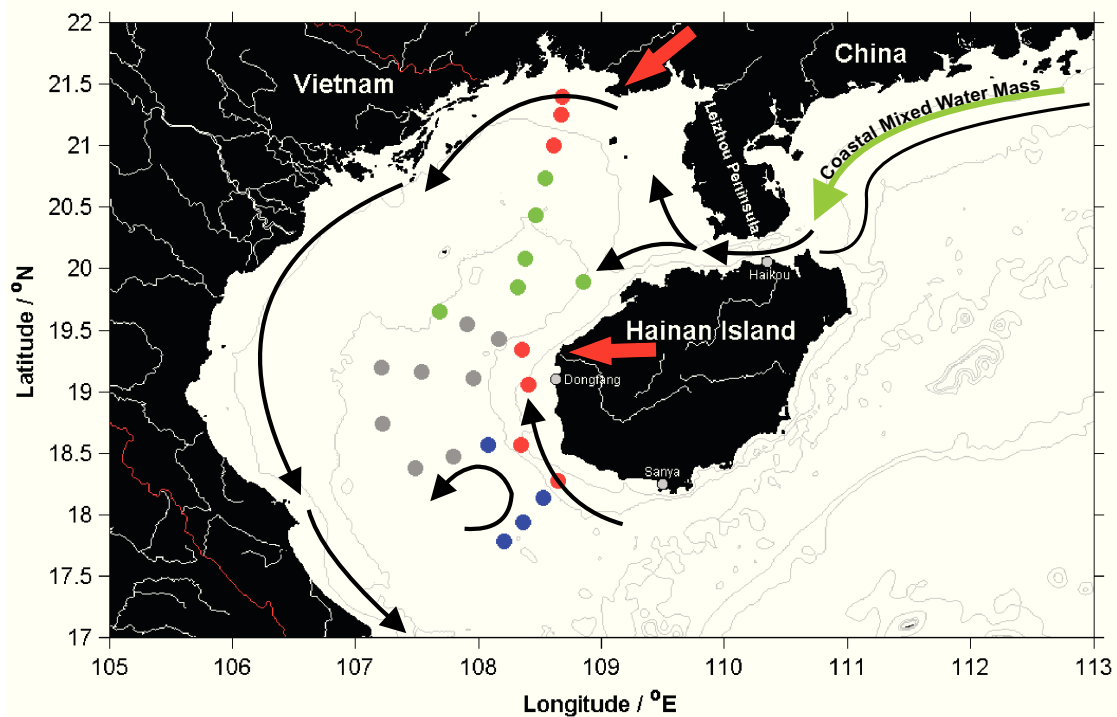


**Figure 3.11:** Proposed current pattern affecting the different zones during the sampling period: general cyclonic circulation with a southward directed flow along the Vietnamese coast and a northward tide-induced residual flow along Hainan Island's west coast. The Coastal Mixed Water Mass (green arrow; Su and Weng [1994]) including Pearl River inflow transported through Qiongzhou Strait and dividing into two current branches influencing BGCoZ and QSZ. The BGCoZ is influenced by river discharge in the north and at the Hainan Island's west coast (red arrows). An inflow of SCS waters and an anticlockwise eddy occur in the southern Beibu Gulf.



The stratified QSZ and BGCEZ are influenced by the same water mass in the deeper layer but different water masses in the upper layers above the thermo- and halocline (Fig. 3.10). In the Beibu Gulf a stratification develops during summer due to sea surface heating whereas the water column is well mixed in winter [Manh and Yanagi, 2000; Tang *et al.*, 2003].

The bottom layer water mass with lower temperature and higher salinity may be tidally transported into the Beibu Gulf from the SCS main basin through the broad opening in the south. Diurnal tidal waves and associated strong tidal currents of up to  $50 \text{ cm s}^{-1}$  propagate northward from the main SCS basin and enter the gulf from the south of Hainan Island [Shi *et al.*, 2002; Hu *et al.*, 2003] (Fig. 3.11). Furthermore, a tide-induced residual flow over the entire water column is stationary in this region and reaches maximum current velocities at the surface of up to  $30 \text{ cm s}^{-1}$  in winter and  $22 \text{ cm s}^{-1}$  in summer [Manh and Yanagi, 2000]. A calculated seasonal variability of residual flow shows that in the bottom layers the currents pass northward along the Hainan Island's west coast into the Beibu Gulf in summer [Manh and Yanagi, 2000] (Fig. 3.11). Consequently, this current re-direction produces a continuous flow of SCS waters into the Beibu Gulf and thereby results in a higher salinity below 30 m water depth in the QSZ and the BGCEZ. The bathymetry, gradually shallowing from the south to the north, may be one reason why the BGCoZ is not affected by this denser bottom water mass.

In comparison to the other zones only the well mixed SBGZ is defined by a completely different water mass. The SBGZ southernmost station (371800) may be under direct influence of SCS waters during sampling period. When the main wind direction changes from SW to NE monsoon in autumn the whole circulation in the Beibu Gulf is affected. As a result the residual flow intensifies in winter, compared to that in summer, and an cyclonic eddy occurs in the lower level (50 m depth) of the southern part of the gulf [Manh and Yanagi, 2000] (Fig. 3.11). This eddy could have developed during the sampling period and, in combination with the stronger residual flow, may result in a turbulent mixing of the water masses and hence a stratification breakdown which apparently already happened in the SBGZ. This situation leads also to the assumption that waters in both QSZ and BGCEZ become mixed when the NE monsoon has been fully developed.

In the Beibu Gulf, winter is the main productive season [Tang *et al.*, 2003] and there-

fore the sampling took place in a period with low primary production. The mean profiles of chlorophyll, nutrients and SPM (Fig. 3.4a-d) and the relatively high standard deviations (Tab. 3.2) in BGCoZ and QSZ indicate a higher variability of water mass properties in these zones compared to BGCEZ and SBGZ during the sampling period.

The highest chlorophyll concentrations are recorded in the BGCoZ. This can be ex-

**Table 3.2:** Mean values and standard deviations for biogeochemical properties in surface and bottom layers as well as maximum concentrations of the mean profile for all parameters in the different zones. The bottom layer is defined as the depth of the shallowest station in one zone.

Zone	Stations	Layer	Chlorophyll [mg m <sup>-3</sup> ]	NO <sub>3</sub> [μM]	PO <sub>4</sub> [μM]	SiO <sub>4</sub> [μM]	SPM [mg l <sup>-1</sup> ]
BGCoZ	6	surface	0.9±0.8	0.4±0.4	0.02±0.02	8.6±2.5	3.1±1.8
		bottom	0.7±0.5	1.2±1.3	0.02±0.02	9.5±3.2	7.6±3.6
	Maximum values (depth/m)		1.0 (7)	1.2 (12)	0.02 (all depths)	9.5 (12)	7.6 (12)
QSZ	6	surface	0.8±0.7	1.1±2.0	0.06±0.1	10.9±3.3	3.5±6.2
		bottom	0.5±0.1	4.4±1.8	0.3±0.2	13.7±4.6	0.9±1.0
	Maximum values (depth/m)		0.9 (20)	4.4 (40)	0.3 (40)	13.7 (40)	3.5 (2)
BGCEZ	8	surface	0.2±0.1	0.3±0.2	0±0.01	6.1±0.8	4.1±2.4
		bottom	0.4±0.2	2.7±0.9	0.2±0.1	10.3±1.6	4.0±1.6
	Maximum values (depth/m)		0.6 (40)	3.1 (50)	0.2 (50)	11.0 (50)	4.1 (50)
SBGZ	4	surface	0.2±0.1	0.2±0.1	0.02±0.04	5.8±1.4	4.0±1.8
		bottom	0.4±0.1	0.7±0.5	0.03±0.04	6.3±1.0	3.1±1.4
	Maximum values (depth/m)		0.6 (30)	0.7 (55)	0.1 (40)	6.3 (55)	4.0 (2)

plained by a high nutrient input into this zone due to riverine inflow which may be an important nutrient source for ecosystems [Su, 2004]. In accordance with the relatively high chlorophyll concentrations the primary production may be enhanced in this area and consequently, due to nutrient uptake by the planktonic organisms, nitrate and phosphate concentrations are depleted. A silicate enrichment observed in the BGCoZ water column also points to the signature of freshwater influx from rivers [Madhupratap

*et al.*, 2003]. Silicates in rivers derive mainly from weathering of silicate minerals along the river course [Gago *et al.*, 2005]. The high silicate concentrations exclude a diatom bloom during the time of the cruise thus indicating other organisms (e.g. dinoflagellates or coccolithophores) being responsible for the high chlorophyll concentrations in the vicinity of the rivers along the coasts of the gulf. The phytoplankton in the area is dominated by freshwater and brackish plankton species, tropical neritic forms are abundant as well [Guo, 1994]. It is also possible that nutrient-rich water masses as well as phytoplankton have been transported from the South China coast east of the Leizhou Peninsula through Qiongzhou Strait in accordance with the previously described circulation patterns. This assumption is corroborated as the QSZ is as well characterized by relatively high chlorophyll and nutrient concentrations in the upper layer. In the QSZ and especially in the BGCEZ the stratification increases chlorophyll concentrations in the vicinity of the thermocline due to increased nutrient concentrations in the deeper layers. The nutricline, the depth in which nitrate reaches concentrations of more than 1  $\mu\text{M}$  for the first time [Fasham *et al.*, 1985], is located in 30-40 m water depth in the BGCEZ, more or less coincident with the thermocline. Due to the stratification the upwelling of nutrients is limited [Tang *et al.*, 2003], therefore, chlorophyll and nutrient concentrations are only enhanced in the vicinity of the thermocline and below. Such a deep chlorophyll maximum is a characteristic feature of seasonally stratified shelf seas and is caused by nutrient pulses into the thermocline through vertical tidally driven mixing processes. The generally low concentrations ( $<1 \mu\text{M}$ ) of dissolved nitrate and phosphate found in the upper layer of BGCEZ and in the entire water column of SBGZ are typical for oligotrophic regions. In all zones dissolved phosphate concentrations are low, therefore phosphorus seems to be the limiting factor for primary production in the surface layer. A calculated N/P molar ratio of 19 in the entire eastern Beibu Gulf, higher than the Redfield ratio of 16, supports the assumption that the Beibu Gulf is phosphorus-limited [Gago *et al.*, 2005].

Enhanced SPM concentrations in the BGCoZ water column point to a strong influence of resuspended sediments. In the Qiongzhou Strait as well as off the west coast of Leizhou Peninsula and Hainan Island, strong tidal currents and thus strong tidal mixing [Tang *et al.*, 2003] lead to sediment resuspension (Fig. 3.1a). Furthermore, sediment resuspension off the southeastern China coast can be transported through Qiongzhou Strait into the gulf, in accordance with the general circulation pattern, and affect the BGCoZ

(Fig. 3.1a). Seasonal differences in water transparency through, e.g. elevated SPM concentrations can limit phytoplankton growth through light limitation [Longhurst, 2007]. Low SPM concentrations in the surface layer and highest concentrations in the bottom layer of QSZ and BGCEZ indicate a tidally driven sediment resuspension at the bottom but exclude an intense sediment transport with currents into these zones from other regions. The tide-driven sediment resuspension can be also responsible for the relatively high chlorophyll concentrations in the bottom layers of QSZ and BGCEZ (the sediment pigment contents will be discussed later). Typhoon KETSANA which passed the study area a few days before the sampling period may have caused the enhanced SPM concentrations in the entire water column of all zones shown in the mean SPM profiles (Fig. 3.4a-d). This strong wind event may induce a strong resuspension of coastal sediments along the coasts of Hainan Island and Leizhou Peninsula as well as the South China east coast which may be transported through Qiongzhou Strait or through the southern boundary into the Beibu Gulf. Moreover, the strong winds may enhance the water mass transport through Qiongzhou Strait and the cyclonic circulation in the gulf. Ekman depth calculations, using the highest wind speeds measured at weather stations on the Hainan Island ( $10.8 \text{ m s}^{-1}$  in Haikou,  $11.8 \text{ m s}^{-1}$  in Dongfang and  $18.5 \text{ m s}^{-1}$  in Sanya), indicate penetration depths for the wind-induced mixing between 79 m in the north and 142 m in the south. This leads to a mixing of the entire water column down to the bottom and thus has the potential to enhance sediment resuspension in all zones. As the Beibu Gulf sediments are fine grained the deposition after the storm takes some time and is therefore substantially slower than the re-stratification of the water column.

### **3.4.2 Differences of sediment characteristics and geochemical properties between the zones**

Mainly two different sediment types are found in the different zones: BGCoZ and BGCEZ are characterized by fine-grained material whereas in QSZ and SBGZ coarser material is deposited. The low variability of the mean grain diameter and clay concentration in the cores collected in the BGCoZ and the BGCEZ indicate a relatively stable depositional environment which allows also fine material to be deposited. The BGCoZ may receive material mainly from rivers entering the Beibu Gulf at the north coast or along Hainan Island's west coasts. In comparison to the Red River, these smaller rivers,

e.g. Nanliu River, provide only a low runoff and thereby the suspended sediments may not be transported far away. Coarse-grained material deposits close to the coast whereas finer sediment fractions are transported into the gulf over longer distances to regions with weaker hydrodynamics and deposit gradually in a 40-50 km wide band along the northern coast of Beibu Gulf and the Hainan Island west coast [Su and Wang, 1994]. For a full tidal cycle (25 h) measured with Aanderaa current meters at station 371600 during the FENDOU 5 cruise a southeasterly directed mean water movement at the surface of  $22.8 \text{ km d}^{-1}$  and at 50 m depth of  $26.8 \text{ km d}^{-1}$  has been calculated. Furthermore, in accordance with the general circulation pattern in the Beibu Gulf and the water masses influencing the BGCoZ as well as the QSZ, the two zones may accumulate fine sediments transported, due to strong tide-induced currents, through the Qiongzhou Strait from the SCS northeastern coastal areas, including sediment load discharged by the Pearl River ( $69 \times 10^6 \text{ t yr}^{-1}$  [Halim, 1991]) as well as material from the Leizhou Peninsula coast. The intensity of river discharges and the transport through Qiongzhou Strait depend on the monsoon season [Tanabe *et al.*, 2003a; Xu *et al.*, 2008]. The large fluctuations of sand proportion in the QSZ sediments indicate a highly dynamic and hence a depositionally unstable environment. Besides material transported through Qiongzhou Strait the QSZ also receives sediments from the Hainan Island north and west coast. The BGCoZ sediments originate mainly from Hainan Island [Xu *et al.*, 2008]. Also here the hydrographical dynamics seem to be weak compared to those in QSZ and SBGZ. The variability in the mean grain size as well as the relatively high proportion of sand in the SBGZ sediment indicates an unstable and dynamic environment present in this zone. As the dynamics are tide-dominated, the sediments may originate mainly from the south and southwest of Hainan Island [Xu *et al.*, 2008]. Otherwise, the changing monsoonal wind system and the resultant changes in circulation patterns may induce material transport from the Vietnamese coast northward into Beibu Gulf [see Manh and Yanagi, 2000], and hence affect the sediments deposited there as well. As sorting is a good indicator for the hydrodynamic forcing these values indicate that the BGCoZ with its moderately sorted sediment is hydrodynamically the calmest zone among all those distinguished. The very poorly sorted sediments in the remaining zones are indicative of depositionally more unstable environments. In addition to tidal currents and river input, strong storms (typhoons), mainly during summer, are also responsible for the sedimentation regime, resuspension and subsequent re-sedimentation, in the Beibu

Gulf.

The sediment pigment contents in the Beibu Gulf remain within the range reported from other Chinese seas (*Liu et al.* [2005], personal communication E. Hua, Ocean University of China, Qingdao). In the QSZ and the SBGZ the surface chlorophyll *a* contents are slightly higher than the contents of the subsurface levels, whereas they are equal in the BGCoZ. Only in BGCoZ the chlorophyll *a* contents in the subsurface are somewhat higher than in the surface layer, which may be taken as evidence of intensive burial of freshly settled plant organic material. The presence of chlorophyll *a* and its contribution to the total plant pigment pool reflects the actual input of fresh plant material, as chlorophyll *a* is very labile and degrades rapidly under aerobic conditions [e.g. *Bianchi et al.*, 2000]. Furthermore, its presence in the subsurface sediments provides evidence of processes, such as bioturbation, leading to organic matter burial in the sediments. In addition, to being buried in the sediment by physical forces or bioturbation, the fresh phytodetritus can be ingested by the benthic fauna [e.g. *Enge et al.*, 2011] and excreted on the sediment surface and beneath it [*Braeckman et al.*, 2011]. The faeces, which can themselves be buried in the sediment, contain degraded plant-derived material the presence of which augments the sedimentary phaeopigment pool [*Shields and Hughes*, 2009]. Also the nature of seafloor sediment itself and its accumulation potential, which in turn is affected by resuspension due to the hydrodynamic regime, are of importance for the distribution of pigments [e.g. *Lund-Hansen et al.*, 1993]. In all zones the phaeopigment contents in the surface sediments are higher than below, which indicates an efficient utilisation of fresh material that has been buried in the subsurface layer. The phytal pigment content in the subsurface sediment is also related to the rate of diagenesis [*Repeta and Gagosian*, 1987; *Sun et al.*, 1993; *Sun and Wakeham*, 1999]. It may be said that the major proportion of the sediment-bound organic material of plant origin is in the degraded form. This is further substantiated by the chlorophyll *a* to phaeopigments ratio in the sediments as a proxy for the "freshness" of the plant material. In all zones, the ratio is below 1 in the surface layer and also in the subsurface layer in BGCoZ, QSZ and SBGZ. Only in BGCoZ the ratio is 1.4. The ratio  $>1$  signifies the prevalence of fresh plant material input over its degradation, and the degree of fresh plant material preservation, whereas the ratio  $<1$  evidences preponderance of *in-situ* degradation of plant material and sedimentation of phytodetritus already degraded in the water column. The sedimentation of plant material is an important means for

transfer organic matter from the water column to the sediments, especially in the BG-CoZ, QSZ and BGCoZ. The distribution of phytal pigments in the Beibu Gulf sediments follows, to some extent, the pattern of water surface productivity. Lowest pigment contents are found in SBGZ, the deepest zone and the one with limited primary production, whereas all other zones differ widely in their pigment contents with high variabilities, especially within the BGCoZ and QSZ, indicated by the high standard deviations. The sediment plant pigment distribution pattern is similar to that emerging from SeaWiFS August 2000 and modelling data for the SCS water surface chlorophyll *a*, presented by *Liu et al.* [2002]. BGCoZ, the region with highest chlorophyll concentrations in the water column, shows the highest signal of "fresh" material supply. In this region, also the material discharge by riverine runoff [e.g. *Bianchi et al.*, 1993] could be a source of plant pigments. The highest accumulation of degraded plant material is found in QSZ probably induced by water masses originating from southern China coastal areas east of Hainan Island, which brought degraded material from a near-shore phytoplankton bloom into the Beibu Gulf. The deposition center in BGCoZ could be affected by tidal currents and therefore a near-bottom transport of pigments from other regions.

The distribution of buried foraminifera shells is influenced by several factors such as water depth, water mass properties (temperature, salinity), nutrient availability, sediment type and currents as transport mechanisms. In general, increased absolute abundance of foraminiferal tests is observed with increasing distance from shore [*Zheng and Fu*, 1994]. Accordingly, the highest abundance of foraminiferal tests is found in the surface sediments of SBGZ (5632 shells/10 g sediment), the lowest in BGCoZ (83 shells/10 g sediment). The low abundance in the BGCoZ is presumably caused by rapid deposition of sediments in the coastal zone diminishing foraminiferal test concentration per amount sediment. In all zones calcareous benthic foraminifera are dominating. The distribution of benthic foraminifera is related to, among others, sediment grain size, bottom water temperature, salinity, organic matter deposition and the current velocity [*Mackensen et al.*, 1990; *Jorissen et al.*, 2007] and is affected by the strong variability of these parameters, especially in shallow waters. The interaction of all these factors is responsible for the distribution of calcareous and agglutinated forms. At that point further investigations are needed. With increasing water depth the ratio of planktonic foraminifera increases from BGCoZ to BGCoZ and SBGZ to up to 25%. One reason is that planktonic foraminifera avoid neritic waters over continental shelves because

they need deep oceanic waters to complete their life cycle [Schmuker, 2000; Kucera, 2007] so that the greatest abundance occurs at the continental slope [Zheng and Fu, 1994]. Additionally, the low abundances of planktonic foraminifera in the BGCoZ can be caused by high turbidity due to the relatively high concentration of SPM in the water column [Schmuker, 2000]. Suspended loads may promote benthic foraminifera which in turn may have a diluting effect on planktonic foraminifera. Distribution and abundance of planktonic foraminifera are strongly linked to current systems and surface-water properties but within the range of normal marine conditions (salinity of 33-36), salinity does not appear to exert any significant influence on them [Hemleben *et al.*, 1989; Zheng and Fu, 1994; Kucera, 2007]. These conditions are only found in the surface waters of BGCoZ, all other zones show lower salinity. Zheng and Fu [1994] described an absence of living planktonic foraminifera in the western Guangdong coastal areas because of coastal currents mixed with river waters and a salinity  $<34$ . Despite that the proportion of planktonic foraminifera reaches 25% also in SBGZ, a zone strongly influenced by the continental shelf water mass and a tide-induced water transport from northwestern SCS to the Beibu Gulf. Therefore, *Neogloboquadrina dutertrei*, a species occurring abundantly in upwelling regions of the tropics and is commonly used to indicate high productivity [Huang *et al.*, 2003] as well as *Globigerina bulloides*, an indicator for high-productivity regimes [Kucera, 2007], are found there. As living organisms as well as their tests can be transported via currents or during storm events away from their ecological optimum [Kucera, 2007] they have probably been transported from SCS into the Beibu Gulf. Particularly in the SCS, the abundance of *Neogloboquadrina dutertrei* generally exceeds 10%.

In general, the investigated surface sediments in the Beibu Gulf are characterized by TOC contents below 1.5%. Besides riverine input, productivity and redox conditions the TOC contents in the top layers depend on the amount of available clay/silt minerals [Keil *et al.*, 1994; Mayer, 1994; Böttcher *et al.*, 2000]. Therefore, TOC contents increase from sandy via silty to clayish sediments.

The down-core compositional changes of the electron acceptors, metabolites as well as the solid phase phosphorus speciation reflect microbial activity in the surface sediments. In typical continental margin sediments, sulphate reduction is the most important final electron acceptor upon anaerobic organic matter decomposition [Jørgensen, 1982; Skyring, 1987; Jørgensen and Kasten, 2006]. Although known from other coastal envi-



ronments (e.g. tidal flats; *Al-Raei et al.* [2009]), dissolved sulphate in the pore waters of the investigated sediments of the Beibu Gulf reflect no significant net sulphate reduction in all zones (Fig. 3.8e). This observation does not exclude near-surface gross sulphate reduction, but may be a further indication for the interaction of dissolved sulphide with ("reactive") metal oxides in the sediments [e.g. *Jørgensen and Kasten*, 2006]. In agreement with this assumption, reactive iron is found in the upper centimeters of the sediments (Fig. 3.9b). Higher contents of reactive iron are found in BGCoZ and SBGZ. Furthermore, the pore water profiles show distinct near-surface maxima of dissolved iron in all zones, and of dissolved manganese in BGCoZ as well as in BGCEZ. These are liberated upon reduction either by heterotrophic bacterial activity or chemically, by the interaction between pore water sulphide and metal oxihydroxides. In QSZ and SBGZ, only slight manganese concentration maxima are found which indicates minor contributions from the reduction of manganese oxides. It has to be remembered that the non-steady state sediment deposition due to re-suspension through tidal forcing or during heavy storms may have lead to the burial of layers enriched in reducible metals. In agreement, changing metal concentrations in the pore waters are partly associated with lithological changes. An elevated accumulation of iron, manganese and metabolites in BGCoZ and BGCEZ occurs due to the presence of medium silty sediments, in comparison to the coarser material in QSZ and SBGZ.

Pore water profiles of phosphate and silica show pronounced near-surface increases in all zones. The accumulation of both, silica and phosphate is caused by the decomposition of diatoms in the surface sediments of the Beibu Gulf. When compared to the expected stoichiometric Si:P ratio of 15:1 for diatom biomass [*Brzezinski*, 1985], the ratio of the liberated concentrations, however, is clearly shifted towards higher silica concentrations (Fig. 3.12). This trend can be explained by further interactions of liberated phosphate with sedimentary iron-oxides or the formation of apatite.

Burial in organic matter, sorption to the surface of iron(III) and aluminum(III) oxyhydroxides, and formation of authigenic minerals are the main routes for P removal from the pelagic part of the ecosystem. The dominant phosphorus sink in the sediments of all zones is apatite-bound phosphorus (Fig. 3.9c), which is a very stable and consequently a long term reservoir. In BGCoZ, QSZ and SBGZ a similar P-Ap concentration level is found while BGCEZ is distinguished by lowest concentrations in depths >4 cm. Highest contents occur in the uppermost sediment layers indicating that most of the apatite

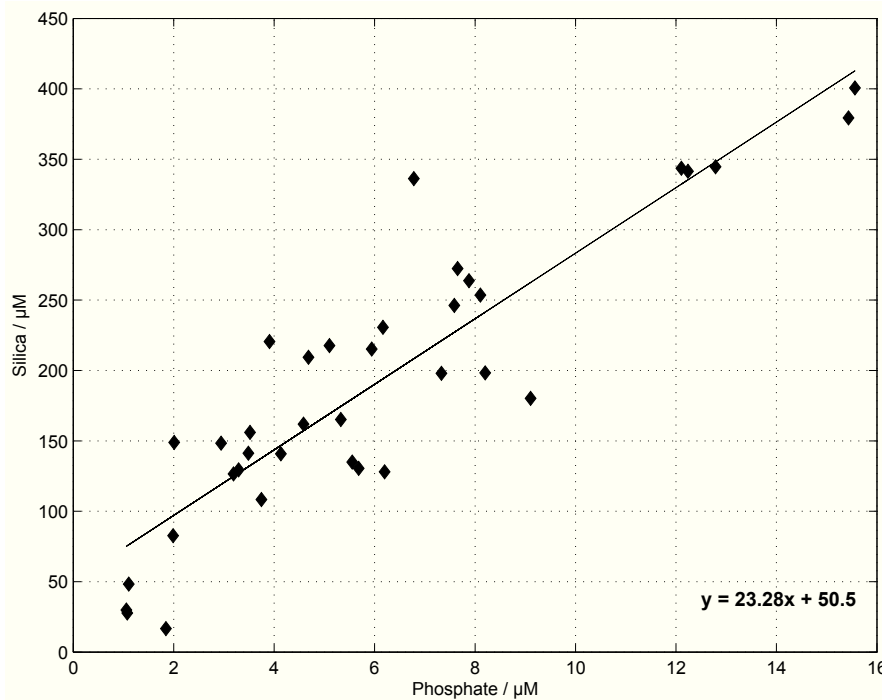


**Figure 3.12:** Covariation of dissolved silica and phosphate in the pore waters of the different zones down to 15 cm sediment depth.

is already formed in the surface sediments by the reaction of liberated phosphate with dissolved calcium and adsorption to carbonate surfaces [Morse, 1986; Ruttenberg and Berner, 1993]. The differences in sedimentary phosphorus speciation and down-core gradients of P-Fe and P-FeAl in the 4 zones indicate that the burial efficiency and the phosphorus retention potential are site-specific. They may depend on different hydrographic conditions and differences in the sedimentology as well as depositional environments and therefore the organic matter contents in the sediments. Highest contents of P-Fe and P-FeAl are found in the surface sediments of BGCoZ (Fig. 3.9d, e), the region with relatively stable depositional conditions, a high influence of river inflow and hence an enhanced primary production.

The reducible pool of iron has to be considered as an important factor for controlling the temporal retention of phosphorus in the sediment and the release rates of dissolved phosphate from the sediment to overlying water [e.g. Anschutz *et al.*, 1998; Jensen and Thamdrup, 1993; Poulton and Raiswell, 2002]. The Iron-bound phosphorus shows a

close correlation with reactive iron trends, which is in agreement with the known close biogeochemical association of phosphorus and iron in near-surface sediments, due to the effective sorption of phosphate by iron(III) oxides [e.g. *Einsele*, 1938; *Hyacinthe and Van Cappellen*, 2004].

### 3.5 Conclusions

Based on hydrographical properties different zones were distinguished in the Beibu Gulf during the sampling period in September/October 2009. The identified zones are mainly influenced by riverine input and tidal mixing in the coastal areas (BGCoZ), water mass transport through Qiongzhou Strait from the southern Chinese coast east of Leizhou Peninsula (BGCoZ and QSZ surface waters) and the influence of SCS waters (bottom water mass of QSZ and BGCoZ as well as SBGZ). Furthermore, the gulf's circulation driven by monsoon winds, tidal currents entering the Beibu Gulf from the south and through Qiongzhou Strait as well as residual water transport through Qiongzhou Strait and the resuspension effect of a typhoon crossing the region during the sampling period influence substantially the biogeochemical properties (chlorophyll, nutrients and SPM) of the water column within the different zones. The shallow BGCoZ and the QSZ show relatively high chlorophyll concentrations and therefore give evidence for enhanced primary production in the entire water column although the sampling took place during low productive season. The grain size, distribution of plant pigments (chlorophyll *a* and phaeopigments) and foraminifera in the surface sediments also reflect the regional hydrodynamic differences and different water masses affecting the zones and, in case of the plant pigments, follow also the pattern of surface water productivity. Additionally, geochemical properties of the sediments depend on the sedimentology, the depositional environment and the organic matter content, and reflect primary production in the water column as well. In the Beibu Gulf, the dominant route of phosphorus removal from the pelagic to the benthic part of the ecosystem is apatite-bound phosphorus.

The first step towards identification of different zones is the understanding of the hydrodynamic variability, deposition patterns associated with it and geochemical processes in the sediments of the Beibu Gulf. Further and more detailed studies are necessary to understand the dynamics in Beibu Gulf and its importance for the SCS.

## 4 Factors affecting the chlorophyll *a* concentration in the central Beibu Gulf, South China Sea

*Bauer & Waniek (2013), Marine Ecology Progress Series: 474, 67-88*

### Abstract

Since in-situ data are sparse a 1D-coupled physical-biological model was used to investigate the complex connection between atmospheric forcing, associated physical water column structure and primary production within the entire seasonal cycle in the central Beibu Gulf for an 11 year period (2000-2010). The results were corroborated by remotely measured SST and surface chlorophyll concentrations in combination with in-situ measurements (temperature and chlorophyll) carried out among others during two German-Chinese cruises FENDOU 5 in September/October 2009 and SONNE in December 2011. Over the 11 year period, 87% of the observed variance in daily SST was captured by the model. The model indicates that the central Beibu Gulf is generally unaffected by water masses from the SCS and the Beibu Gulf coastal regions. Thereby most of the primary production is locally generated. A strong stratification and a DCM develop during summer, vanishing in autumn when the stratification breaks down due to the change from the weak southwest to the stronger northeast monsoon. Deep mixing brings a higher nutrient supply to the surface waters leading to a phytoplankton bloom which lasts on average for about 6 months. Along with the semi-annual wind system change, temporally short, strong wind events affect the primary productivity in the region. Typhoon crossings can enhance the primary production by up to 275% relative to the summer background chlorophyll concentration at the surface according to our modeling results. These events play an important role in primary production and the

corresponding biogeochemical cycling in this oligotrophic region during the summer and the autumn low-productive periods.

### 4.1 Introduction

Primary production and the associated energy transfer into higher trophic levels due to grazing [Ross, 2004], as well as nutrient recycling through biomass sinking and decomposition play a major role in the biogeochemical cycling of oceanic regions [Chen *et al.*, 2003]. For this, phytoplankton is fundamentally important for the functioning of marine ecosystems [e.g. Waniek and Holliday, 2006] and crucial for oceanic carbon fixation which in turn has an impact on the atmospheric carbon dioxide content [Chen *et al.*, 2003].

The growth of phytoplankton depends on the availability of nutrients, incident solar irradiance and grazing pressure and varies regionally through different oceanic conditions [Yoder *et al.*, 1993]. Compared to land-based primary producers phytoplankton are subject to the strong variability of the turbulent marine environment. This means their occurrence, regional distributions and seasonal cycles are determined by physical processes [Ward and Waniek, 2007] such as currents, vertical mixing, particularly through tides generating a near-bottom turbulence and wind-stress creating additional turbulence near the sea surface [Tett *et al.*, 1986], and stratification. As a result phytoplankton always has to cope with rapid vertical attenuation of light [Sharples, 1999] and the limitation of nutrient supply from the deeper waters in stratified regimes.

Tides, wind, solar radiation and their interactions affect motion and mixing of the water column [Dickey, 1988] and lead to the characteristic seasonal cycles in the mixed layer thickness [Williams and Follows, 2003]. From autumn to spring (in the northern hemisphere), a low surface heating and a steady influence of wind and tides lead to the eroding of the seasonal thermocline and hence to a deep mixing. Depending on the water depth, this mixing can even reach the bottom which is common in shallow shelf regions. The deep mixing leads indeed to a high nutrient supply in the euphotic zone which could immediately trigger a phytoplankton bloom. This has been identified as the determinant of the primary production in, for instance, the western part of the Mediterranean Sea [Klein and Coste, 1984]. It is the availability of light which makes the difference in the timing of the phytoplankton bloom between regions in high and those in low latitudes.

Seasonal cycles in subtropical waters show highest surface chlorophyll concentrations during winter, e.g. in the SCS [e.g. *Liu et al.*, 2002], and lowest in summer contrary to polar and subpolar waters [*Howard and Yoder*, 1997] which are dominated by a spring bloom [*Yoder et al.*, 1993], e.g. Northeast Atlantic [*Waniek*, 2003]. Furthermore, depending on the depth of the oceanic region, due to the deep mixing and tidally driven turbulence, phytoplankton may be vertically transported below the euphotic depth and can not conduct photosynthesis anymore [*Lauria et al.*, 1999] (e.g. North Atlantic [cf. *Ward and Waniek*, 2007]). If the influence of solar irradiance overcomes the capacity for tidal mixing in deep regions or regions with low tidal currents, the vertically homogeneous water column can not be maintained anymore and thermally stratifies in spring and summer [*Sharples*, 2008]. Then the algal cells and nutrients are trapped in the surface layer and may induce a spring phytoplankton bloom.

As an important physical barrier, the seasonal thermocline separates the wind-mixed surface layer from the, particularly, tidally-mixed deeper waters [*Ross and Sharples*, 2007] and inhibits the transfer of properties, like nutrients, algal cells and oxygen [e.g. *Klein and Coste*, 1984; *Sharples et al.*, 2001]. Many regions show oligotrophic conditions during the period of vertical stratification [*Varela et al.*, 1992] due to the fast consumption of the only limited available nutrients and the prevented replenishment of those. In those regions, a DCM, which in most studies represents a real maximum in phytoplankton biomass [*Sharples et al.*, 2001], is commonly observed within the thermocline. The DCM is caused by not steady pulses in the strength of the mixing processes bringing nutrients into the thermocline [*Klein and Coste*, 1984; *Sharples and Tett*, 1994] such as periodical tidally-induced motion, surface breaking waves, wind events and internal wave instabilities [*Lauria et al.*, 1999]. These pulses lead to an oscillation of the thermocline supporting a nutrient flux into the surface layer. Due to episodic weakening of the thermocline and consequent nutrient input to the surface waters, the variability in the surface wind stress, especially during storm events like typhoons, also contributes to the formation of the subsurface chlorophyll maximum [*Klein and Coste*, 1984; *Sharples and Tett*, 1994] and are important especially in the subtropical/tropical regions.

To understand the temporal and spatial variability of primary production in marine environments, the connection between primary production and the seasonal variability of the vertical water column stability [*Sharples*, 1999; *Ross*, 2006] needs to be investi-

gated. The timing, strength and duration of the phytoplankton bloom is known to play a fundamental role for growth and survival of organisms of higher trophic levels and hence the functioning of biological communities [e.g. *Ridderinkhof*, 1992; *Waniek and Holliday*, 2006; *Sharples*, 2008]. For the northeast Atlantic meteorological factors (solar heating, wind mixing) have been shown to be responsible for timing and strength of the spring bloom [*Waniek*, 2003].

To investigate the complex connection between atmospheric forcing, associated physical water column structure and the primary production, a continuous and extensive sampling within the respective study area is necessary. In most regions this is impossible, we can, however, use numerical models as tools to explain intermittently observed distributions.

The first aim of this study is therefore to examine the timing of stratification and phytoplankton growth in the Beibu Gulf throughout an annual cycle using a simple 1-dimensional model. Due to a lack of empirical *in-situ* data little is known about the oceanic and biological processes, including spatial and seasonal variation of phytoplankton concentration in this region [*Tang et al.*, 2003], which plays an important role in biogeochemical cycling in the northwestern region of the SCS [*Song*, 2010]. The modeling results are compared to satellite as well as *in-situ* measurements and literature values from all seasons in different years. Since the Beibu Gulf is affected by tidal currents with velocities up to  $0.6 \text{ m s}^{-1}$  [*Manh and Yanagi*, 1997] and occasional typhoon crossings, another two questions arise: 1) What effect does the spring-neap tidal cycle have on the primary production in the Beibu Gulf, especially within the thermocline in relation to the DCM, and 2) to what extent do strong wind events ( $>10 \text{ m s}^{-1}$ ) affect phytoplankton growth? It is known that both forces can contribute to the enhancement of nutrient flux from the deeper into the surface water layers which in turn can cause the development of a phytoplankton bloom [*Williams and Follows*, 2003]. Finally, important factors in generating inter-annual variability in the timing of stratification and the phytoplankton bloom will be discussed.

## 4.2 Material and Methods

### 4.2.1 Study area

The Beibu Gulf, also known as the Gulf of Tonkin, is a hydrodynamically variable region influenced by the Asian monsoon system, tidal currents and occasional typhoon activity. It is a marginal sea of the SCS located within the broad Sunda-Arafura Shelves Province [Longhurst, 2007].

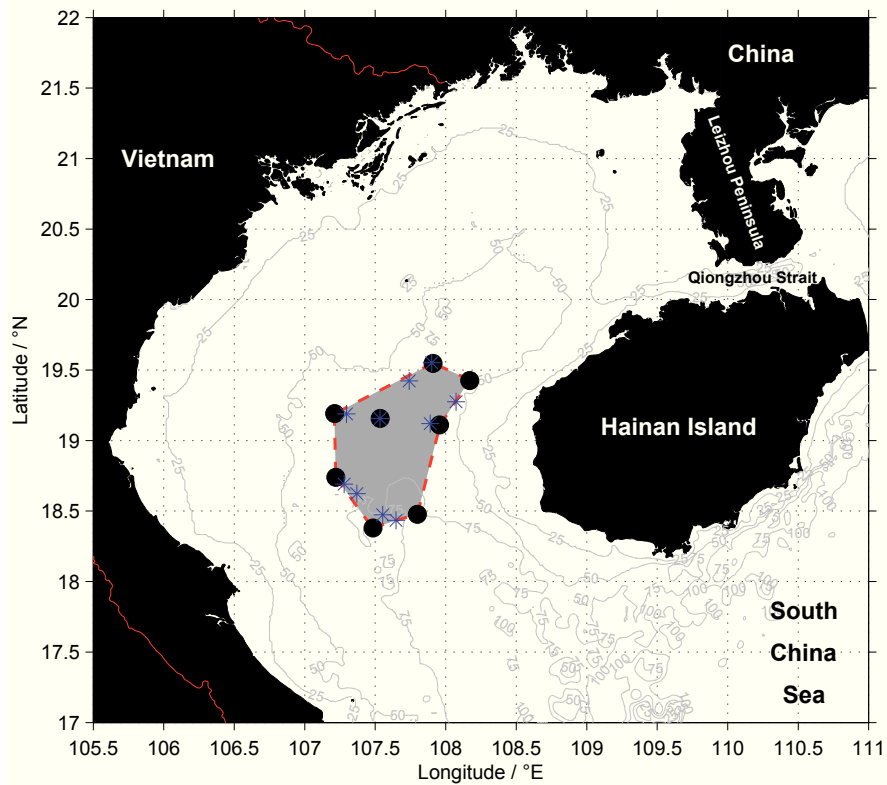


**Figure 4.1:** The study area of the FENDOU 5 cruise in September/October 2009 in the eastern Beibu Gulf. Filled circles indicate sampling stations and the grey area covers the central Beibu Gulf. The blue stars indicate the sampling stations within the central Beibu Gulf of the SONNE cruise in December 2011.

The region is characterized by a large riverine discharge in the north and northwest, a broad opening in the south connecting the gulf with the SCS and the Qiongzhou Strait, a narrow opening to the South China coastal area in the northeast. A year-round west-



ward mean water transport through the Qiongzhou Strait forces a gulf-wide cyclonic circulation pattern in all seasons [Shi *et al.*, 2002; Wu *et al.*, 2008].

In this study we concentrate on the central Beibu Gulf (Fig. 4.1) a region which may only be affected by external water masses to a small degree in comparison to other regions within the gulf [Bauer *et al.*, in press]. Therefore most of the primary production should be locally generated with a small amount being transported through Qiongzhou Strait or from the SCS during strong wind events.

The central Beibu Gulf is an area with a depth between 54 and 78 m and a summer stratification with a strong thermocline between 20 and 50 m depth [Huang *et al.*, 2008; Bauer *et al.*, in press]. Surface chlorophyll-*a* concentrations are low in summer ( $<0.5 \text{ mg m}^{-3}$ ) and show a seasonal peak in winter due to the strong northeast monsoonal winds [Hu *et al.*, 2003; Tang *et al.*, 2003]. Typically for oligotrophic regions only low surface nitrate (up to  $0.5 \text{ }\mu\text{M}$ ) and phosphate (at detection limit) concentrations were found in the central Beibu Gulf with an N:P ratio  $>16$  indicating phosphate limitation [Bauer *et al.*, in press]. Due to the strong stratification in summer, nutrient supply from the deeper nutrient-rich water is limited and enhanced chlorophyll concentrations are located in the vicinity of the thermocline, where sufficient nutrient concentrations and light are available. This DCM lies typically in around 30-50 m depth with a maximum chlorophyll-*a* concentration of about  $0.6\text{-}1 \text{ mg m}^{-3}$  [Huang *et al.*, 2008; Wu *et al.*, 2008; Bauer *et al.*, in press].

### 4.2.2 In situ data for model validation

Observational data were collected during the German-Chinese FENDOU 5 cruise in September/October 2009 and the SONNE cruise in December 2011. Using an IOW mini PUMP CTD system [Strady *et al.*, 2008] depth profiles of hydrographical parameters (temperature, conductivity and oxygen) were recorded at 8 stations within the central Beibu Gulf during FENDOU 5 cruise. For hydrographic profiling and water sampling a Seabird CTD was used during the SONNE 219 cruise. Water samples were taken at different depths during the upcast for chlorophyll and nutrient analysis ( $\text{NO}_2$ ,  $\text{NO}_3$ ,  $\text{PO}_4$  and  $\text{SiO}_4$ ). The samples were low vacuum filtered through  $0.7 \text{ }\mu\text{m}$  Whatman GF/F glass fibre filters, which were pre-combusted for preparing water samples for nutrient analysis, and frozen at around  $-20^\circ\text{C}$ . Extracted chlorophyll samples [JGOFS, 1994]

were analyzed fluorometrically (Turner 10-AU) without correction for phaeopigments. According to standard methods [Hansen and Koroleff, 1999] an autoanalyzer (Evolution III, Alliance Instruments) was used to process nutrient samples (detection limits:  $\text{NO}_2$ :  $0.02 \mu\text{M}$ ,  $\text{NO}_3$ :  $0.05 \mu\text{M}$ ,  $\text{PO}_4$ :  $0.02 \mu\text{M}$ ,  $\text{SiO}_4$ :  $0.1 \mu\text{M}$ ).

Furthermore, in-situ CTD data (temperature) and surface chlorophyll concentrations from August 2009, August 2010 and September 2011 provided by the SCS Branch of the State Oceanic Administration (SOA) and from the WOCE Upper Ocean Thermal (WOCE UOT, 2006, <http://doi.pangaea.de/10.1594/PANGAEA.361180?format=html>) from January 1992 were used for model validation.

### 4.2.3 Simple 1D coupled physical-biological model

To investigate the link between the physical environment, especially stratification and mixing of the water column, and the phytoplankton growth in the central Beibu Gulf a simple 1-D coupled physical-biological model established by Sharples [1999] was used. This model is limited to depths less than 200 m and can be applied to regions from estuaries to the shelf edge [Sharples, 1999]. The physical module of the model simulates daily mean vertical profiles of temperature ( $^{\circ}\text{C}$ ), u-component of currents (zonal,  $\text{m s}^{-1}$ ) and turbulent mixing ( $\text{m}^2 \text{s}^{-1}$ ) with 1 m depth resolution. An oscillating sea surface slope, with two tidal constituents, drives the tidal currents. Only the  $\text{M}_2$  and  $\text{S}_2$  tidal constituents are used because those are mainly responsible for the Spring-Neap tidal cycle [Sharples, 2008]. This allows investigation into the effect of varying kinetic energy levels in the bottom layer caused by the strongest and weakest tidal currents for a semimonthly time period. Meteorological data, daily mean wind u- and v-components (zonal and meridional,  $\text{m s}^{-1}$ ), daily mean dewpoint temperature ( $^{\circ}\text{C}$ ) and daily mean solar irradiance ( $\text{W m}^{-2}$ ), are used by the physical module to calculate heat fluxes across the air-sea boundary and wind-driven momentum flux transmitted into the water column by using a quadratic stress boundary condition at the sea surface [Sharples, 1999]. The daily mean vertical profiles of the PAR ( $\text{W m}^{-2}$ ) are calculated by the model determining the surface PAR as a fraction of the incident solar radiation (Tab. 4.1). PAR is then distributed through the water column by using a vertical absorption coefficient [Sharples, 1999] (Tab. 4.1). As the attenuation coefficient for PAR changes seasonally within each region it has been calculated after Kirk [2011] by using the mean Secchi

depth of 9.2 m determined from all, only sparsely available Secchi depths measured from the FENDOU 5 and SONNE cruises.

The biological component of the model is a simple cell quota, threshold-limitation scheme after *Tett et al.* [1986] simulating vertical profiles of phytoplankton biomass (in mg chlorophyll  $\text{m}^{-3}$ ) and DIN (in  $\text{mmol m}^{-3}$ ). This module has the same vertical (1 m) and temporal (daily) resolution as the physical component. Phytoplankton growth depends on the availability of light, driven by the mean PAR within a model grid depth element [*Sharples*, 1999], and DIN. Both potentially limiting resources lead to respiration if there is insufficient growth due to the light environment or nutrient limitation [*Sharples et al.*, 2006]. A fixed grazing rate that recycles nutrients acts on phytoplankton biomass throughout the year and in addition, remineralized nitrogen diffuses from the seabed. To simulate the behavior of zooplankton feeding when it is energetically favorable, the assumed linear grazing (Tab. 4.1, grazing exponent) is only allowed to take place if the biomass is greater than a threshold value [*Sharples and Tett*, 1994]. This threshold value is set to  $0.16 \text{ mg Chl m}^{-3}$  the lowest remotely measured surface chlorophyll concentration for the central Beibu Gulf in 2009. Phytoplankton biomass and DIN are vertically mixed by turbulence calculated by the physical module. Initialization parameters used for both modules (physical and biological) are summarized in Tab. 4.1.

The maximum depth of the central Beibu Gulf averages 63 m, this was chosen as well as the mean latitude of  $19^\circ\text{N}$ . Current data was only obtained during the spring tide leading to a calculated mean  $M_2$  amplitude of  $0.6 \text{ m s}^{-1}$ . For the neap tide a lowering of this amplitude is expected which would lead to a lower mean  $M_2$  amplitude. Therefore, for all model runs the  $M_2$  amplitude was set to the mean value of  $0.15 \text{ m s}^{-1}$ , containing several tidal cycles, estimated from *Manh and Yanagi* [1997] as well as *Zu et al.* [2008] for the central Beibu Gulf. Published tidal ellipse polarisations for the Beibu Gulf are conflicting [e.g. *Manh and Yanagi*, 1997; *Zu et al.*, 2008]. For this reason, the tidal cycles recorded during the FENDOU 5 cruise at different depths were used to define the tidal ellipse polarisation as a degenerated one. The mean  $S_2$  tidal amplitude (0.98) which is expressed as a fraction of  $M_2$  is calculated from the predictions provided by harmonic analysis for the current records [*Emery and Thomson*, 2001]. Changing the mean  $S_2$  tidal amplitude did not show any significant effect in the model output. As a result of the  $S_2$  tidal amplitude activation from 0 to 1, a cooling of about 0.2% in the

**Table 4.1:** Initialisation parameters for the model runs used in the physical and biological module of the model.

Parameter [unit]	Value	Reference
<b>Physical module</b>		
Depth [m]	63	
Maximum eddy viscosity and diffusivity [ $\text{m}^2 \text{s}^{-1}$ ]	0.1	<i>Sharples</i> [1999]
Bottom quadratic drag coefficient	$3.0 \times 10^{-3}$	<i>Sharples</i> [1999]
Latitude [ $^{\circ}\text{N}$ ]	19	
Background viscosity and diffusivity [ $\text{m}^2 \text{s}^{-1}$ ]	$1.0 \times 10^{-5}$	<i>Sharples</i> [1999]
Amplitude of $M_2$ tidal current [ $\text{m s}^{-1}$ ]	0.15	<i>Zu et al.</i> [2008] <i>Manh and Yanagi</i> [1997]
$S_2$ tidal amplitude (as fraction of $M_2$ )	0.98	this study
Light attenuation coefficient [ $\text{m}^{-1}$ ]	0.1	<i>Kirk</i> [2011]
Heat shading coefficient [ $\text{m}^2 (\text{mg chl})^{-1}$ ]	0.012	<i>Sharples</i> [1999]
Initial homogeneous temperature [ $^{\circ}\text{C}$ ]	24.41	Satellite SST
Fraction of solar radiation that is PAR	0.45	<i>Sharples</i> [1999]
Attenuation coefficient for PAR [ $\text{m}^{-1}$ ]	0.15	this study
Pigment absorption cross section [ $\text{m}^2 (\text{mg chl})^{-1}$ ]	0.012	<i>Sharples</i> [1999]
Max near bed DIN concentration [ $\text{mmol DIN m}^{-3}$ ]	2.12	this study
Benthic nutrient input rate [ $\text{s}^{-1}$ ]	$2.3 \times 10^{-7}$	<i>Sharples</i> [1999]
<b>Biological module</b>		
Subsistence quota [ $\text{mmol N (mg chl)}^{-1}$ ]	0.2	<i>Sharples</i> [1999]
Max quantum yield [ $\text{mg C (mg chl)}^{-1} \text{day}^{-1} (\text{W m}^{-2})^{-1}$ ]	4.1	<i>Sharples</i> [1999]
Cell chl:carbon ratio [ $\text{mg chl (mg C)}^{-1}$ ]	0.02	<i>Sharples</i> [1999]
Max cell quota [ $\text{mmol N (mg chl)}^{-1}$ ]	1.0	<i>Sharples</i> [1999]
Recycled proportion of grazed nutrients	0.5	e.g. <i>Tett et al.</i> [1981] <i>Sharples</i> [1999] <i>Ross and Sharples</i> [2008]
Max specific growth rate [ $\text{day}^{-1}$ ]	1.2	<i>Sharples</i> [1999]
Max nutrient uptake rate [ $\text{mmol DIN (mg chl)}^{-1} \text{day}^{-1}$ ]	2.0	<i>Sharples</i> [1999]
Nutrient concentration for half max uptake [ $\text{mmol DIN m}^{-3}$ ]	0.5	e.g. <i>Waniek</i> [2003] <i>Sharples et al.</i> [2006] <i>Waniek and Holliday</i> [2006]
Grazing threshold limit [ $\text{mg chl m}^{-3}$ ]	0.16	this study
Respiration rate [ $\text{mg C (mg chl)}^{-1} \text{day}^{-1}$ ]	3.5	<i>Sharples</i> [1999]
Grazing rate [fraction standing stock $\text{day}^{-1}$ ]	0.12	e.g. <i>Sharples and Tett</i> [1994] <i>Sharples</i> [1999] <i>Sharples et al.</i> [2006]
Grazing exponent	1.0	<i>Sharples</i> [1999]
Limiting nitrate concentration [ $\text{mmol DIN m}^{-3}$ ]	0.32	this study

upper 49 m of the water column and a warming of about 0.9% in the bottom waters was produced.

The initial homogeneous temperature is taken from remotely measured SST (see subsection "Meteorological and comparative satellite data") at December 31<sup>st</sup> from the previous year, taking into account that the central Beibu Gulf is well-mixed in winter (Tab. 4.2). The maximum near bed DIN concentration is estimated from the zonally

averaged bottom nitrate concentrations measured during the FENDOU 5 cruise. The parameters in the initial phytoplankton file describe a simple, neutrally buoyant phytoplankton species [Sharples, 1999]. Within the model only DIN is used as nutrient but based on our measurements the Beibu Gulf seems to be phosphate limited [Bauer *et al.*, in press]. In general, phytoplankton assimilates phosphate whenever available and accumulates it within the cells allowing ongoing growing during poor living conditions (personal communication M. Nausch, Leibniz-Institute for Baltic Sea Research). To include non-modeled phosphate the phosphate detection limit of  $0.02 \mu\text{M}$  was used to calculate the corresponding nitrate concentration using the Redfield ratio. The calculated limiting nitrate concentration of  $0.32 \text{ mmol DIN m}^{-3}$  is equivalent to the  $0.3 \text{ mmol DIN m}^{-3}$  external concentration on which phytoplankton is generally capable to take up DIN actively [Reynolds, 2006].

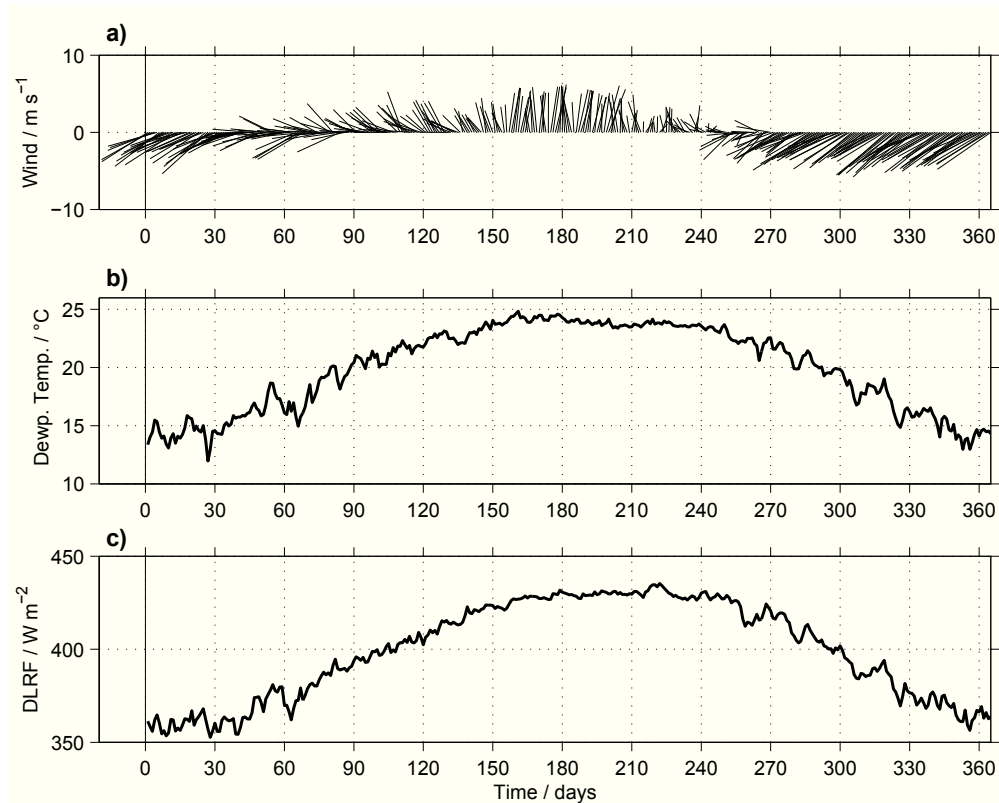


**Figure 4.2:** Mean meteorological forcing for a time period of 11 years (2000-2010): (a) wind velocity ( $\text{m s}^{-1}$ ), (b) dewpoint temperature ( $^{\circ}\text{C}$ ), (c) solar irradiance as downward longwave radiation flux (DLRF in  $\text{W m}^{-2}$ ).

### 4.2.4 Meteorological and comparative satellite data

The model is forced with daily surface u- and v-components of wind, dewpoint temperature, calculated after *Wanielista et al.* [1997] using air temperature and relative humidity, and downward longwave radiation flux all taken from NCEP obtained at <http://www.esrl.noaa.gov> for 11 years (2000-2010, Fig. 4.2, Fig. S1a-c in the supplement). As the spatial resolution of the NCEP Reanalysis data set is  $2.5^{\circ} \times 2.5^{\circ}$  [Kalnay *et al.*, 1996], the Beibu Gulf area has been cubically interpolated to a resolution of  $0.1^{\circ} \times 0.1^{\circ}$ . The interpolated meteorological data were averaged for the entire area in the central Beibu Gulf to force the model ( $18.3\text{--}19.6^{\circ}\text{N}$   $107.2\text{--}108.2^{\circ}\text{E}$ , Fig. 4.1).

Comparative satellite data for daily SST were taken from <http://www.remss.com> (TMI SST), resolution  $0.25^{\circ} \times 0.25^{\circ}$ ) and used for the comparison with the predicted SST. To compare the modeled primary production monthly SeaWiFS (2000-2010) and MODIS (07/2002-2010) surface chlorophyll concentrations from <http://gdata1.sci.gsfc.nasa.gov> were used and averaged between 07/2002 and 2010 because of gaps in both data sets. The satellite data were averaged for the entire central Beibu Gulf region as well.

## 4.3 Results

All model simulations for the years 2000 to 2010 started at the same initial conditions for the physical and biological module (Tab. 4.1). The only differences were in the meteorological forcing and in the initial homogeneous temperature which was taken from satellite SST for the previous year on December 31<sup>st</sup> (Tab. 4.2). A comparison of a three years run using meteorological data from 2009 shows a similar vertical temperature distribution for each year, indicating stability of the numerical scheme. Despite that, an initial leg of one year was introduced to allow a better adaptation of the biological components.

**Table 4.2:** Relevant forcing parameters and calculated values for the modeled mean year and the years 2000 to 2010: Initial temperature (T), mean, minimum (Min) and maximum (Max) values of meteorological forcing: wind velocity ( $\text{m s}^{-1}$ ), solar irradiation as downward longwave radiation flux (DLRF in  $\text{W m}^{-2}$ ) and dewpoint temperature (dT in  $^{\circ}\text{C}$ ), modeled surface and bottom temperature ( $T_{sfc}$  and  $T_{bot}$  in  $^{\circ}\text{C}$ ) as well as modeled surface chlorophyll concentration ( $\text{Chl}_{sfc}$  and annual integrated surface biomass concentration (Annual  $\text{Chl}_{sfc}$ ) in  $\text{mg m}^{-3}$ ), start and termination of stratification (strat) and phytoplankton bloom (both day in year). For all mean values the standard deviation is given as well. Besides the modeled mean year the bloom length (days) relates to the phytoplankton bloom between two years. Values are inscribed in the respective second year.

Parameter	Mean	2000	2001	2002	2003	2004	2005	2006	2007	2008	2009	2010
<b>Initial T</b>	23.82	22.29	23.85	23.30	24.26	23.76	24.22	23.38	24.29	23.81	24.41	24.48
<b>Mean Wind</b>	6.5 $\pm$ 1.3	6.3 $\pm$ 3.1	6.4 $\pm$ 2.8	6.5 $\pm$ 3.0	6.4 $\pm$ 2.4	6.0 $\pm$ 2.4	6.8 $\pm$ 2.7	6.5 $\pm$ 2.6	6.9 $\pm$ 2.8	7.0 $\pm$ 2.8	6.3 $\pm$ 2.8	6.9 $\pm$ 2.9
<b>Min Wind</b>	3.7	0.2	0.03	1.1	0.4	0.5	0.2	0.6	0.3	0.2	0.1	0.7
<b>Max Wind</b>	9.9	16.4	16.5	38.9	13.4	13.7	16.9	15.4	18.1	16.7	17.5	15.5
<b>Mean DLRF</b>	399 $\pm$ 26	400 $\pm$ 28	403 $\pm$ 27	401 $\pm$ 26	400 $\pm$ 29	395 $\pm$ 29	400 $\pm$ 28	400 $\pm$ 28	397 $\pm$ 30	395 $\pm$ 32	398 $\pm$ 31	403 $\pm$ 27
<b>Min DLRF</b>	353	312	328	334	314	315	319	324	301	297	305	339
<b>Max DLRF</b>	435	446	446	440	445	448	445	442	439	440	449	442
<b>Mean dT</b>	19.9 $\pm$ 3.6	19.8 $\pm$ 4.3	20.1 $\pm$ 3.8	19.7 $\pm$ 4.0	19.7 $\pm$ 4.1	19.8 $\pm$ 4.2	19.9 $\pm$ 4.7	20.0 $\pm$ 4.4	20.0 $\pm$ 4.2	19.8 $\pm$ 4.7	20.0 $\pm$ 4.0	20.5 $\pm$ 4.0
<b>Min dT</b>	12.0	6.3	9.7	4.2	7.4	6.8	4.2	4.7	6.0	4.9	8.0	6.6
<b>Max dT</b>	24.8	26.3	26.0	26.5	27.2	28.4	27.0	26.2	27.3	26.9	27.3	27.6
<b>Mean <math>T_{sfc}</math></b>	28.6 $\pm$ 4.0	26.3 $\pm$ 3.7	26.9 $\pm$ 3.6	26.4 $\pm$ 3.2	26.6 $\pm$ 3.6	27.0 $\pm$ 3.7	26.2 $\pm$ 3.6	26.8 $\pm$ 3.6	26.2 $\pm$ 3.6	25.8 $\pm$ 4.2	26.7 $\pm$ 3.7	26.7 $\pm$ 3.2
<b>Min <math>T_{sfc}</math></b>	22.5	20.1	21.3	20.9	20.4	20.4	19.5	20.8	20.2	17.8	20.8	21.8
<b>Max <math>T_{sfc}</math></b>	35.0	32.3	33.2	31.5	32.4	33.5	31.8	32.0	31.5	32.5	32.6	32.1
<b>Mean <math>T_{bot}</math></b>	23.6 $\pm$ 0.8	21.2 $\pm$ 0.8	22.5 $\pm$ 0.8	22.4 $\pm$ 1.3	21.8 $\pm$ 0.9	21.7 $\pm$ 0.9	21.0 $\pm$ 1.2	22.0 $\pm$ 0.9	21.5 $\pm$ 1.0	19.3 $\pm$ 1.1	22.0 $\pm$ 0.9	23.1 $\pm$ 0.9
<b>Min <math>T_{bot}</math></b>	22.5	20.1	21.3	20.9	20.5	20.5	19.5	20.8	20.2	17.8	20.8	21.8
<b>Max <math>T_{bot}</math></b>	25.2	23.4	24.3	25.4	24.1	23.7	23.9	23.9	24.4	21.9	24.2	25.0
<b>Mean <math>\text{Chl}_{sfc}</math></b>	0.6 $\pm$ 0.7	0.8 $\pm$ 0.7	0.8 $\pm$ 0.8	0.9 $\pm$ 0.9	0.6 $\pm$ 0.6	0.6 $\pm$ 0.7	0.7 $\pm$ 0.6	0.7 $\pm$ 0.7	0.7 $\pm$ 0.7	0.7 $\pm$ 0.7	0.7 $\pm$ 0.7	0.9 $\pm$ 0.8
<b>Min <math>\text{Chl}_{sfc}</math></b>	0.16	0.16	0.16	0.16	0.16	0.16	0.16	0.16	0.16	0.16	0.16	0.16
<b>Max <math>\text{Chl}_{sfc}</math></b>	2.3	2.5	2.4	2.7	2.3	2.4	2.4	2.3	2.3	2.3	2.4	2.5
<b>Annual <math>\text{Chl}_{sfc}</math></b>	234	273	295	326	217	228	236	262	260	240	251	317
<b>Start strat</b>	38	64	73	35	18	44	18	64	31	52	31	52
<b>End bloom</b>	88	120	127	97	99	106	102	120	123	103	119	119
<b>End strat</b>	330	319	318	265	329	343	324	336	315	342	321	305
<b>Start bloom</b>	285	285	278	260	275	295	256	266	274	273	267	273
<b>Bloom length</b>	169		207	184	204	196	172	229	222	194	211	217

### 4.3.1 Mean annual cycle

In order to investigate the effect of the meteorological forcing a mean annual cycle was modeled using the mean meteorological forcing calculated as the average over the years 2000-2010 (Fig. 4.2 and Fig. 4.3). The analysis of the model results focuses on the annual cycle of physical factors, e.g. vertical temperature distribution, mixed layer depth (MLD, depth where the difference of 0.5°C between SST and temperature at the depth is reached), euphotic depth (1% of the surface PAR) and biological properties, e.g. chlorophyll distribution representing primary production. The mean modeled temperature distribution for 2000-2010 for the entire water column down to the mean depth of 63 m for the central Beibu Gulf shows a surface heating in summer with an associated stratification and a winter deep mixing (Fig. 4.3a). The stratification establishes on average in spring around day 38 and exists until end of November (day 330, Fig. 4.3a, b). The beginning of stratification is defined as the first day in spring when surface and bottom temperatures are not equal anymore whereas the end of stratification is defined as the first day in autumn when both temperatures are equal again (Fig. 4.3b). During summer the MLD persists on average in about 18 m depth and shows a deepening during winter (January and December) due to strong vertical mixing (Fig. 4.3a).

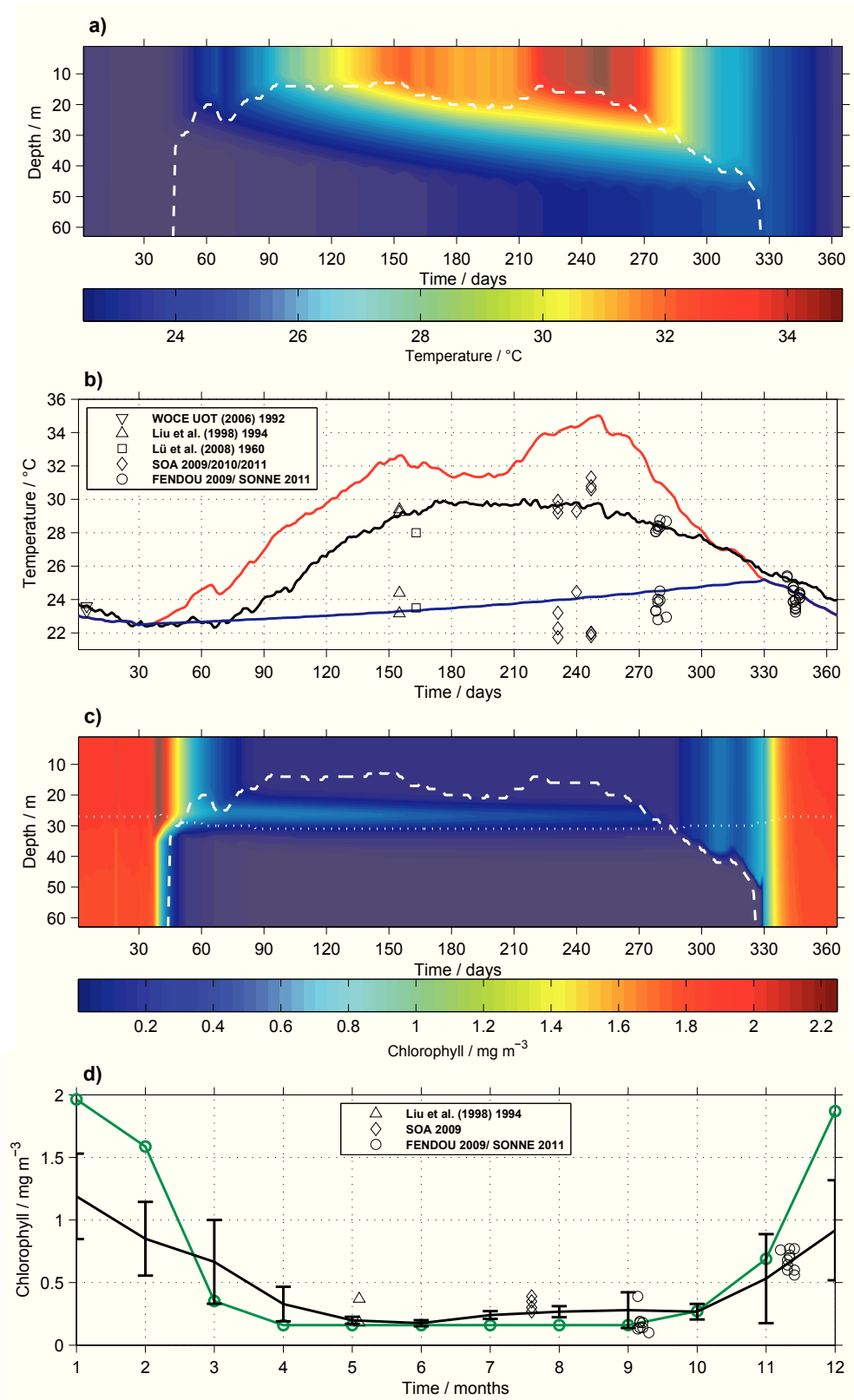
To validate the model predictions simulated mean daily SST is compared to satellite derived SST which is averaged over the 11 years period (2000-2010) and in-situ

---

**Figure 4.3 (following page):** Simulated mean annual cycle using mean meteorological forcing for a time period of 11 years (2000-2010) in the central Beibu Gulf: (a) Temperature (°C) distribution over the entire water column. The white dashed line indicates the calculated MLD. (b) Simulated daily mean SST (°C, red line) in comparison to remotely measured SST (°C, black line) averaged over the 11 years and in-situ observations (symbols). The blue line represents the modeled daily mean bottom temperature (°C) and the respective observations (symbols). (c) Chlorophyll ( $\text{mg m}^{-3}$ ) distribution over the entire water column. The white dashed line indicates the calculated MLD, the white dotted line indicates the euphotic depth (1% of surface PAR). (d) Simulated monthly mean sea surface chlorophyll concentrations ( $\text{mg m}^{-3}$ , green line) in comparison to satellite derived monthly mean surface chlorophyll concentrations ( $\text{mg m}^{-3}$ , black line). The sources for the values indicated by the black symbols are given in the legend. The black bars indicate the standard deviations of the remotely measured chlorophyll concentrations.



Chapter 4: Factors affecting chlorophyll *a* concentration



data (Fig. 4.3b). The model simulates correctly the annual cycle of temperature rising during spring and summer and its decreasing in autumn and winter due to reduced solar irradiance (Fig. 4.3b). Modeled and satellite derived SST agree considerably well during winter but deviate from each other during summer. The model overestimates the SST by up to 5.3°C in late summer. In winter the modeled SST is slightly lower than the remotely measured by up to 1.1°C. Higher temperatures during summer, especially in late summer, may result from the functional principle of the 1-dimensional model as always the same water body is heated. Lateral transport as well as a cloud cover factor are not taken into account by the model. In the mean run due to averaging, wind peaks, normally responsible for a surface temperature cooling by mixing processes, were smoothed which results in higher surface temperatures as well. As a result the higher dewpoint temperature and solar radiation in summer lead to an increasing SST. Using mean solar irradiance, mean dewpoint temperature but realistic wind from 2009 reduces the temperature difference between modeled and remotely measured SST in the period of highest variation, caused by highest typhoon activity, in late summer and autumn between days 207 and 287 by up to 5.5°C. The strong winds in this period decrease SST on average by  $2.4 \pm 1^\circ\text{C}$ . Observed winter surface and bottom temperature data from the SONNE cruise and the WOCE UOT (2006) at stations within the central Beibu Gulf corroborate the model results (Fig. 4.3b). Also the bottom temperature data from the FENDOU 5 cruise as well as published bottom temperatures of *Liu et al.* [1998] and *Lü et al.* [2008] agree well with the model results (Fig. 4.3b). In summer and autumn the in-situ SST values corroborate the satellite data but not the SST of the mean year. The modeled SSTs are remarkably consistent with the remotely measured SSTs over the 11 year period studied. The model captured 87% of the observed variance in daily surface temperatures (Fig. 4.4). In winter the modeled SSTs are slightly too low, in summer slightly too high. The modeled chlorophyll distribution shows an annual cycle with a productive season during winter time due to the deep mixing and the formation of a DCM during summer because of the strong stratification and the nutrient depletion in the surface water layer (Fig. 4.3c). The DCM establishes in March when the MLD reaches 20 m depth and the stratification begins to develop (Fig. 4.3c). During summer the DCM is located in around 26 m depth, somewhat shallower than the euphotic depth (31 m). Due to the strong vertical mixing during January and December the phytoplankton bloom signal is transported down to the bottom below

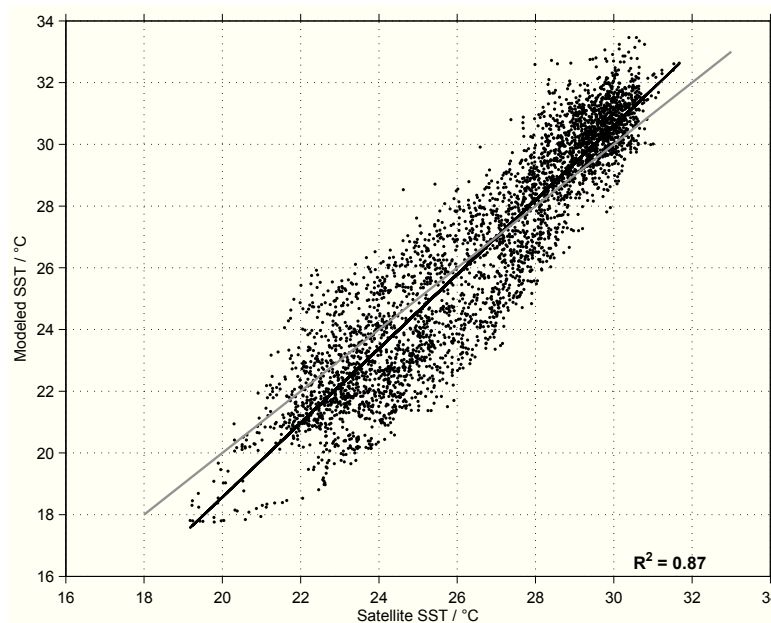


**Figure 4.4:** Correlation between model and satellite data of all daily SST for the period 2000 to 2010. The grey line indicates the regression line with a slope of 1.

the euphotic depth which is permanently located in around 25-31 m depth (Fig. 4.3c). During summer the monthly mean surface chlorophyll concentrations of about 0.1 to 0.2 mg m<sup>-3</sup> are captured very well by the model compared to the satellite derived concentrations averaged for the 11-years period and in-situ measurements (Fig. 4.3d). The decrease of surface chlorophyll concentration in spring (February and March) and the increase in autumn and winter (October to December) are also well modeled but with differences of up to 0.8 mg m<sup>-3</sup>. In January and February as well as November and December higher chlorophyll concentrations were modeled than measured by satellites. On the other hand slightly lower concentrations were modeled for March and April as well as July to September. The standard deviations represent the interannual variability of satellite monthly surface chlorophyll concentrations (Fig. 4.3d). From January to March and from November to December highest standard deviations were calculated for the remotely measured chlorophyll concentrations indicating that highest interannual variability occurs during winter.

Vertical depth profiles of temperature, chlorophyll and DIN from different cruises during summer/autumn corroborate the model results averaged over the summerly strat-

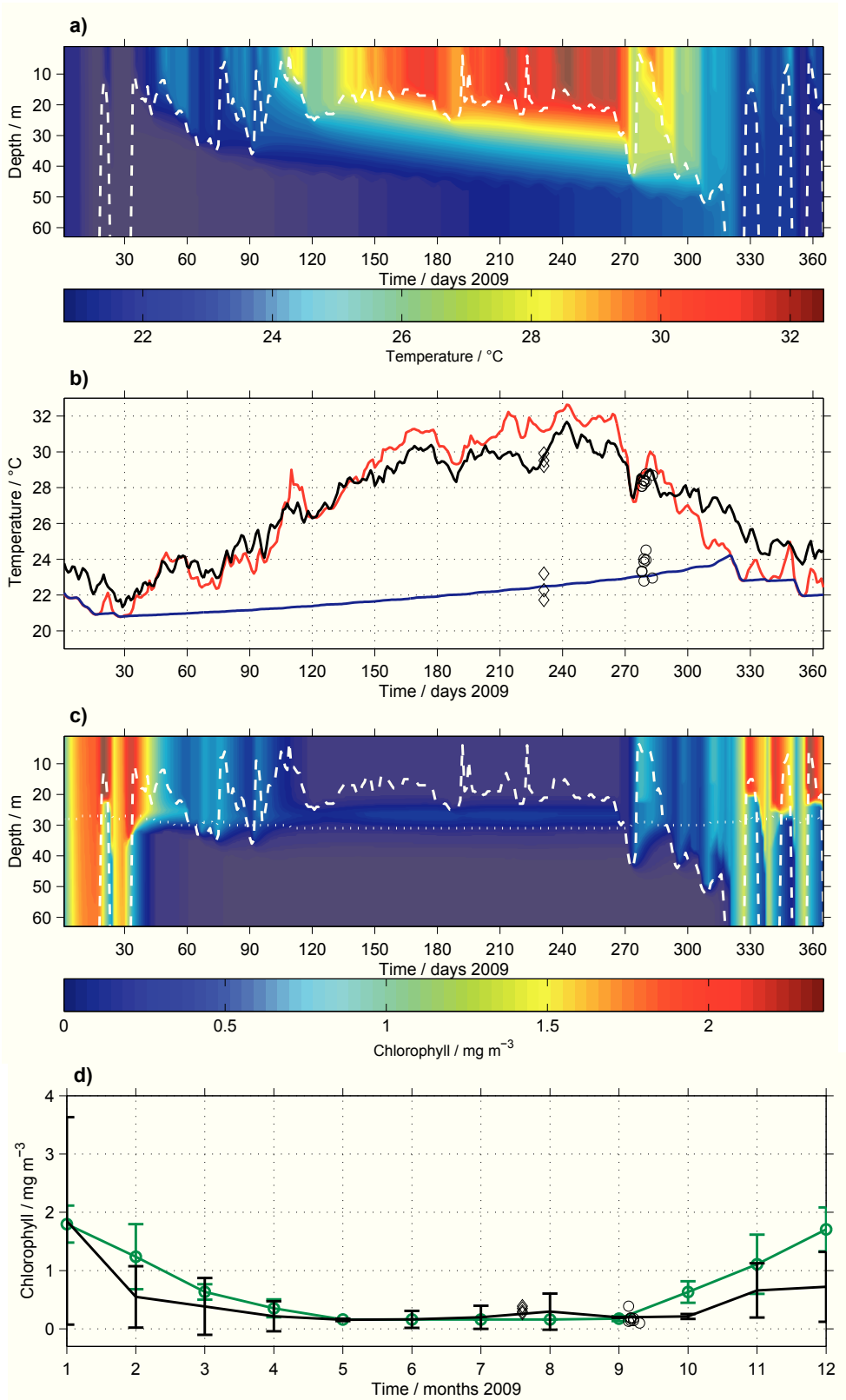
ification period with regard to the depth of the thermocline, the depth of the DCM and the DIN distribution (see Fig. S1).

### 4.3.2 Annual cycle 2009

In 2009 a weak stratification establishes at the beginning of February (day 31) and continues developing to a fully stratified water column in spring until autumn (around days 102 to 274, Fig. 4.5a). Correspondingly, the MLD reaches the bottom during the winter season and shallows in February when weak stratification occurs (Fig. 4.5a). During spring and summer the MLD persists on average in about 20 m depth followed by the seasonal deepening starting end of September due to strong wind events and culminating in full mixed water column during winter. Modeled and satellite derived SST are consistent from day 35 (February) to day 144 (May, Fig. 4.5b). From that day on the modeled SST shows slightly higher values until day 293 (October) and lower values than the remotely measured from October to December (days 294-365). Nevertheless, the annual mean deviation of SST reaches only  $-0.08^{\circ}\text{C}$ . The highest temperature of  $32.6^{\circ}\text{C}$  is modeled in September at day 242 in comparison to the remotely measured maximum temperature of  $31.7^{\circ}\text{C}$  at the same day. The lowest temperature of  $20.8^{\circ}\text{C}$  is modeled during winter at day 28 (January) while  $21.3^{\circ}\text{C}$  were measured at day 29. Around day 265 (September) a sudden temperature decrease of about  $4.6^{\circ}\text{C}$  within 10

---

**Figure 4.5 (following page):** Simulated annual cycle for 2009 in the central Beibu Gulf: (a) Temperature ( $^{\circ}\text{C}$ ) distribution over the entire water column. The white dashed line indicates the calculated MLD. (b) Simulated daily mean SST ( $^{\circ}\text{C}$ , red line) in comparison to remotely measured SST ( $^{\circ}\text{C}$ , black line) and observations (symbols). The blue line represents the modeled daily mean bottom temperature ( $^{\circ}\text{C}$ ) and the respective observations (symbols). (c) Chlorophyll ( $\text{mg m}^{-3}$ ) distribution over the entire water column. The white dashed line indicates the calculated MLD, the white dotted line indicates the euphotic depth (1% of surface PAR). (d) Simulated monthly mean sea surface chlorophyll concentrations ( $\text{mg m}^{-3}$ , green line) in comparison to satellite derived monthly mean surface chlorophyll concentrations ( $\text{mg m}^{-3}$ , black line). The black circles indicate observations during FENDOU 5 cruise, the black diamonds observations provided by SOA in 2009. The black and green bars are the standard deviations of the remotely measured and modeled chlorophyll concentrations representing the spatial and temporal variability of the data sets.



days took place induced by a typhoon which passed the study area. After that the water column was well mixed down to 44 m depth for around 7 days (271-277, Fig. 4.5a). Then the water column stratified again for a short period of around two weeks (days 276-291) and transits slowly to the winterly conditions. The bottom temperature shows a persistent warming from day 26 (January) with 20.9°C to day 321 (November) with 24.2°C (Fig. 4.5b). From the end of November the bottom water temperature decreases again due to the winter mixing of the entire water column and reduced solar radiation as well as decreased dewpoint temperature during this time of the year. The observed surface and bottom temperature data from the FENDOU 5 (2009) cruise and received from SOA at the stations within the central Beibu Gulf corroborate the model results (Fig. 4.5b).

After the MLD reached its shallowest depth (around 3 m) and the stratification is fully developed in April the DCM establishes (Fig. 4.5c). The summerly DCM is located at around 27 m depth, again shallower than the euphotic depth (30 m). The phytoplankton bloom in January with 1.9 mg m<sup>-3</sup> chlorophyll and the low concentrations of about 0.1 to 0.2 mg m<sup>-3</sup> chlorophyll during summer are modeled quite well (Fig. 4.5d). In general, the surface chlorophyll decrease in spring (February and March) and increase in autumn and winter (October to December) are well captured with differences of up to 0.9 mg m<sup>-3</sup>. During winter the model results show higher concentrations than remotely measured (Fig. 4.5d). The standard deviations indicated by the green and black bars (Fig. 4.5d) indicate the temporal and in case of the satellite data also spatial variability of monthly mean surface chlorophyll concentrations (Tab. S1 in the supplement). Highest variability occurs during winter and spring (between January and April as well as November and December). The measurements and the overlapping standard deviations point to a good agreement between the modeled and the remotely measured monthly mean surface chlorophyll concentrations.

### 4.3.3 Effects of strong wind events

The wind forcing at the surface is demonstrated in fig. 4.6a for a time period of 40 days including the passing of typhoon KETSANA (25.-30.09.2009, days 268-273) with maximum wind speeds of up to 17.5 m s<sup>-1</sup> in the central Beibu Gulf around day 272. The stratification is very strong during summer prior to the typhoon crossing and the

MLD only reaches down to 20 m depth (Fig. 4.6b). During the typhoon (day 272) the temperature of the surface layer decreases rapidly from around 32 to 27°C, the thermocline deepens and destabilizes and the mixed layer reaches 44 m depth (Fig. 4.6b). As a consequence, between days 271 and 274 the nutrient concentration in the surface waters exceeds 0.32 mmol DIN m<sup>-3</sup>, the defined limiting nitrate concentration or nutricline (Fig. 4.6c). This in turn leads to an enhanced primary production in the surface layer above the euphotic depth which is visible with a lag of about 2 days (Fig. 4.6d). The chlorophyll concentration increases from values of around 0.16 mg m<sup>-3</sup> to 1 mg m<sup>-3</sup> at day 278 at the surface. The nutrient concentration reached the maximum (0.35 mmol m<sup>-3</sup>) at the same day (272) the wind reached its maximum velocity whereas the maximum in chlorophyll concentration within the upper 20 m depth is reached five days (277-278) later.

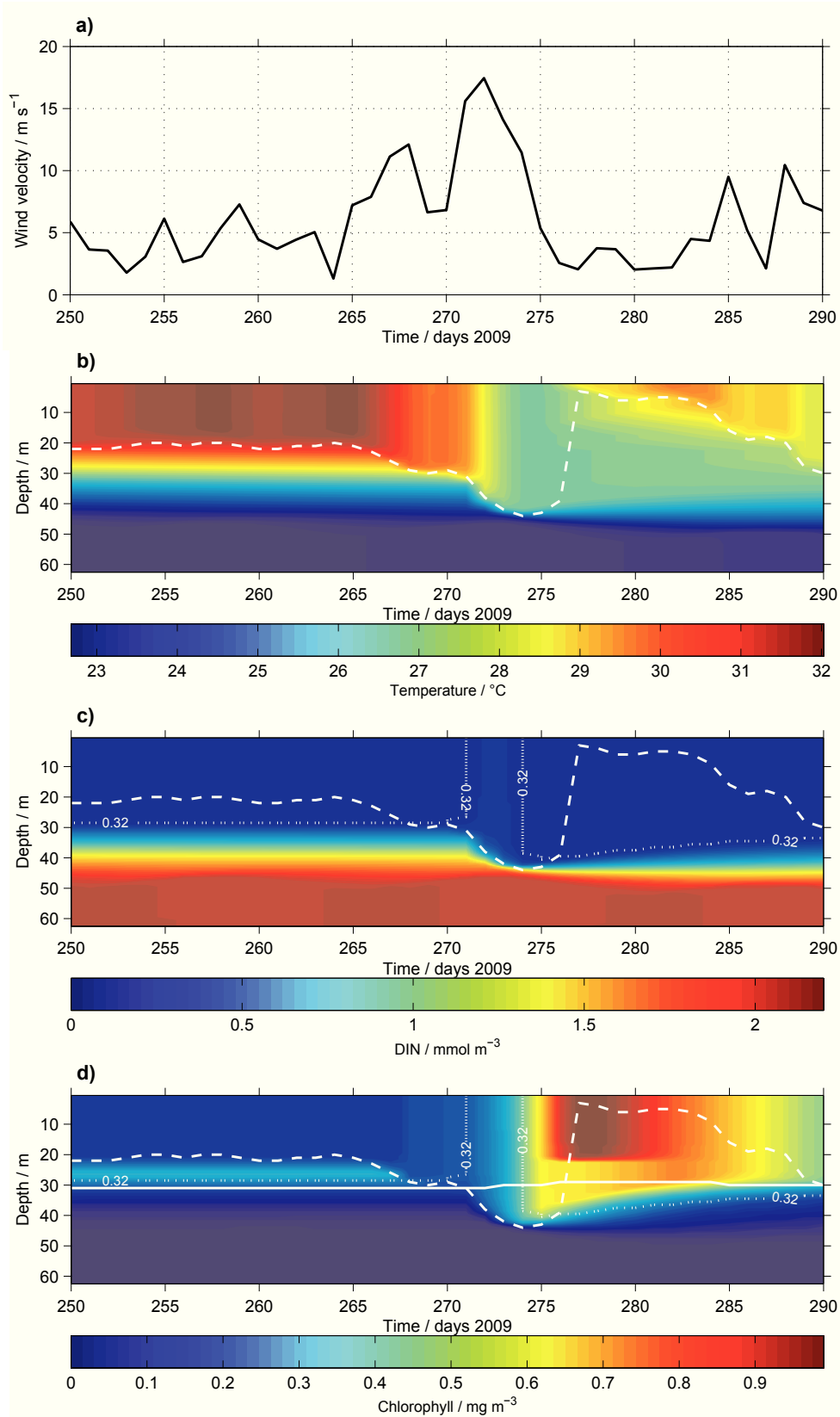
#### 4.3.4 Effects of tides

Fig. 4.7a-c show the effect of tidal forcing on the DCM within a 50 day period from July to September 2009. The resulting DCM from a model run with tides (Fig. 4.7b) is more developed than the DCM of a model run without tides ( $M_2$  and  $S_2$  tidal amplitudes set to 0, Fig. 4.7a). Maximum chlorophyll concentrations for the model run without tidal forcing reach 0.31 mg m<sup>-3</sup> in around 26.5 m depth in comparison to 0.42 mg m<sup>-3</sup> for the model run with tides at similar depth. This is an increase of around 36%. Besides the higher concentrations the tidally forced DCM is also slightly broader with a thickness (determined as the part of the chlorophyll depth profiles showing higher values than surface background chlorophyll concentration of 0.16 mg m<sup>-3</sup>, Fig. 4.7c) of around 12 m compared to 9 m for the run without tides (Fig. 4.7c) which is an increase of around 33%. Due to the maximum tidal forcing during spring tide the modeled DCM

---

**Figure 4.6 (following page):** A 40 days section (September/October) of the year 2009 (days 250-290) showing the effect of a typhoon passing throughout the region based on (a) absolute wind velocity (m s<sup>-1</sup>), (b) vertical temperature distribution (°C), (c) vertical distribution of DIN (mmol m<sup>-3</sup>) and (d) vertical chlorophyll distribution (mg m<sup>-3</sup>). The white dashed line is the MLD (b-d), the white dotted lines indicate the limiting nitrate concentration of 0.32 mmol m<sup>-3</sup> (c-d) and the white solid line in (d) is the euphotic depth.

## Chapter 4: Factors affecting chlorophyll *a* concentration





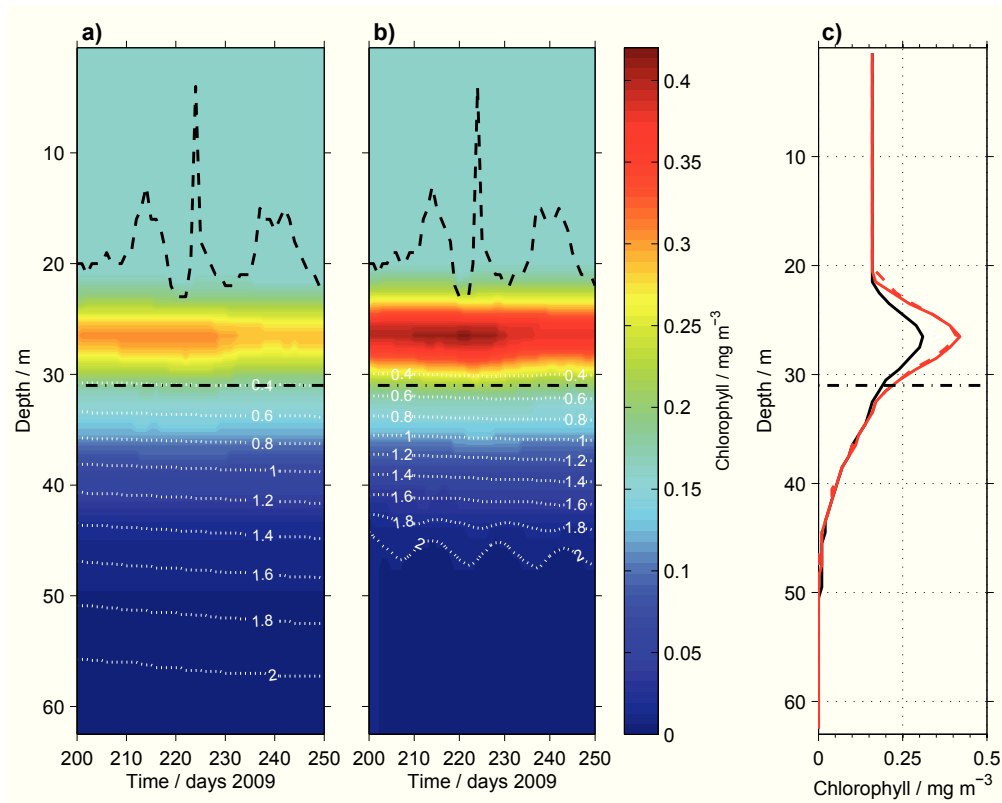


**Figure 4.7:** Simulated 50 days section of daily mean vertical chlorophyll ( $\text{mg m}^{-3}$ ) distribution and DIN ( $\text{mmol m}^{-3}$ ) isolines for model runs (a) without and (b) with tidal forcing in the year 2009. (c) Chlorophyll profiles at one day for a model run without tidal forcing (black solid line, day 220), for a neap tide (red solid line, day 220) and for a spring tide (red dashed line, day 212). The black dashed line is the MLD and the dash-dotted line is the euphotic depth.

(Fig. 4.7c) is slightly shifted towards the surface by around 1 m at the upper boundary of the DCM. Furthermore, during spring the rate of turbulent dissipation at the base of the thermocline increases and leads to an eroding of the stratification and hence to nutrient fluxes into the water layer above the thermocline [e.g. *Sharples et al.*, 2001]. The differences in thickness and strength of the DCM are a result of higher nutrient supply within the euphotic zone (Fig. 4.7a, b) and utilization of DIN by the phytoplankton due to the optimal living conditions within this layer. The tidally induced turbulence pushes the DIN isolines towards the surface. The  $2.0 \text{ mmol m}^{-3}$  isoline is located on average in about 56 m depth in the model run without tides but in about 45 m during a spring tide. As the tides in the central Beibu Gulf are weak this effect deflates relatively fast towards

the surface which causes only 1 m difference in the position of the 0.4 mmol DIN m<sup>-3</sup> isoline. Despite this weak elevation of the nutrient richer water layers into the thermocline the primary production within the DCM is enhanced by a third.

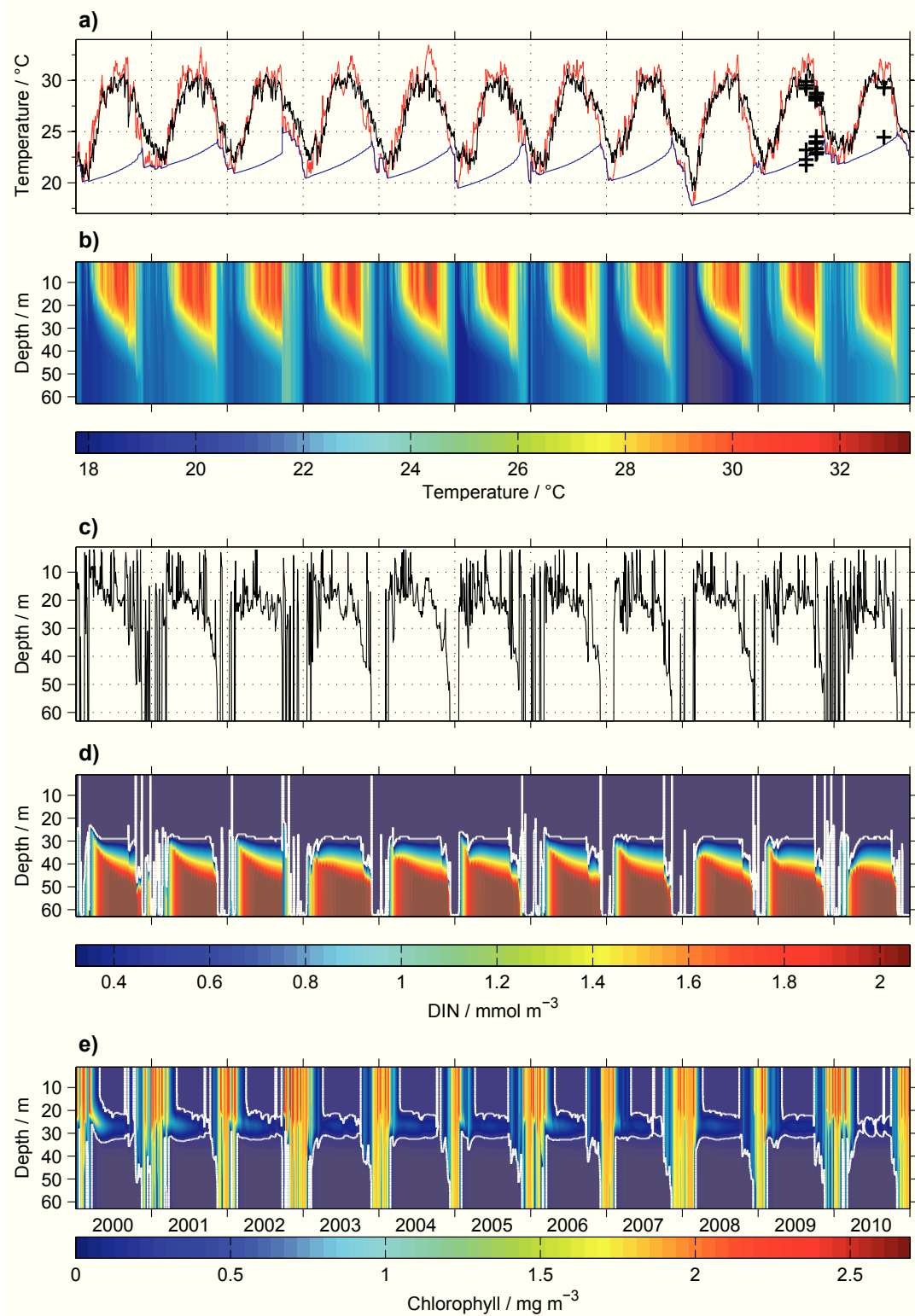
### 4.3.5 Interannual variability

As typical for the Beibu Gulf region the absolute wind shows lower velocities during summer when the southwest monsoon is predominant and highest velocities in winter during the northeast monsoon in the time period between 2000 and 2010 (Fig. S2 in the supplement). Wind peaks during late summer and autumn (August to November) indicate strong wind events, such as tropical storms or typhoons. The downward longwave radiation flux (DLRF, W m<sup>-2</sup>) displays the typical annual cycle with high insolation in summer (Fig. S2). In winter the irradiance is lower but, typical for the region, still high with values between 300 and 400 W m<sup>-2</sup>.

Maximum and minimum wind forcing in each year are mirrored by the temperature distribution (Fig. 4.8a and b) and the MLD (Fig. 4.8c). Longer periods of low wind speeds, e.g. in summer 2001 (days 224-239), 2004 (days 218-239), 2007 (days 227-233) and 2009 (days 233-243) lead to an increase of temperature in the surface water layer and a shallowing of the MLD, in 2004 for instance from 27 m to 3 m depth and in 2007 from 30 m to 2 m depth. On the other hand strong wind events in late summer and autumn, e.g. in 2000 (day 288), 2001 (day 222), 2002 (day 265), 2007 (day 276), 2009 (day 272) and 2010 (day 277), cause a cooling of the surface water between 0.6 and 6.7 °C, depending on the strength of maximum wind (Tab. 4.3), and a deepening of the MLD for instance from around 6 m to 50 m in 2000, from 19 m to 63 m in 2002 and in 2009 from 20 m to 44 m.

---

**Figure 4.8 (following page):** Interannual comparison of the years 2000-2010: (a) Daily mean surface (red line) and bottom (blue line) temperature (°C) as well as satellite SST (black line). The crosses indicate measurements during the FENDOU 5 cruise and cruises conducted by SOA (August 2009 and 2010). (b) Daily mean temperature distribution over the entire water column (°C). (c) Calculated daily MLD (m). (d) Daily mean DIN distribution over the entire water column (mmol m<sup>-3</sup>). The white line indicates the defined limiting nitrate concentration of 0.32 mmol m<sup>-3</sup>. (e) Daily mean chlorophyll distribution (mg m<sup>-3</sup>). The white line emphasizes the DCM.



The start of sustained stratification and vertical mixing is indicated by the surface and bottom temperature trends when SST and bottom temperature begin to diverge in spring and converge again in autumn, respectively (Fig. 4.8a). Periods of mixing and/or weak stratification occur between the middle of September and the middle of March of the following year. The beginning of the main period of stratification is defined as the first day after last day of entire vertical mixing, the end as the first day of total vertical mixing in one year (Fig. 4.8a, Tab. 4.2). In the Beibu Gulf the winter period is the main productive season [Hu *et al.*, 2003; Tang *et al.*, 2003]. The termination of the thermal stratification in autumn/winter is the most important factor for the timing of nutrient supply from the bottom waters (Fig. 4.8d) and hence the initiation and timing of the phytoplankton bloom. On average the termination of stratification takes place in November with a strong nutrient input into the surface layer in most of the years directly after the stratification breakdown indicated by shallowing of the nutricline (Fig. 4.8d, white line). In all years the limiting nitrate concentration of about  $0.32 \text{ mmol m}^{-3}$  (which is equivalent to a phosphate concentration of  $0.02 \text{ mmol m}^{-3}$  necessary for phytoplankton growth) lies on average in 29 m depth during summer, with higher values below and a nutrient depleted surface water body (Fig. 4.8d). In autumn and winter when the mixed layer deepens nutrient inputs from the bottom water layer into the surface layer enhance nutrient concentrations within the euphotic zone (Fig. 4.8d).

In some years (e.g. 2001, 2004 and 2010) this nutrient input is not visible because it is directly ingested by phytoplankton in the model. In autumn 2002 a strong wind event at day 265 (Fig. S1) terminated the stratification by September which led to a strong nutrient input into the surface layer and hence an early phytoplankton bloom (Fig. 4.8d, e). In all years a phytoplankton bloom developed between autumn and winter and persisted until spring (Fig. 4.8e). At the turn of the year 2000/2001, 2002/2003, 2005/2006 and 2007/2008 the phytoplankton bloom is well developed. By contrast the bloom is less pronounced between 2001/2002, 2004/2005, 2006/2007 and 2008/2009 (Fig. 4.8e). Due to the maximum MLD (63 m) during winter the signal of the bloom reaches the bottom in every year. The stratification vanishes in autumn between day 265 and 343 but the already established phytoplankton bloom starts between day 256 and 295 (Tab. 4.2). Strong wind events as well as the change from the weaker southwest to the stronger northeast monsoon lead to a weakening of the thermocline in autumn, to episodic nutrient supply into the surface waters and hence a phytoplankton bloom

establishing already before the stratification breaks down completely.

On average a bloom persists for about 204 days or more than 6 months. The spring stratification starts between day 17 and 72 whereas the phytoplankton bloom ends between day 97 and 127 (Tab. 4.2). The shortest bloom occurred between 2004 and 2005 (172 days, Tab. 4.2). Between 2005 and 2006 the bloom lasted for the longest time (229 days, Tab. 4.2). Within this 11 years the well-developed bloom between the years 2002 and 2003 shows the highest chlorophyll concentrations with  $2.7 \text{ mg m}^{-3}$  (Tab. 4.2). The highest annual integrated surface biomass concentration of  $326 \text{ mg m}^{-3}$  was calculated for 2002, the lowest with  $218 \text{ mg m}^{-3}$  for 2003 (Tab. 4.2).

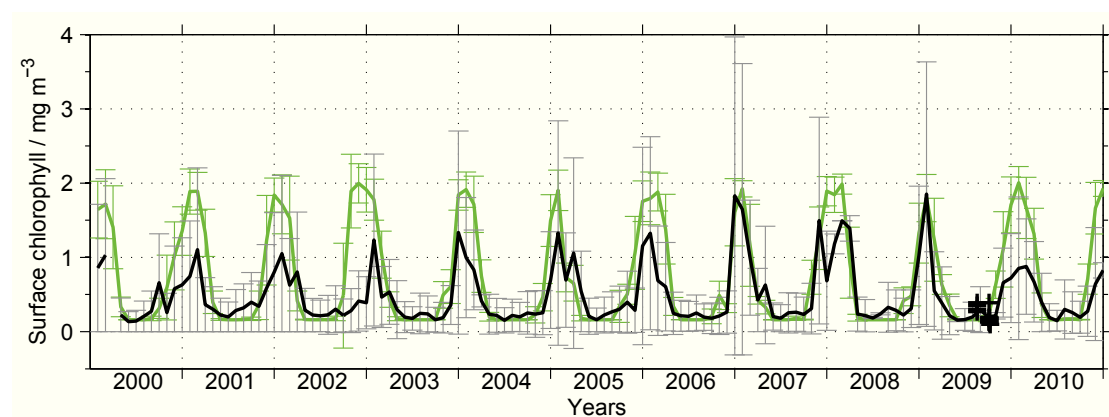


**Figure 4.9:** Interannual variability of the modeled (green line) and remotely measured (black line) monthly mean surface chlorophyll concentrations ( $\text{mg m}^{-3}$ ) for the time period from 2000 to 2010. The grey bars indicate the spatial availability of satellite chlorophyll data for the central Beibu Gulf, the crosses show measurements during the FENDOU 5 cruise and a cruise conducted by SOA (August 2009).

The modeled monthly mean surface chlorophyll concentrations in almost all years are higher compared to the remotely measured concentrations (Fig. 4.5). On average the modeled bloom has a  $0.6 \text{ mg m}^{-3}$  higher chlorophyll concentration than remotely measured and a shift of up to 2 months between both signals can be seen, for example between 2002 and 2003 (Fig. 4.9). While the satellite observed blooms start in November/December and continue until April/May, the modeled bloom start between September and December and continue until January to March (Fig. 4.9).

**Table 4.3:** Wind events classified in Tropical storm (TS), typhoon (TY), tropical depression (TD) and strong wind events (WE,  $>10 \text{ m s}^{-1}$ ) which affected the primary production in the central Beibu Gulf (2000 to 2010) with corresponding SST decrease including the lag between wind peak and lowest SST in brackets. The production increase expressed as a percentage is related to the background  $0.16 \text{ mg m}^{-3}$  chlorophyll concentration found in the central Beibu Gulf during summer. For wind events initiating the phytoplankton bloom the end of the increased primary production (PP) is not detectable. Cyclone classification and data are from the Joint Typhoon Warning Center (<http://www.usno.navy.mil/JTWC/>; <sup>1</sup>JTWC [2000], <sup>2</sup>JTWC [2001], <sup>3</sup>Furze and Engel [2002], <sup>4</sup>Furze and Preble [2003], <sup>5</sup>Atangan and Preble [2005], <sup>6</sup>O'Hara and Falvey [2006], <sup>7</sup>O'Hara and Falvey [2007], <sup>8</sup>Cooper and Falvey [2008], <sup>9</sup>Cooper and Falvey [2009], <sup>10</sup>Angove and Falvey [2010]).

Year	Name	Cyclone type	Period	Estimated max intensity (gusts) [ $\text{m s}^{-1}$ ]	Daily mean NCEP wind speed [ $\text{m s}^{-1}$ ] (day)	SST decrease [ $^{\circ}\text{C}$ ] (lag)	Start increase of PP [day]	End increase of PP [day]	Maximum production [ $\text{mg m}^{-3}$ ] (day)	Production increase [%]
2000	Kaemi <sup>1</sup>	TS 19W	20.-23.Aug	23.2 (28.3)	15.5 (235)	2.2 (1)	235	246	0.3 (237)	87.5
2000	Wukong <sup>1</sup>	TY 23W	05.-10.Sep	48.9 (59.2)	15.9 (254)	4.4 (1)	254	282	0.6 (259)	275
2000	Noname <sup>1</sup>	TS 28W	06.-13.Oct	20.6 (25.7)	16.4 (288)	5.0 (5)	285	bloom initiated		
2001	Usagi <sup>2</sup>	TS 13W	08.-11.Aug	20.6 (25.7)	12.5 (222)	1.0 (1)	222	227	0.2 (224)	25
2001	Noname	WE			11.2 (254)	2.1 (2)	253	264	0.2 (256)	25
2001	Lingling <sup>2</sup>	TY 27W	06.-12.Nov	59.2 (72.0)	16.5 (318)	4.1 (6)	within bloom			
2002	Vongfong <sup>3</sup>	TS 20W	15.-20.Aug	28.3 (36.0)	14.2 (230)	1.4 (2)	230	241	0.3 (233)	87.5
2002	Mekkhala <sup>3</sup>	TS 24W	23.-27.Sep	28.3 (36.0)	38.9 (265)	6.7 (4)	260	bloom initiated		
2003	Nepartak <sup>4</sup>	TY 25W	12.-19.Nov	38.6 (46.3)	11.7 (314)	2.1 (3)	within bloom			
2004	Noname	WE			11.7 (276)	2.2 (4)	276	287	0.2 (279)	25
2005	Washi <sup>5</sup>	TS 08W	28.-31.Jul	23.2 (28.3)	11.6 (212)	0.6 (2)	213	214	0.2 (213)	25
2005	Vicente <sup>5</sup>	TS 16W	14.-18.Sep	25.7 (33.4)	16.2 (261)	1.6 (1)	256	bloom initiated		
2005	Damrey <sup>5</sup>	TY 17W	20.-27.Sep	46.3 (56.6)	17.2 (270)	2.0 (2)	within bloom			
2006	Noname <sup>6</sup>	TD 17W	21.-25.Sep	64.3 (77.2)	12.9 (268)	2.3 (2)	266	bloom initiated		
2006	Xangsane <sup>6</sup>	TY 18W	25.Sep-02.Oct	15.4 (20.6)	15.4 (274)	1.2 (2)	within bloom			
2007	Noname	WE			11.2 (218)	1.2 (1)	218	234	0.3 (225)	87.5
2007	Noname	WE			10.7 (267)	1.7 (1)	266	273	0.2 (268)	25
2007	Lekima <sup>7</sup>	TY 16W	29.Sep-03.Oct	36.0	18.1 (276)	2.5 (1)	274	bloom initiated		
2008	Mekkhala <sup>8</sup>	TS 20W	26.-30.Sep	28.3	15.3 (274)	4.2 (1)	273	bloom initiated		
2008	Noname <sup>8</sup>	TS 22W	12.-15.Oct	18.0	16.7 (288)	2.7 (1)	within bloom			
2009	Ketsana <sup>9</sup>	TY 17W	23.-29.Sep	46.3	17.5 (272)	4.9 (2)	267	bloom initiated		
2010	Noname	WE			10.7 (198)	1.1 (2)	198	205	0.2 (201)	25
2010	Noname	WE			10.6 (236)	1.1 (2)	236	247	0.2 (238)	25
2010	Noname <sup>10</sup>	TD 14W	04.-06.Oct	15.4	15.5 (277)	3.9 (3)	273	bloom initiated		

In all years a DCM was detected more or less developed with a thickness between 19 m (e.g. in 2001) and 33 m (e.g. in 2004, Fig. 4.8e, emphasized by the white line which indicates the  $0.2 \text{ mg chl m}^{-3}$  isoline). In some years short-lived blooms prior to the main phytoplankton bloom were modeled. These blooms are associated with strong wind events in late summer and autumn (Fig. S1) for example in 2000, 2005-2010 (Fig. 4.8e).

### 4.4 Discussion

Considering that the model works simply with vertical exchange and does not include advective flows the models success to capture 87% of the observed variance in daily surface temperatures indicates that surface water masses from the SCS or the Beibu Gulf coastal regions do not strongly affect the central Beibu Gulf. This agrees with the general cyclonic circulation pattern in the Beibu Gulf [Wu *et al.*, 2008]. Therefore the local meteorological forcing seems to be the most important factor for the formation of the vertical water column temperature distribution. The approximately 14% over- and underestimation for summer and winter temperatures, respectively, can be explained by the structure of the 1-D model itself, as it always warms up and cools down the same body of water, because lateral transports of water masses are not taken into account by the model. Another reason is the missing cloud cover correction within the model. The surface dewpoint temperature (minimum of  $4.2^{\circ}\text{C}$  in winter and maximum of  $28.4^{\circ}\text{C}$  in summer, Tab. 4.2) and the high solar irradiance (typically ranging between  $297$  and  $449 \text{ W m}^{-2}$ , Tab. 4.2) result in a strong stratification during summer with SSTs of up to  $33.5^{\circ}\text{C}$ . It is the wind and its effects on water column stability that seem to play the most important role for the phytoplankton growth in the central Beibu Gulf. The assumption was tested using the model with only one changed meteorological forcing parameter (dewpoint temperature, solar irradiance and wind velocities) for 2009 in each run. The minimum and maximum values of the respective forcing parameter were used to act throughout the year. The differences in the resulting annual mean of surface chlorophyll concentrations between the model runs forced with the minimum and maximum value of every meteorological input are 4% for the solar irradiance (min =  $305 \text{ W m}^{-2}$ , max =  $449 \text{ W m}^{-2}$ ), 63% for the surface dewpoint temperature (min =  $8.0^{\circ}\text{C}$ , max =  $27.3^{\circ}\text{C}$ ) and 90% for the wind velocities (min<sub>*u*</sub> =  $-0.0017 \text{ m s}^{-1}$ ,

$\min_v = -0.041 \text{ m s}^{-1}$ ,  $\max_u = -11.99 \text{ m s}^{-1}$ ,  $\max_v = -14.95 \text{ m s}^{-1}$ ). This supports our conclusion that wind is the most important parameter for phytoplankton growth in the central Beibu Gulf. This is already known from the Arabian Sea, an also monsoon-influenced region [e.g. *Bauer et al.*, 1991]. Based on observations, *Bauer et al.* [1991] identified the wind forcing as the primary factor influencing the MLD and hence pigment biomass in the monsoon season.

As the light regime is relatively constant throughout the year the phytoplankton growth depends mainly on the availability of nutrients, which in turn is affected by the water column structure and physical forces acting upon it. Due to the strong water column stratification (see Fig. S2a) most pronounced between February and November, the central Beibu Gulf is nutrient depleted in the upper water layer during this period (Fig. S2c). As a result only minimum phytoplankton growth takes place in the surface waters and a DCM develops in around 20-30 m depth where the nutricline and euphotic zone overlap (see Fig. 4.6d). The depth of the DCM seems to depend on the depth of the nutricline rather than on the euphotic depth (Fig. 4.6d), which has been described by *Cullen and Eppley* [1981] for the Southern California Bight. They found the depth of the DCM in about 20-50 m more correlating with the depth of the nutricline (15-45 m, 15-6% of the surface irradiance available) than with the euphotic depth (33-66 m). For the mean modeled year the calculated PAR in the mean depth of the DCM (26 m) is about 4% of the surface PAR. The link between the nutricline and the DCM results in a gradual deepening of the nutricline and the DCM within the thermocline, which has been shown for the western English Channel by *Sharples et al.* [2001].

The mean modeled DCM is located somewhat shallower than the depth range for the DCM in the central Beibu Gulf of about 30-50 m published by *Huang et al.* [2008], *Wu* [2008] and *Bauer et al.* [in press]. Own measurements and literature values [*Liu et al.*, 1998] indicate a relatively high variability in the depth of the DCM as well as in its strength. The mean modeled DCM shows maximum chlorophyll concentrations of around  $0.5 \text{ mg m}^{-3}$  (Fig. 4.3c) whereas the maximum chlorophyll concentrations within the DCM vary between 0.2 and  $1.1 \text{ mg m}^{-3}$  (Fig. 4.8e) for the different years and, particularly for different periods within the years which agrees well with the range of  $0.6\text{-}1 \text{ mg m}^{-3}$  reported by *Wu* [2008] and *Bauer et al.* [in press]. If enough nutrients and light, to compensate loss processes through photosynthesis, are available a net phytoplankton blooming occurs when cells are trapped near the surface [*Sverdrup*, 1953;



Ward and Waniek, 2007]. Despite the strong stratification during summer, the existence of a DCM implies that a complete decoupling of the surface and bottom waters does not occur [Sharpley and Tett, 1994]. The continuous presence of the DCM throughout the summer is caused by the variability in surface wind stress driving occasional events introducing DIN into the system [Sharpley and Tett, 1994], rather than by tidally-driven turbulence as discussed later. Depending on the strength and quantity of these events the DCM is more or less strongly developed within the different years. The DCM can disappear for periods when the time between the entrainment events is longer than the utilization time scale of DIN [Sharpley and Tett, 1994], this is clearly happening in autumn 2004 and summer 2010 (Fig. 4.8d).

Due to the strong northeast monsoon beginning in autumn the stratification breaks down between October and December and allows the development of a phytoplankton bloom. The onset of the phytoplankton bloom around day  $273 \pm 22$  (Tab. 4.2), some 47 days before the disappearance of stratification on day  $320 \pm 55$ , leads to the assumption that the stratification is already weakened in autumn due to tides, storms and the change of the wind system to the stronger northeast monsoon, before it finally disappears. The stronger wind-driven turbulence induced at the surface deepens the MLD [Bauer *et al.*, 1991] and leads to a nutrient input into the surface water layer through the thermocline. In turn this allows a phytoplankton bloom to start before the stratification breaks down. Differences in the strength and quantity of nutrient inputs lead to a different timing and development of the phytoplankton bloom [cf. Waniek, 2003]. Ongoing strong winds and the further decrease in solar irradiance then enable a mixing down to the seabed and full development of the bloom. The spring stratification starts on average around day  $44 \pm 19$  whereas the phytoplankton bloom ends around day  $112 \pm 15$  (Tab. 4.2). It takes about 69 days until the stratification is fully developed and nutrients within the surface water layer are depleted. About 2 months after stratification occurs the phytoplankton growth is terminated indicating a very slow onset of full stratification, probably with periodic nutrient inputs in the surface layer due to tidal forcing, a low nutrient uptake rate, slow remineralisation or a low grazing pressure acting on the phytoplankton. According to Chung *et al.* [2012] phytoplankton blooms are terminated due to herbivore grazing rather than nutrient depletion or sedimentation: a model test with deactivated grazing showed that a strong phytoplankton bloom would persist over the entire year. Despite nutrient depletion during summer zooplankton grazing seems to be the most important

factor for the termination of the phytoplankton bloom in the central Beibu Gulf. The variability in the beginning and ending of stratification and phytoplankton bloom, indicate that the timing of the bloom is less variable than the timing of the stratification [e.g. *Sharples et al.*, 2006]. This also supports the conclusion that wind forcing is the most important factor driving primary production in the central Beibu Gulf.

Differences between both developments of modeled and remotely measured monthly mean surface chlorophyll concentration could be caused by lateral transport which is not contained in the model (Fig. 4.9). Through currents and tide-induced lateral transport nutrients for phytoplankton growing or phytoplankton itself as well as grazers may be transported to/from the central Beibu Gulf from/to other regions. This would have an effect on the surface chlorophyll concentration within the central Beibu Gulf. The standard deviations for the satellite data (Fig. 4.9) display the spatial variability of the remotely measured surface chlorophyll concentrations. Between 0 and 121 pixel per month were recorded by SeaWiFS within the central Beibu Gulf (Tab. S1). During winter, satellite data for the central Beibu Gulf is sparse probably due to a higher cloud cover caused by activity of tropical storms. The differences between the surface chlorophyll concentrations and the beginning of the phytoplankton bloom can therefore be attributed to the lack of available satellite data. The small standard deviations on the output data indicate that the model successfully simulated the surface chlorophyll concentrations for the region.

The low variability in meteorological forcing is mirrored in the model results (Tab. 4.2). Surface and bottom water temperatures as well as surface chlorophyll concentrations do not show great differences between the years, variations are the result of strong wind events. In correspondence with the strong wind events the SST declines due to entrainment of colder, subsurface water masses into surface waters [*Price*, 1981] by 0.6-6.7°C (Tab. 4.3), depending on the winds strength, comparable to measured SST responses between -2.5 and -9°C *Chang et al.* [1996]; *Lin et al.* [2003]; *Walker et al.* [2005]; *Shi and Wang* [2007]; *Zheng and Tang* [2007]. The lag between the wind peak and the lowest SST is about 1-6 days [cf. *Shi and Wang*, 2007], depending as well on the winds intensity and the duration of strong winds influence or the transit time of the respective typhoon. Despite the pronounced summer stratification, strong wind events like tropical storms lead to a deepening of the MLD [*Price*, 1981; *Jiang et al.*, 2009] and hence to a higher nutrient supply in the surface water layer resulting in a short-lived en-

hancement of the primary productivity or a phytoplankton bloom [e.g. *Zheng and Tang*, 2007]. These results are supported by several studies based on satellite data or in-situ measurements describing such blooms for different typhoon- or hurricane-influenced regions [e.g. *Chang et al.*, 1996; *Fogel et al.*, 1999; *Shiah et al.*, 2000; *Lin et al.*, 2003; *Babin et al.*, 2004; *Zheng and Tang*, 2007; *Chung et al.*, 2012; *Lin*, 2012]. Wind velocities (Fig. S1) show that typically more than one strong wind event influenced the central Beibu Gulf region during almost every year from 2000 to 2010 in late summer and autumn. In the 11 year period 11 events were detected which initiated a small bloom prior to the highly developed bloom, statistically one event per year (Tab. 4.3). On average the estimated temporary increase in primary production induced by these strong wind events accounts for 65% with an averaged duration of  $11 \pm 7$  days. This result corresponds well to the 11 days bloom duration after the crossing of Hurricane Katrina in the Gulf of Mexico in August 2005 [*Shi and Wang*, 2007]. About 1-7 days lagged between the wind-stress peak and the modeled chlorophyll peak at the surface (Tab. 4.3) which is comparable to the 3-4 days lag postulated by *Walker et al.* [2005] for the Hurricane Ivan, the 4 days lag described by *Shi and Wang* [2007] for the Hurricane Katrina, both in the Gulf of Mexico, and the 3-6 days lag described by *Zheng and Tang* [2007] for the Typhoon Damrey in the SCS. The modeled lag between the lowest SST and the chlorophyll peak of up to 6 days agrees well with the 4 days lag described by *Zheng and Tang* [2007].

However, to what extent a typhoon will affect an oceanic region depends on the wind's intensity, the transit time as well as the ocean's precondition, which means how deep or shallow the nutrient-rich water body lies [*Lin*, 2012]. Is any condition unfavorable the oceans response will be weakened [*Lin*, 2012]. For example, the modeled typhoon Washi enhanced the surface chlorophyll concentration in the central Beibu Gulf to up to  $0.2 \text{ mg m}^{-3}$  at a maximum wind speed of  $11.6 \text{ m s}^{-1}$  but enhanced the maximum surface chlorophyll concentration by up to  $0.9 \text{ mg m}^{-3}$  (around 3.8 times before the typhoon) in the SCS at wind speeds of around  $18 \text{ m s}^{-1}$  [*Chen and Tang*, 2011]. The greatest effect on the chlorophyll increase was seen from the passage of the typhoon WUKONG through the region in 2000 (Tab. 4.3). This storm initiated a bloom lasting for 28 days with a maximum surface chlorophyll concentration of  $0.6 \text{ mg m}^{-3}$ , an increase of 275% compared to the summer background surface chlorophyll concentration of  $0.16 \text{ mg m}^{-3}$ . Along with these temporary bloom events, tropical storms can also ini-

tiate a phytoplankton proliferation, for example in 2000, 2002, 2005-2010, resulting in a bloom as early as mid-September such as those in 2002 or 2005. The effect of strong wind events on surface chlorophyll concentration during the fully developed bloom is difficult to estimate.

Contrary to our expectations the effect of the tides on the primary production within the central Beibu Gulf is only moderate. This may be a result of the relatively great depth (63 m), the distance from shore, the associated small tidal forcing in this region and the lateral transport initiated by tides, which is not included in the model, or a combination of those. The strong stratification can reduce the already weak tidal forcing which therefore only has a minor effect on mixing in the surface water column during summer. In spite of the weak tides ( $0.15 \text{ m s}^{-1}$  for amplitude of  $M_2$  tidal currents) in this region the tidally generated turbulence increases the strength of the DCM by up to 36% and its thickness by up to 33% as well. According to the results of *Sharpley et al.* [2006] a tidal current amplitude of  $0.4 \text{ m s}^{-1}$  can offset the influence of the heating in stratifying the water column. The result of this would be a weakly stratified water column and a breakdown of stratification that occurs earlier in the year. Ultimately, due to the intense nutrient input from the deep water to the surface layer it would strongly enhance the primary production within the surface water layer throughout the year. The rising bathymetry from south to north in the region means the shallow northern or coastal regions may be considerably more affected by tidal currents than the relatively deep central part of the gulf. In a system which is strongly influenced by tides a constant competition between tidal turbulence in the bottom layer and wind-driven turbulence in the surface layer determine the position of the thermocline and its associated DCM [*Sharpley*, 1999]. During spring tides, when the maximum currents occur, the tidal turbulence pushes the thermocline towards the sea surface while during neap tides, with only weak currents, the wind-driven turbulence pushes the thermocline deeper in the water column [e.g. *Sharpley*, 1999]. These forces cause periodic pulses of nutrients to the euphotic zone and hence higher chlorophyll concentrations within the DCM. In the central Beibu Gulf the influence of the spring-neap tidal cycle on the elevation of the DIN isolines is only visible to a depth of 40 m (Fig. 4.7b). Hence the expected periodic pulses of higher chlorophyll concentrations within the DCM do not occur.

### 4.5 Conclusions

As typical for subtropical/tropical shelf seas the central Beibu Gulf shows an annual cycle with a strong stratification during summer and a deep mixing down to the seabed in winter. The physical structure of the water column is reflected in the seasonal cycle of primary production. A phytoplankton bloom develops when the wind system changes in autumn into the stronger northeast monsoon, the solar irradiance decreases, deep mixing occurs and nutrients from bottom waters are supplied to the surface waters and therefore are available for phytoplankton. During summer, due to the strong stratification, the surface waters are nutrient depleted and therefore only low phytoplankton growth is possible. At a depth of around 20-30 m, where euphotic depth and nutricline co-exist a DCM developed in all modeled years.

The model simulated successfully the observed stratification, SST and bottom temperature as well as the chlorophyll distribution. Differences in the SST and the monthly mean surface chlorophyll concentrations are a consequence of the absent horizontal advection and the missing cloud cover in the model as well as attributable to the lack of satellite data.

The water depth of 63 m, the distance from shore and associated weak tidal forcing explain the weak tidal influence in the central Beibu Gulf. However, tides lead to an enhanced nutrient supply within the euphotic zone and hence to a considerable increase in strength and thickness of the DCM.

Although the interannual variability is generally low, the timing of the stratification breakdown and the establishment of a phytoplankton bloom are variable within a time-frame of about 2.5 months and around 1 month in autumn/winter. Besides these features, strong wind events play an important role in the primary production within the central Beibu Gulf. Single events strongly enhance primary production during the usually low productive summer season and are able to initiate a prior phytoplankton bloom. In summary, the monsoon winds and the occasionally strong wind events are the most important forces driving the primary production in the central Beibu Gulf.

Our study helps to compensate the lack of remotely measured and in-situ data for the central Beibu Gulf and hence contributes to a more comprehensive understanding of processes influencing the primary production in that region.

## Supplementary Material

Meteorological forcing used for the modeled years 2000-2010, more in-situ data for model validation and pixels available for the central Beibu Gulf from SeaWiFS.

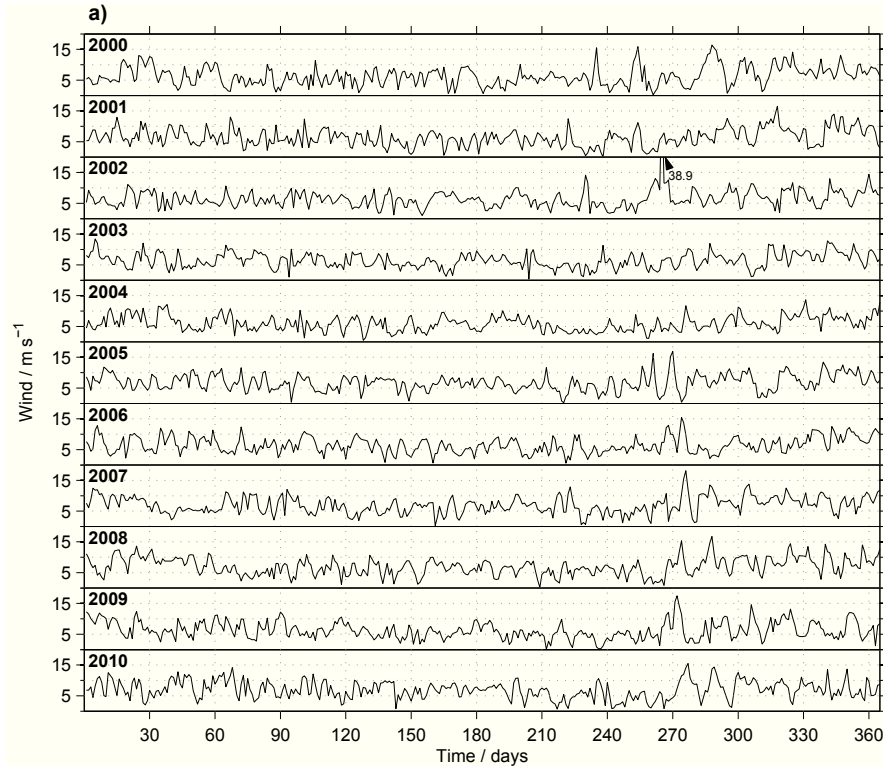


**Figure S1:** Daily meteorological forcing for the years from 2000 to 2010: (a) absolute wind velocity ( $\text{m s}^{-1}$ ), (b) dewpoint temperature ( $^{\circ}\text{C}$ ) and (c) solar irradiance as downward longwave radiation flux (DLRF in  $\text{W m}^{-2}$ ). It is noticeable that there is an apparent shift of the timing of the first strong wind event in autumn from year to year. In 2000 it appeared at the end of August and shifted towards the beginning of October in 2010, whereas the years 2003 and 2004 differ and show a relatively consistent wind forcing without very strong wind events in late summer and autumn.

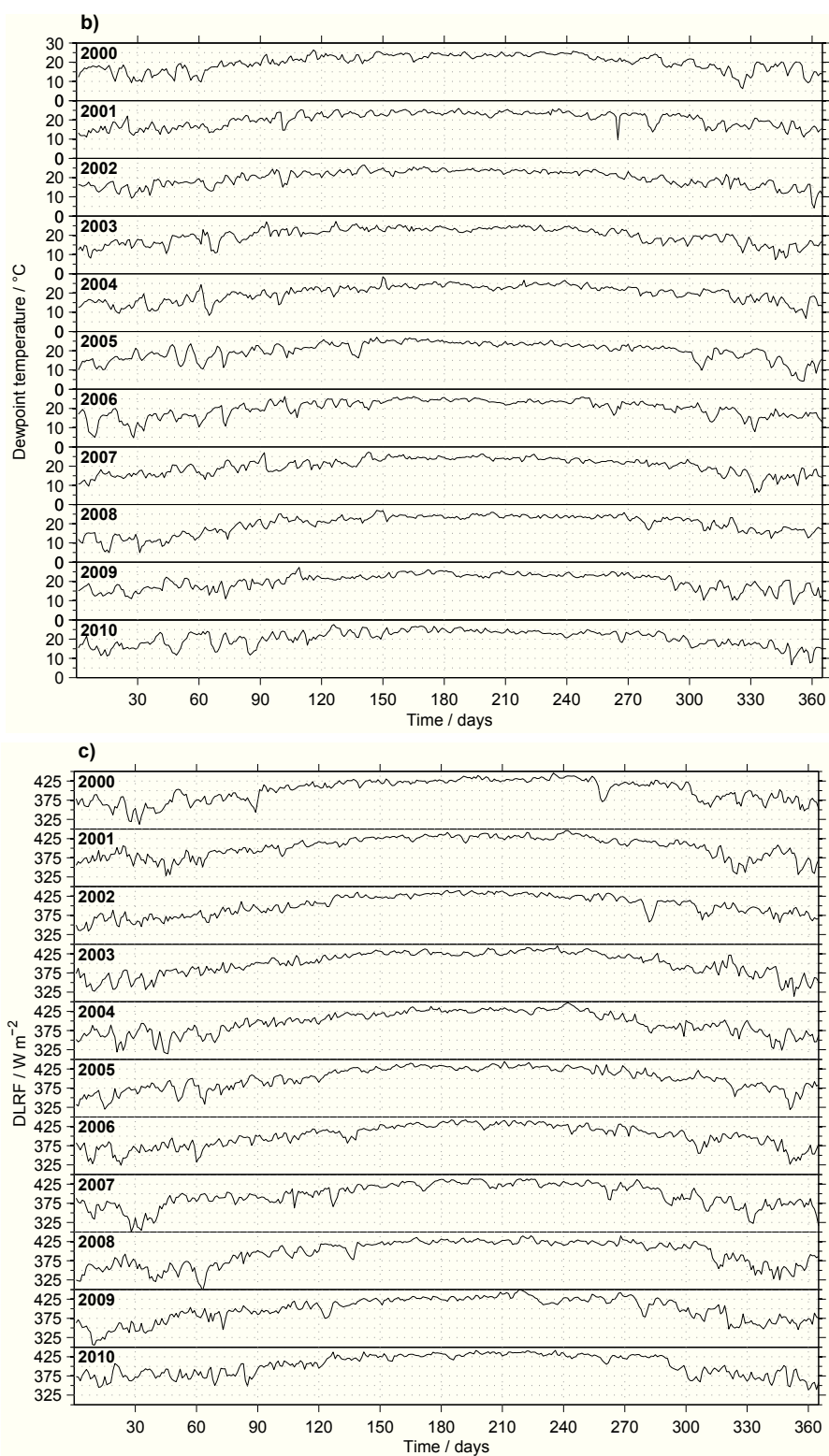


**Figure S1: Continued.**

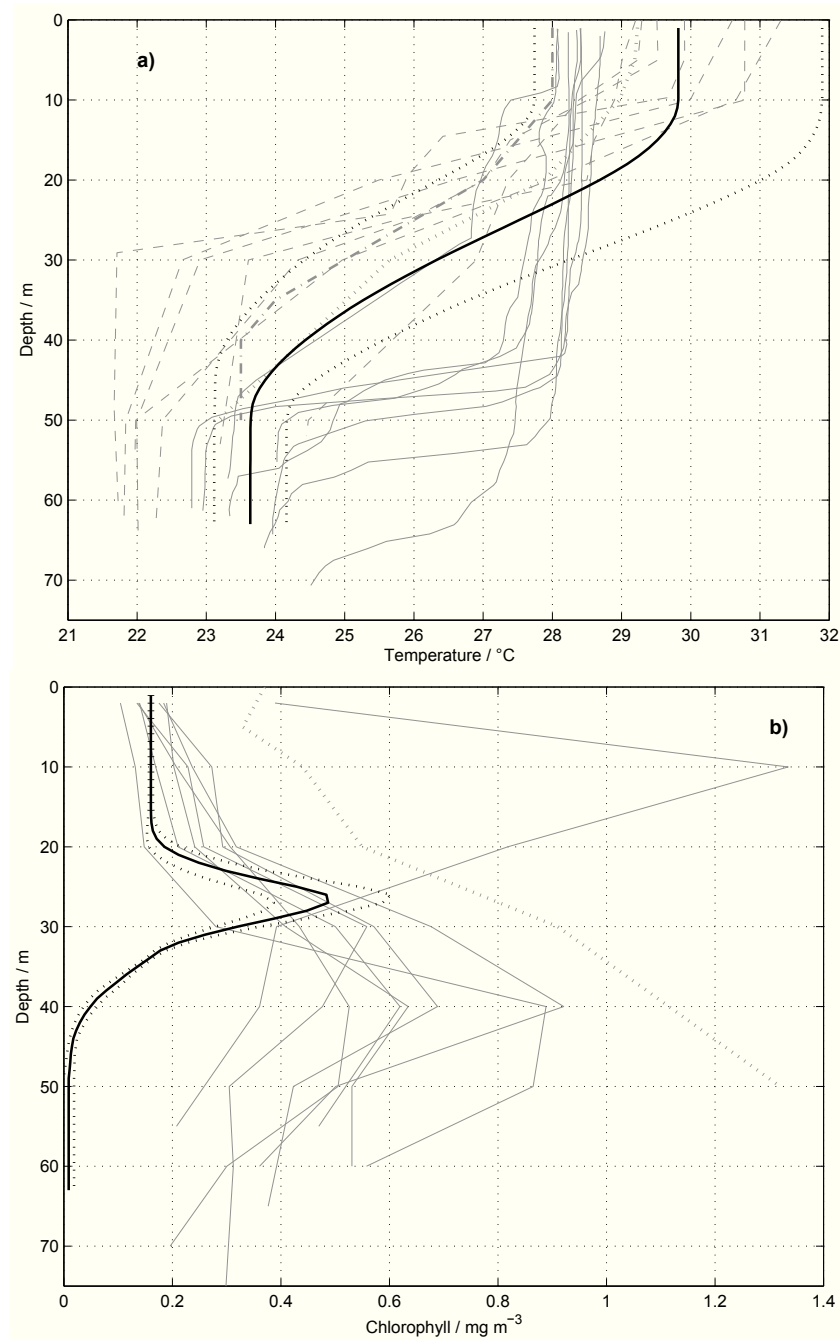


**Figure S2:** For the period of stratification averaged temperature, chlorophyll and DIN depth profiles (black line) with respective standard deviations (black dotted line) of the mean modeled year. The grey solid lines are in-situ measurements during FENDOU 5 cruise (September/October 2009), the grey dashed line are in-situ measurements conducted by SOA (August 2009, August 2010, September 2011), the grey dotted lines indicate data published by *Liu et al.* [1998] (May/June 1994) and the grey dash-dotted lines are values published by *Lü et al.* [2008] (June 1960).



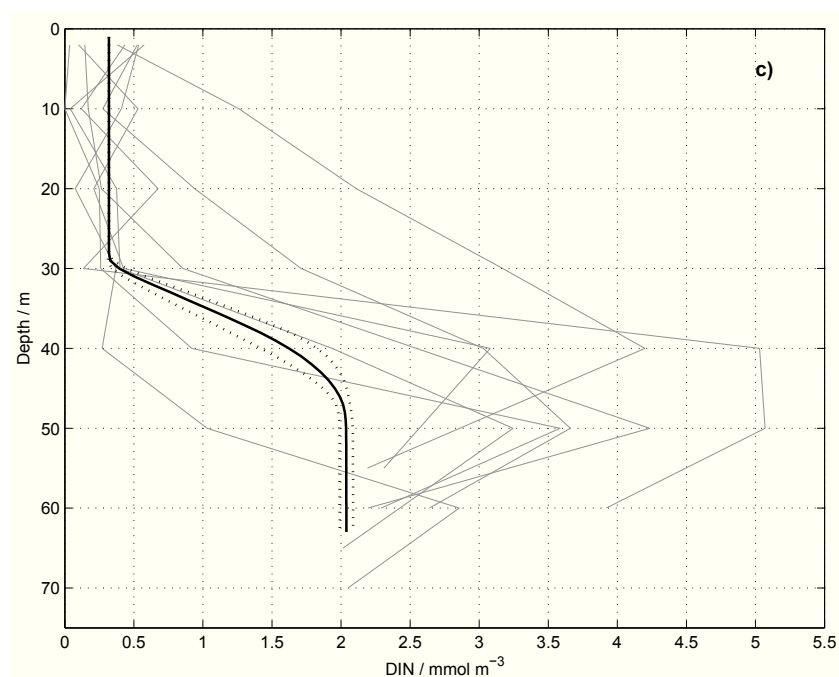


**Figure S2:** Continued.

**Table S1:** Number of pixels of surface chlorophyll concentration available for the central Beibu Gulf from SeaWiFS.

	2000	2001	2002	2003	2004	2005	2006	2007	2008	2009	2010
<b>January</b>	71	30	8	27	30	21	32	11	0	60	40
<b>February</b>	10	45	100	103	101	11	87	15	0	114	84
<b>March</b>	0	71	12	64	0	1	12	13	0	1	89
<b>April</b>	101	86	121	121	121	78	118	117	68	121	43
<b>May</b>	69	120	94	116	121	121	121	70	98	0	121
<b>June</b>	105	91	121	78	121	90	121	121	0	65	30
<b>July</b>	112	98	115	121	118	117	121	121	0	120	85
<b>August</b>	121	113	121	121	121	121	114	111	92	121	92
<b>September</b>	121	98	97	111	119	115	121	108	93	0	120
<b>October</b>	121	114	121	121	91	111	116	118	112	0	93
<b>November</b>	116	118	97	99	99	120	115	72	99	46	19
<b>December</b>	35	78	48	1	11	10	13	32	20	19	0

## 5 Sediment resuspension patterns and the diffusive boundary layer in the Beibu Gulf, South China Sea

*Bauer et al.: Manuscript*

### 5.1 Introduction

Sediment resuspension is known from all kinds of marine environments [Tengberg *et al.*, 2003] and, in addition to river discharge is, one of the important processes determining sediment concentration in the water column and hence the magnitude of suspended sediment transport [Guillén *et al.*, 2002]. Sediment stirring is naturally caused by water motion due to density differences, strong winds and tidal currents. Especially in shelf sea areas, the combination of shallow waters, strong tidal currents, wind and waves creates a complex pattern of sediment resuspension, transport and deposition dynamics [Guinder *et al.*, 2009], that are of environmental significance. Frictional effects of the water against the sea floor lead to a shear stress which erodes and resuspends sediments into the water column after exceeding a critical value [Yuan *et al.*, 2009].

The interaction of tidal and wind-induced flow with the bottom roughness is responsible for the turbulence at the seabed which results in a tidally driven boundary layer, providing a significant interface between the seabed and the water column for the exchange of particles, nutrients and organisms [Grant and Madsen, 1986; Werner *et al.*, 2003]. This layer is also important for the longshore near-coast transport of pollutants, for example, oil spill originating from accidental leakages [Holmedal and Myrhaug, 2008]. Furthermore, this flow may determine conditions for phytoplankton growth and transport in the ocean [Holmedal and Myrhaug, 2008]. The thickness of the bottom boundary layer depends on the current strength, bottom roughness and vertical stratification

[Werner *et al.*, 2003]. As a result, particles, depending on their grain size, weight, sorting, degree of compactness and the acting current strength, are transported along the sea floor by currents [Tengberg *et al.*, 2003] over varying distances. Fine sediments like clay and silt will be already eroded under weak flow conditions whereby coarse sediments keep undisturbed. Other mechanisms resuspending sediments are bioresuspension and bioturbation, induced by animals actively moving particles [Graf and Rosenberg, 1997] and anthropogenic perturbations like trawling, dredging [Tengberg *et al.*, 2003], sand mining and land reclamation.

Concentrations of SPM in the water column vary on different time scales, as a result of fluctuations in river discharge, the prevailing hydrodynamics or throughout a tidal cycle [Velegarakis *et al.*, 1997]. The specific role of tidal flows causing sediment resuspension arise from the flow structure as it is determined by periodical acceleration and deceleration [Grant and Madsen, 1986]. Velegarakis *et al.* [1997] showed that the SPM concentrations in the water column are significantly varying throughout the tidal cycle caused by horizontal advection and vertical material exchange (resuspension and deposition). In general, the tide-induced shear stress near the bottom increases shoreward; the sediment grain size usually becomes coarser in the same direction [Guillén *et al.*, 2002]. Resuspension of fine-grained sediments takes place during the energetic parts of the tidal cycle but deposition occurs only during slack water [Jago *et al.*, 1993], whereas coarse-grained sediments may be also deposited during less energetic stages of the tides [Velegarakis *et al.*, 1997]. Tengberg *et al.* [2003] reported a necessary bottom current strength of  $40 \text{ cm s}^{-1}$  to induce resuspension of fine-grained, soft and muddy sediments on the West Coast of Sweden.

The importance of the sediment resuspension lies, first of all, in the sediment transport itself which is crucial for the understanding of geological records [Grant and Madsen, 1986]. Coupled with the sediments, also deposited pollutants, benthic fluff, which is organic-rich SPM of biological origin, and benthic communities (e.g. benthic foraminifera) will be mixed, resuspended, transported by currents [Grant and Madsen, 1986; Jago *et al.*, 2002] and deposited in calmer regions. A study by Tengberg *et al.* [2003] showed that resuspension also affects the fluxes of total carbonate, oxygen and nutrients from the bottom sediments into the water column due to mixing of sediment pore waters which is very important for the benthic-pelagic exchange [Jago *et al.*, 2002]. Resuspension and deposition of organic-rich SPM further moderates the redox-climate

at the seabed, controls organic matter remineralization and nutrient supply to the substrate [Jago *et al.*, 2002]. Despite an induced nutrient supply by resuspension which would enhance primary production, suspended matter concentrations may also lead to enhanced turbidity causing poor light conditions and consequently reduced photosynthesis rates.

Important for the exchange rate between the seabed and the water column is the development of a diffusive boundary layer (DBL). This sediment-water interface, with a thickness of a few millimeters to centimeters, is formed due to friction retard of the water movement at the seabed, depending on sediment surface roughness, resulting in dominating viscous forces and a velocity approaching to zero [Jørgensen and Des Marais, 1990]. Hence, the DBL can influence biogeochemical cycles by allowing fluxes of dissolved reactive compounds, nutrients and gases across the sediment-water interface through molecular diffusion [Jørgensen and Des Marais, 1990; Santschi *et al.*, 1991; Kelly-Gerreyn *et al.*, 2005]. By altering the diffusion time through the DBL, changes in thickness, due to different current speeds, influence reaction rates in the sediment, such as oxidation of organic matter, denitrification and sulphate reduction [Kelly-Gerreyn *et al.*, 2005], which may have consequences for nutrient and carbon budgets.

Aim of this study is to characterize bottom currents and associated sediment resuspension as well as to determine different thicknesses of the DBL during tidal stages at various stations in the eastern Beibu Gulf in September/October 2009.

As a semi-enclosed shallow shelf sea, the Beibu Gulf is mainly governed by strong monsoon winds and tides, both responsible for strong currents and the cyclonic circulation pattern [e.g. Wu *et al.*, 2008], affecting resuspension, transport and deposition processes. Although many geological surveys have been done in this region in the past, until now, only limited knowledge exist about tide- and wind-induced resuspension dynamics, which is important to understand recent sedimentation patterns and geochemical processes near and in the seabed. This work is particularly important as a fundamental research of the relationship between currents and sediment dynamics in the Beibu Gulf and hence crucial for further geochemical investigations on element and energy fluxes within the small-scale DBL.

Bauer *et al.* [in press] demonstrated that the eastern Beibu Gulf can be partitioned into four zones for the study period, related to hydrography, water column biogeochemistry, sediment properties and deposition. A coastal zone exists in the north and along Hainan

Island west coast. One zone lies in the vicinity of the Qiongzhou Strait, an important passage for water exchange with the south-east China coast. The central Beibu Gulf represents the third and the transition area between Beibu Gulf and SCS waters in the southern part of the Gulf the fourth zone. These zones will be used to provide a more comprehensive picture of resuspension processes during the study period.

## **5.2 Material and methods**

### **5.2.1 Current records and their analysis**

Current velocity profiles were recorded using a ship-mounted ADP (SonTek, 500 kHz) during the FENDOU 5 cruise in September/October 2009 (Fig. 5.1). The ADP uses the so-called Doppler shift to measure current velocity. The system is equipped with three transducers having different orientations and generating a narrow beam of sound that is projected through the water column and reflected or "scattered" from particles (SPM, organic matter, air bubbles, [SonTek/YSI, 2005]). The measured current velocities for each of the transducer are transformed into "East-North-Up" coordinates by the ADP system. Current velocity and direction profiles were recorded every 10 or 30 s with a vertical resolution of 1 m. As the measurements took place on a moving vessel the ADP was set to the bottom-track mode to remove vessel motion and to obtain the absolute water current speed and direction. An echo intensity (beam 1-3) exceeding a value of 100 indicates the bottom. All profiles has been cut at this value.

To obtain mean, minimum and maximum velocities influencing the water column and sediment sampling the bottom current records from the ADP measurements were averaged for a 10 km radius around the position of each station (Fig. 5.1).

To calculate the geostrophic currents between adjacent stations first the geopotential anomaly of each station has been computed by integrating the specific volume anomaly upward from the bottom after *Pond and Pickard* [1983] using depth profiles of temperature, salinity and pressure. The geostrophic velocity was then computed after *Mascarenhas Jr. et al.* [2004] depending on pressure, the distance between two stations, the Coriolis parameter and the latitude.

To investigate the penetration depth of the wind forcing and its effect on the measured currents the Ekman depth and velocity has been calculated. For this, daily surface u- and

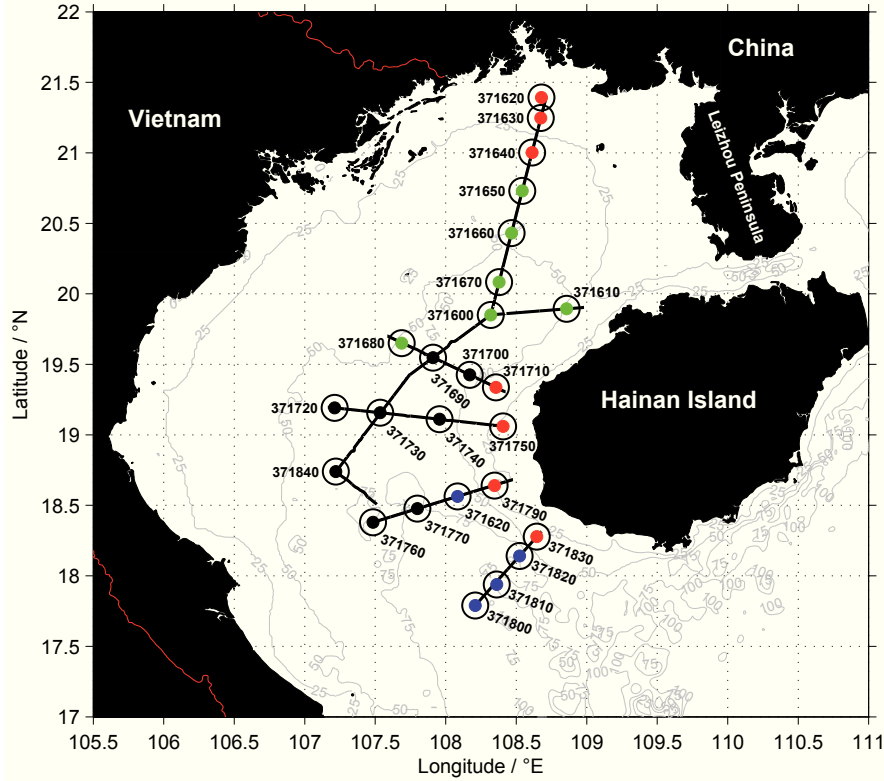


**Figure 5.1:** ADP lines (black) and stations for water sampling. Colors indicate the different zones distinguished by *Bauer et al.* [in press]: Beibu Gulf Coastal Zone (red), Qiongzhou Strait Zone (green), Beibu Gulf Central Zone (black) and Southern beibu Gulf Zone (blue). Black circles indicate 10 km radii for data averaging.

v-components of wind has been taken from NCEP obtained at <http://www.esrl.noaa.gov> for the study period. The NCEP Reanalysis data set [Kalnay *et al.*, 1996] has a coarse spatial resolution of  $2.5^\circ \times 2.5^\circ$ . Thus, the data grid over the Beibu Gulf has been cubically interpolated to a resolution of  $0.1^\circ \times 0.1^\circ$ . For the Ekman calculations first the surface wind stress has been computed following Alvarez *et al.* [2008] using drag coefficients as a function of wind speed taken from Gill [1982] after Smith [1980]. The Ekman depth, or the depth of frictional influence, as well as the Ekman velocities down to the Ekman depth have been calculated following Pond and Pickard [1983].

The DBL thickness (in  $\mu\text{m}$ ) is calculated by the empirical relationship after Tengberg *et al.* [2004]:  $\text{DBL} = 76.18(u_*)^{-0.933}$ ; where  $u_*$  is the shear velocity (in  $\text{cm s}^{-1}$ ) which has been computed from the current velocity ( $U_{100}$ , at a height of 100 cm above the sea

bottom) using the quadratic stress law

$$u_* = U_{100} \sqrt{C_d},$$

with the drag coefficient  $C_d = 2.5 \times 10^{-3}$  [Santschi *et al.*, 1991].

### **5.2.2 Water and sediment sampling**

Hydrographic profiling (temperature, conductivity) and water sampling were done by using an IOW mini PUMP CTD system based on *Strady et al.* [2008] at 25 stations. For the sampling of SPM 0.5-1 l sea water was low vacuum filtered through 0.7  $\mu\text{m}$  pre-weighted Whatman GF/F glass fibre filters. The filters were washed with deionized water and weighted again after drying in a compartment dryer at 60°C for 24 h. The SPM concentration is calculated from the weight difference between the empty and the loaded filter and the amount of filtered water.

Surface sediment samples at all stations were taken by a box corer. Grain size was determined using a diffraction particle size analyzer (Mastersizer 2000) at the Guangzhou Marine Geological Survey in China for a particle range from 0.01 to 2000  $\mu\text{m}$ . The sediment classification followed *Shepard* [1954] and the grain size parameters were calculated according to *McManus* [1988].

### **5.2.3 Tidal model**

To estimate the tidal stages at which the ADP lines were recorded and the stations sampled a tidal model has been set up using MATLAB. For 32 stations along the Chinese and Vietnamese coasts in the Beibu Gulf tidal levels were predicted by WXTide32 software (<http://www.wxtide32.com/>) for September/October 2009 with an interval of five minutes. The tidal levels along the coasts has been cubically interpolated over the Beibu Gulf area (16-22°N, 105-111°E) to a resolution of 0.1° x 0.1° for every time step. This allows the output of the tidal cycle at almost every location within the Beibu Gulf. To validate the predicted tides by the tidal model, a 25 h current record obtained on fixed position during the FENDOU 5 cruise for a spring-tide using the ADP (recording interval 30 or 60 s) and in parallel an Aanderaa RCM (recording interval one minute) in 50 m depth has been used.

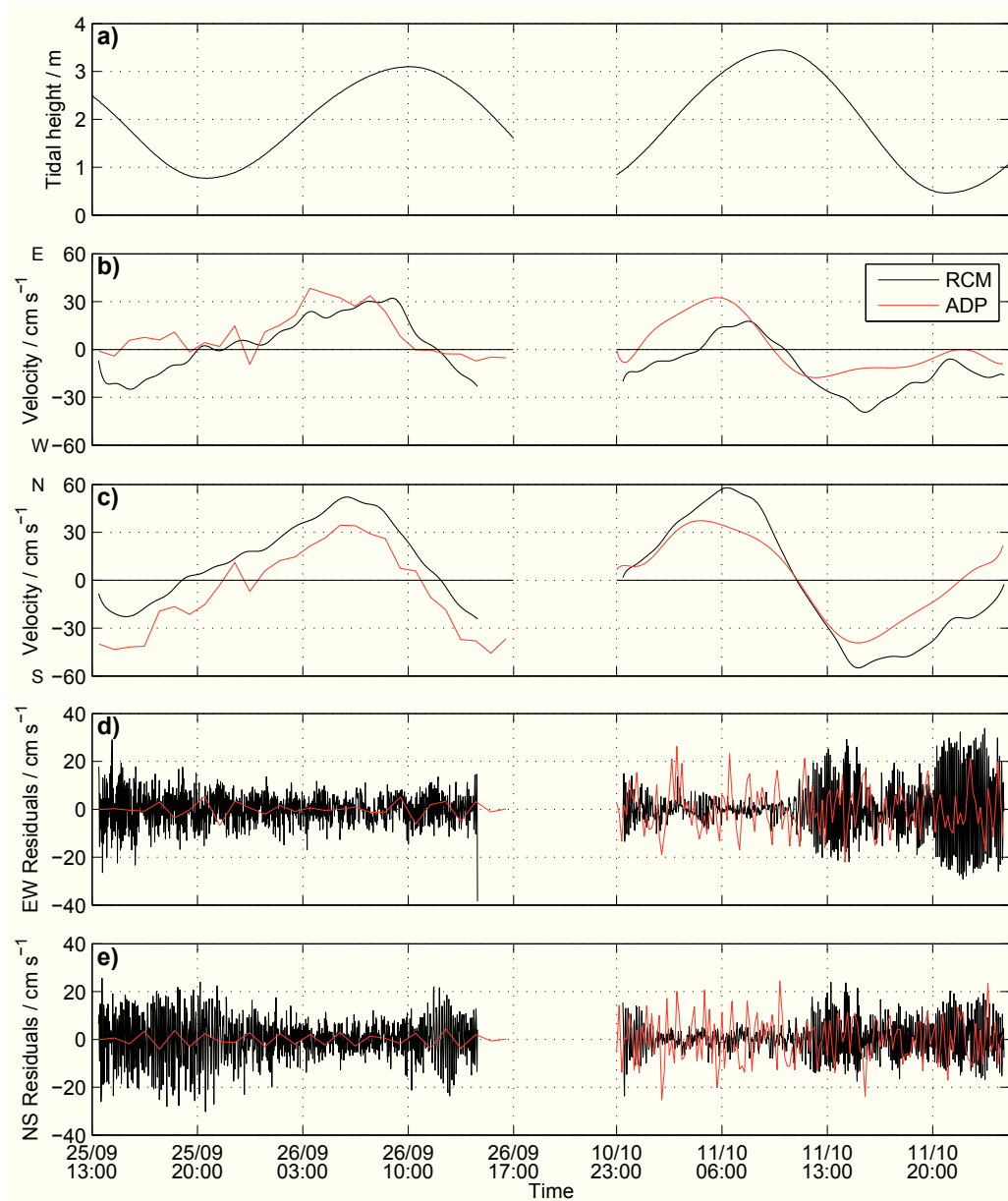


**Figure 5.2:** a) Tidal heights for the station 371600 from 25.-26.09.2009 as well as from 10.-12.10.2009 given by the tidal model (resolution five minutes). The time axis between both measurements is squeezed for graphical reasons. b) Results of the harmonically analyzed u-components of the RCM (black, resolution one minute) and ADP (red, hourly and 10-minute resolution) records in 50 m depth for the same station and the same time. c) The same as b) but for the v-components. d) Residuals for the harmonically analyzed u-components: RCM (black) and ADP (red). e) Residuals for the harmonically analyzed v-components. The different temporal resolutions of the ADP measurements cause the differences in the residuals.



The results from harmonic analysis, carried out as described by *Emery and Thomson* [2001], of the RCM and ADP current records as well as the results of the tidal model for this station are shown in Fig. 5.2. At the time of ebb and flood, indicated by the low and high water levels, respectively (Fig. 5.2a), the velocities of the current's u- and v-components are lowest (slack water), roughly zero, due to the current direction changes in this phase (Fig. 5.2b, c). During flood, the time period of rising water level, currents are north-east directed at this station, while they change to a south-west direction during ebb, when the water level falls (Fig. 5.2a-c). Incoming tidal waves propagate mainly through the southern opening from the SCS into the Beibu Gulf [e.g. *Fang et al.*, 1999; *Shi et al.*, 2002; *Chen et al.*, 2009] and are therefore north-east directed in the study area. As the graphs (water level and componential current velocity) show a good temporal agreement for the tidal phases, the model will be used for predicting tidal stages during the study period.

The directions and the times of slack water of the u- and v-components for the RCM and the ADP records correspond relatively well (Fig. 5.2b, c). Differences in the current velocities between both records arise from the different measuring methods and resolutions. Because of a gap in data within the measurements the first ADP record has been harmonically analyzed with an hourly resolution, the second one with a 10 minute resolution, whereas the RCM record has been analyzed for every minute. The residuals (tidal and non-tidal variations) shown in Fig. 5.2d/e indicate that in 50 m depth a current fraction exists which is not captured by harmonic analysis [*Boon*, 2004]. This fraction may be determined by tidal constituents which were not included in the harmonic analysis or wind effects. For the second measurement the residual curves of the ADP and RCM measurement are relatively similar. The large differences between both curves in the first measurement arise from the insufficient resolution of the ADP measurements (Fig. 5.2c, d).

From the tidal model determined tidal stages for the start and the end points of the ADP lines vary only to a small degree. Therefore, for one line, both stages were combined and taken as the tidal phase at which the ADP line has been recorded.

## 5.3 Results and discussion

### 5.3.1 Tidal cycle

For an analysis of sedimentation patterns, first, the current structure itself needs to be investigated as currents are the driving force for sediment dynamics. In the Beibu Gulf, currents in the upper water layers (15 and 35 m depth) show much higher velocities compared to the near-bottom currents in about 64 m depth, which are affected by bottom friction (Fig. 5.3).

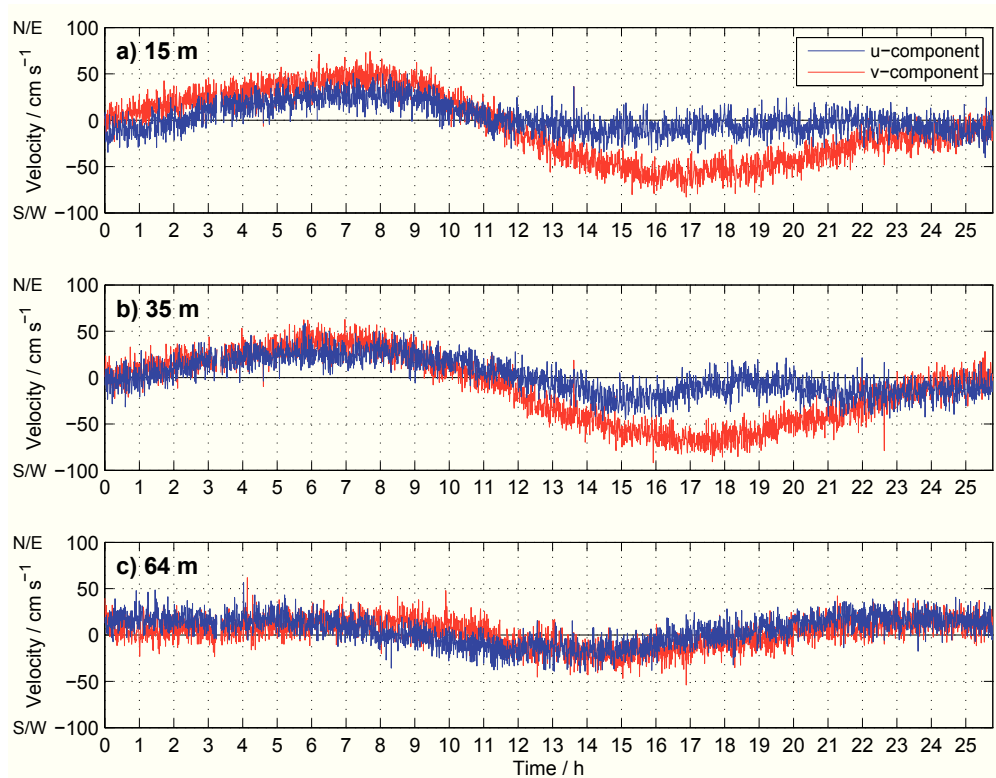


**Figure 5.3:** U (east-west) and v (north-south) current components measured with an ADP for 25 h (10.-12.10.2009) at station 371600 in a) 15 m, b) 35 m and c) 64 m depth.

At the 25 h (10.10.-12.10.2009) station 371600, mean current speeds of  $36.6 \text{ cm s}^{-1}$  for 15 m,  $38.3 \text{ cm s}^{-1}$  for 35 m and only  $20.6 \text{ cm s}^{-1}$  for 64 m depth were measured with a mean south-east current direction indicating a stronger ebb phase. While the

wind is acting on the surface inducing water movements, this effect can be transferred through friction between the water layers down to the depth. Up to which depth this influence acts (Ekman depth) depends on the strength of the wind. The surface wind, with a mean velocity of  $5.1 \text{ m s}^{-1}$  ( $u = -2.5 \text{ m s}^{-1}$ ,  $v = -4.4 \text{ m s}^{-1}$ ) over the three days leads to a calculated Ekman velocity of  $-10.4 \text{ cm s}^{-1}$  for the u-component (representing east-west) and of  $5.3 \text{ cm s}^{-1}$  for the v-component (representing north-south) at a depth of 15 m and of  $1.1 \text{ cm s}^{-1}$  and  $1.9 \text{ cm s}^{-1}$  for the u- and v-component, respectively at 35 m depth (Fig. 5.3a, b). This result shows that 32% of the currents in 15 m depth can be attributed to the wind over the measuring period. The wind's effect weakens down the water column and reduces to only 6% of the measured current velocities in 35 m depth. The calculated total geostrophic currents from/to station 371600 to/from stations 371610, 371670 and 371690 for all depths lie between  $3.9 \times 10^{-7}$  and  $1 \times 10^{-5}$ , account for a fraction far below 1% of the absolute current velocity and can therefore be neglected at all depths.

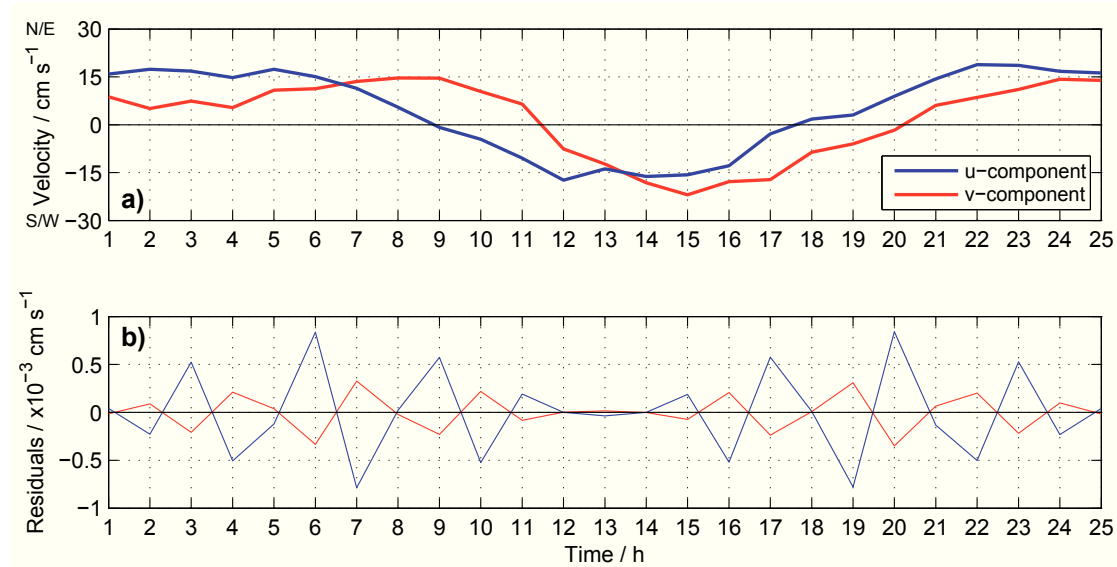


**Figure 5.4:** a) Results of the harmonic analysis of the ADP bottom current measurement (hourly resolution) for a 25 h period (10.-12.10.2009). b) Residual currents of the harmonic analysis.

As the mean Ekman depth reaches  $37.7 \pm 14.5 \text{ m}$ , all current records below can be assumed to be less affected by wind forcing during this measurement. Hence, the currents in 64 m depth may be mainly affected by tidal forcing (Fig. 5.3c), which is corroborated

by the harmonic analysis of hourly averaged values of this tidal record, describing the tidal influence (Fig. 5.4a).

For the 25 h cycle, the mean tidal contribution to the near-bottom current velocity accounts for almost 100% for the u- and v-component. The residuals are very small, in the order of  $10^{-3} \text{ cm s}^{-1}$ , and therefore can be neglected as they do not significantly contribute to the total currents (Fig. 5.4b).

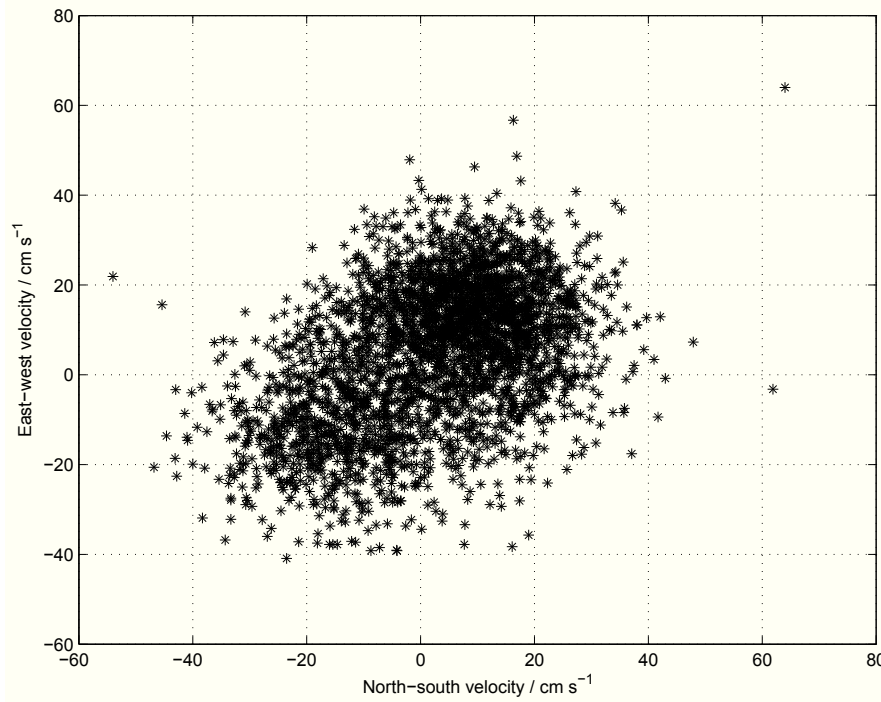


**Figure 5.5:** Bottom north-south versus east-west velocity at station 371600.

The zonally mean Ekman depths, averaged over all days sampling took place in each zone, of  $17 \pm 9$  m in the Beibu Gulf Central Zone (BGCEZ) with water depths between 45-50 m and of  $10 \pm 7$  m in the Southern Beibu Gulf Zone (SBGZ) with depths of 57 to 94 m [Bauer *et al.*, in press] indicate that the wind did not affect bottom currents causing sediment resuspension itself, due to wave action, in these regions. In contrast, in the Qiongzhou Strait Zone (QSZ) with a depth range between 36-42 m the mean Ekman depth of  $34 \pm 19$  m could have reached the bottom similarly to the Beibu Gulf Coastal Zone (BGCoZ), which shows a depth of 12-30 and an Ekman depth of  $23 \pm 1$  m in the north and a depth between 25 and 35 m [Bauer *et al.*, in press] in the east part of the Beibu Gulf and during the sampling period in this zone an Ekman depth of  $15 \pm 8$  m.

At the bottom, the maximum velocities measured during the ebb (south-west directed) are slightly larger than the maximum velocities of the flood (north-east directed, Fig. 5.3c). In general, for the 25 h period, the current velocities for all tidal phases do not show great differences between the north-south and east-west components for currents not influenced by wind driven velocities (Fig. 5.5). The main fraction of the current velocities is between  $-30$  and  $30 \text{ cm s}^{-1}$  for both components, with values ranging from  $-41$  to  $64 \text{ cm s}^{-1}$  for the  $u$ -component and from  $-54$  to  $64 \text{ cm s}^{-1}$  for the  $v$ -component (Fig. 5.5).

### 5.3.2 Sedimentation patterns

Near-bottom SPM concentrations at all stations were between  $0$  and  $9.6 \text{ mg l}^{-1}$  during the observation (Fig. 5.6). A dependence on the tidal phases as well on the zones determined by *Bauer et al.* [in press] can not be distinguished, as high and low SPM concentrations are measured everywhere at all times (Fig. 5.6). On average, the SPM concentrations measured in the BGCoZ, BGCoZ and SBGZ differ only slightly ( $3.8$ – $4.4 \text{ mg l}^{-1}$ ), whereby the QSZ shows the lowest concentration of about  $1.6 \text{ mg l}^{-1}$  (Fig. 5.6a).

It has been shown that horizontal advection and vertical exchanges of material (resuspension and deposition) contributing to temporal variations in SPM concentrations, are associated with tidal-current fluctuations [*Velegarakis et al.*, 1997]. SPM moves near the seabed in clouds with different sizes [*Yuan et al.*, 2009]. In the Beibu Gulf the mean SPM concentrations are highest for ebb ( $3.7 \text{ mg l}^{-1}$ ) and lowest for slack water ( $2.8 \text{ mg l}^{-1}$ ), but differ for all tidal phases only to a minor degree (Fig. 5.6b). Apparently, currents in the Beibu Gulf are strong enough leading to sediment resuspension and the establishment of a near-bottom resuspension layer existing throughout. Such a pattern has been observed for the western Yellow Sea, where small particle clouds, consisting of silts and clays, were found to be existent throughout two semi-diurnal tidal cycles near the seabed [*Yuan et al.*, 2009].

The measured SPM concentrations do not need to be induced by near-bottom currents acting on the seabed directly during the sampling. They are rather a reflection of the previous tidal cycles and current strengths, influence of strong winds (typhoons), water mass transport from/to other regions including river discharge, especially in coastal re-

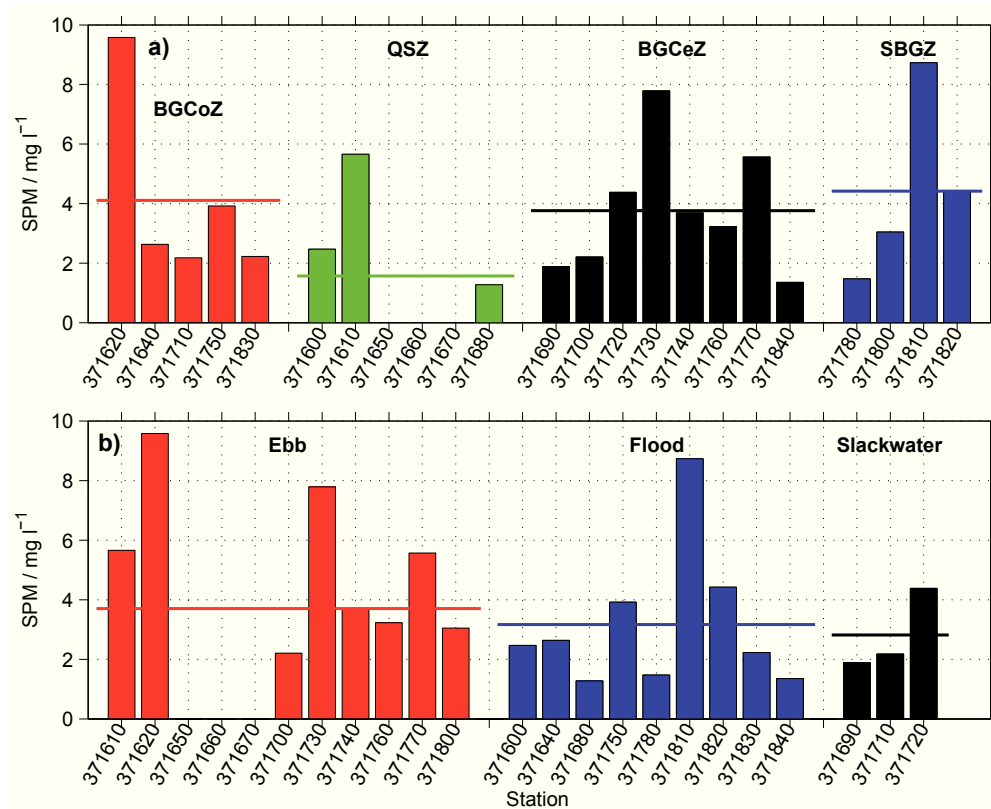


**Figure 5.6:** Near-bottom SPM concentrations (mg l<sup>-1</sup>) measured at stations a) in the Beibu Gulf Coastal Zone (BGCeZ), Qiongzhou Strait Zone (QSZ), Beibu Gulf Central Zone (BGCoZ) and Southern Beibu Gulf Zone (SBGZ) and b) during different tidal phases (ebb, flood, slack water). The horizontal lines indicate mean values for the respective groups.

gions, and the sediment grain size. The total amount of flow transported suspended load is larger if the sediment grain size available for resuspension is smaller [Hoitink and Hoekstra, 2005]. According to the resuspended particle size, the material needs some time to deposit again. But not only sediments contribute to SPM, also, for example, phytoplankton blooms, enhancing particle agglutination and hence the settling velocity, as well as zooplankton, egesting faecal pellets [Krivtsov *et al.*, 2009]. Especially the fine-grained deposition of biological origin, the benthic fluff, may be resuspended more easily also during weaker currents [Velegarakis *et al.*, 1997]. For the Beibu Gulf, relatively high plant pigment contents in the surface sediments and an increased water column chlorophyll concentrations near the bottom were found, indicating that these

biogenic deposits has been resuspended [Bauer *et al.*, in press].

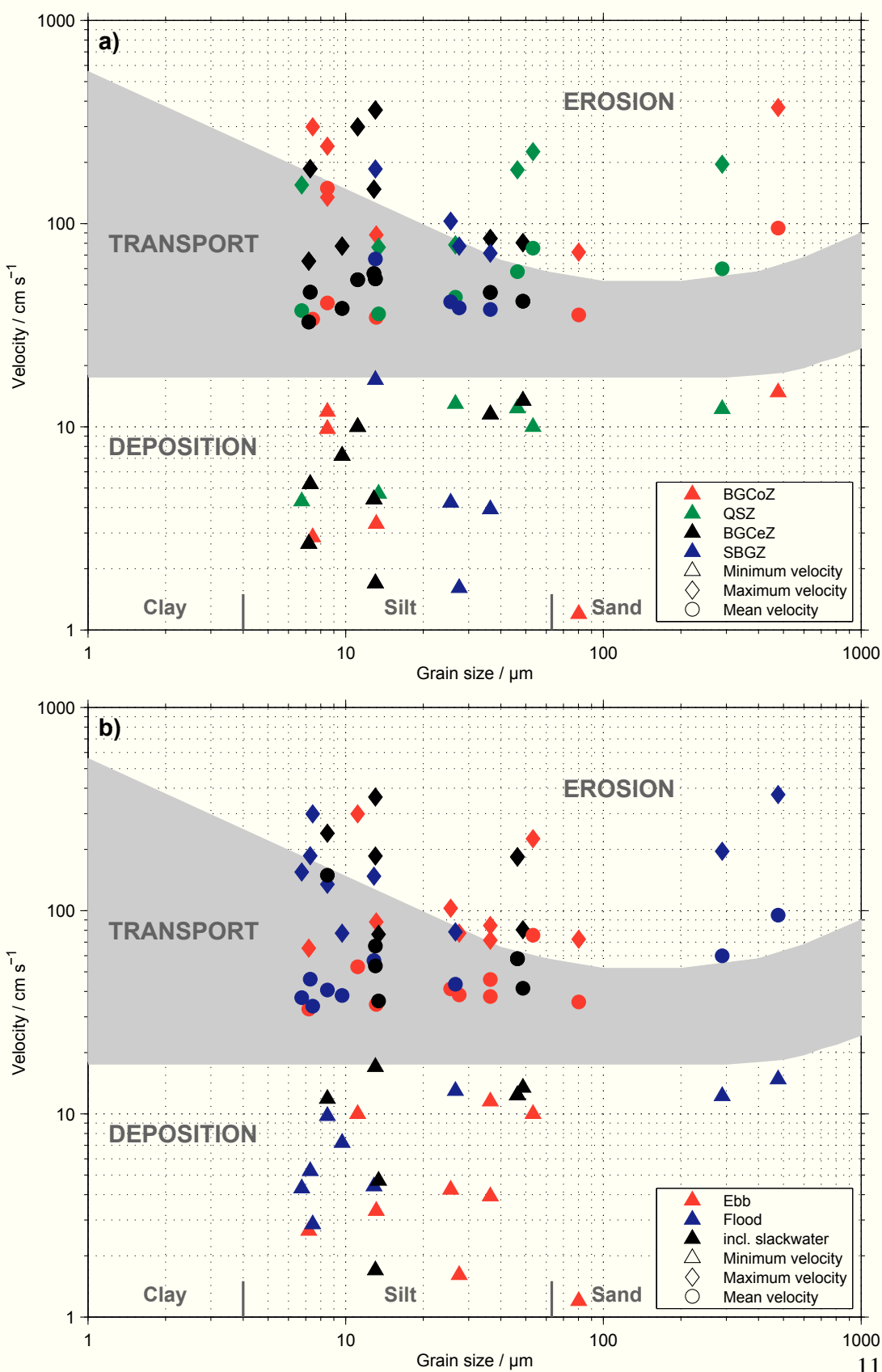
Fine-grained material can be comparatively easily resuspended by tidal flows [Hoitink and Hoekstra, 2005]. In general, sediments in the Beibu Gulf are relatively fine, with a grain size between 7 and 500  $\mu\text{m}$ , mainly consisting of silt and clay.

Depending on the grain size and the currents acting on the sea bed, sediments are deposited, transported or eroded. The relationship between the current strength and the sediment grain size, allowing to decide if sediment deposition, transport or erosion occurs, is described by the Hjulström diagram (Fig. 5.7). According to this diagram, deposition takes place during lowest current velocities ( $<18 \text{ cm s}^{-1}$ ), which were recorded during all current measurements around the stations and during all tidal phases (Fig. 5.7a, b).

For most stations in all zones the mean current velocity leads to a sediment transport and shows similar values. The relatively similar mean currents for all stations indicate low variability of the near-bottom current velocities within the study area in respect to the different zones. For three stations, belonging to the BGCoZ and QSZ, relatively large grain sizes (50-480  $\mu\text{m}$ , silty sand to sand) in combination with relatively high mean velocities (60-95  $\text{cm s}^{-1}$ ) result in sediment resuspension (Fig. 5.7a). Although at one station in the BGCoZ (371750) the highest mean velocity of about 149  $\text{cm s}^{-1}$  is recorded, due to the small grain size of 8  $\mu\text{m}$  (clayey silt), at this station only sediment transport may occur. For this station, located at Hainan Island's west coast where maximum tidal currents (on average 40-50  $\text{cm s}^{-1}$ ) has been reported [Hu *et al.*, 2003], a current velocity of about 180  $\text{cm s}^{-1}$  would be necessary for sediment resuspension which is not reached during the sampling period. The finer the sediments, stronger currents are needed for erosion, due to stronger cohesiveness between the particles [Seibold

---

**Figure 5.7 (following page):** Hjulström diagram [Hjulström, 1935] showing the relation between near-bottom currents and the sediment grain size deposition, transport (grey area) and erosion (after Sundborg [1956] and Seibold and Berger [1996]). a) All stations sampled during the FENDOU 5 cruise in September/October 2009 are color coded according to the zones defined by Bauer *et al.* [in press]: Beibu Gulf Coastal Zone (BGCoZ), Qiongzhou Strait Zone (QSZ), Beibu Gulf Central Zone (BGCoZ) and Southern Beibu Gulf Zone (SBGZ). b) Colors indicate the tidal phase of the ADP records around every station. Symbols indicate minimum, maximum and mean current velocities around the respective station.





and Berger, 1996] which is indicated by the leftward sloping grey area in the Hjulström diagram (Fig. 5.7). To resuspend clay a current velocity between 250-560 cm s<sup>-1</sup> is necessary, compared to 58-250 cm s<sup>-1</sup> for silt and 52-58 cm s<sup>-1</sup> for fine sand.

Maximum currents (up to 372 cm s<sup>-1</sup>), strong enough to erode, are recorded in all zones, for stations with finer and coarser surface sediments (Fig. 5.7a), indicating a possible resuspension pattern also for stations with fine-grained sediments (fine silt) in the course of a tidal cycle. In the Beibu Gulf during all tidal phases current speeds leading to deposition, transport and erosion of the sediments has been observed (Fig. 5.7b). According to the results of Yu *et al.* [2011] obtained at one station in the southern Beibu Gulf, the suspended sediment concentration increases with increasing ebb as well as flood flows. Peak and minimums in suspended sediment concentration were measured during maximum currents and slack water, respectively. This coincides with our results, as sediment resuspension mostly takes place for the maximum currents and minimum currents contribute to sediment deposition. During spring tides, the suspended sediment consists of very fine sand, during neap tides of very coarse silt [Yu *et al.*, 2011] in the southern Beibu Gulf. Based on our data, however, no final conclusions can be made about the relationship of spring-neap currents and sediment grain size, as all stations were sampled for different points in time of a spring-neap tidal cycle during the FENDOU 5 cruise.

It should be noted that the maximum as well as the minimum values are only measurements representing a single point in time. If and to what extend sediments are resuspended or deposited depends also on the acting time of minimum and maximum current velocities. Further, the proportion of fine and coarse sediments determines as well a potential resuspension effect. The sediments in the Beibu Gulf contain different clay/silt/sand-ratios (for a comparison of the zonal mean ratios see chapter 3). Hence, the used grain size mirrors this composition only roughly. In the Beibu Gulf the sediment dynamics is mainly driven by tidal currents [cf. Yu *et al.*, 2011]. The region seems to be highly variable with tidal currents not necessarily leading to sediment resuspension but on average to a sediment transport within all zones (Fig. 5.7a, b). Also deposition takes place in all zones during periods of low current speeds (Fig. 5.7a, b). Based on the Ekman depth, at stations in the BGCoZ and the QSZ also the wind could have contributed to the measured current velocities and intensified those, especially during typhoons, which have the potential to influence the entire water column.

### 5.3.3 Diffusive Boundary Layer

According to *Kelly-Gerreyn et al.* [2005] a DBL may establish only for current velocities below  $8 \text{ cm s}^{-1}$ . For an entire tidal cycle (25 h, hourly averaged) 24% of the u-component and 44% of the v-component currents may allow a DBL to develop (Fig. 5.8).

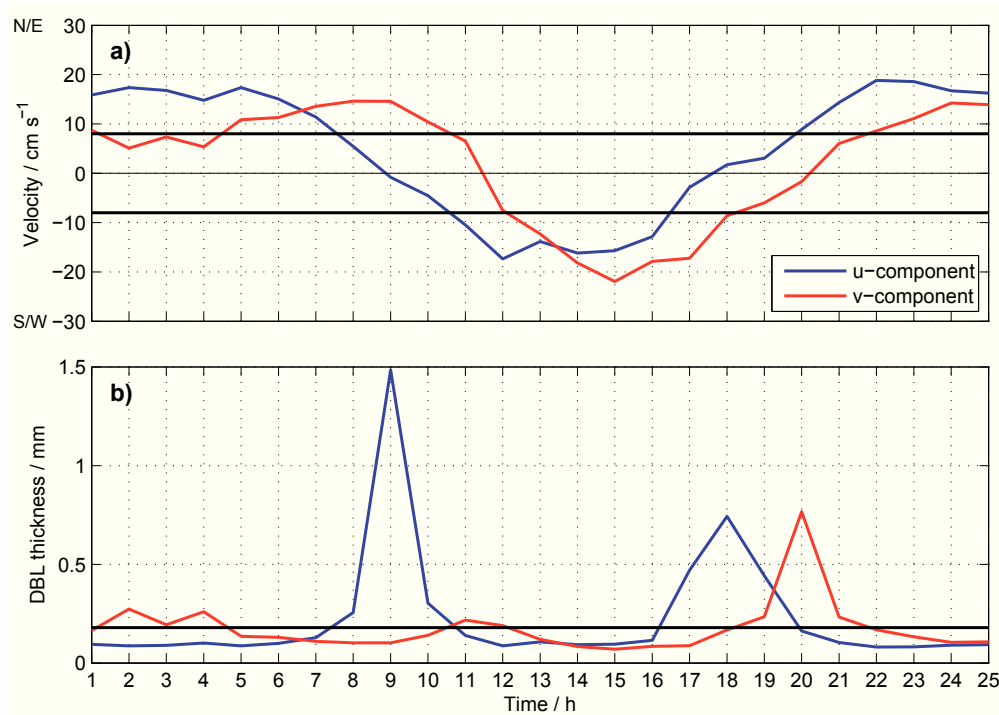


**Figure 5.8:** a) Hourly averaged current velocity u- and v-components ( $\text{cm s}^{-1}$ ) and b) the calculated DBL thickness (mm) for these velocities. The black horizontal lines in a) indicate the  $-8$  to  $8 \text{ cm s}^{-1}$  range for which the establishment of a DBL is possible, and in b) indicates the respective DBL thickness for a current velocity of  $8 \text{ cm s}^{-1}$ . Thicknesses below  $0.18 \text{ mm}$  are artificial.

These results are comparable to 31% of the current velocities for which DBLs can be determined given by *Kelly-Gerreyn et al.* [2005] for a 3.5 months sampling period in Southampton Water (UK). Although the velocities for the v-component currents are more often between  $-8$  and  $8 \text{ cm s}^{-1}$ , low u-component velocities lead to thicker DBLs (Fig. 5.8a). The DBL may establish mainly around the slack water phase, when currents tend to reach  $0 \text{ cm s}^{-1}$ , but also during flood (hour 2-4) velocities lower than  $8 \text{ cm s}^{-1}$

were detected and may lead to DBL establishment (Fig. 5.8b).

At all stations, the mean and maximum velocities show values greater than  $8 \text{ cm s}^{-1}$  during the sampling period, indicating that in the Beibu Gulf the mean currents and the currents for high energetic tidal phases are too strong for establishment of a DBL (Fig. 5.9a). The required low velocities were measured for the minimum currents at only 13 stations (Fig. 5.9b).

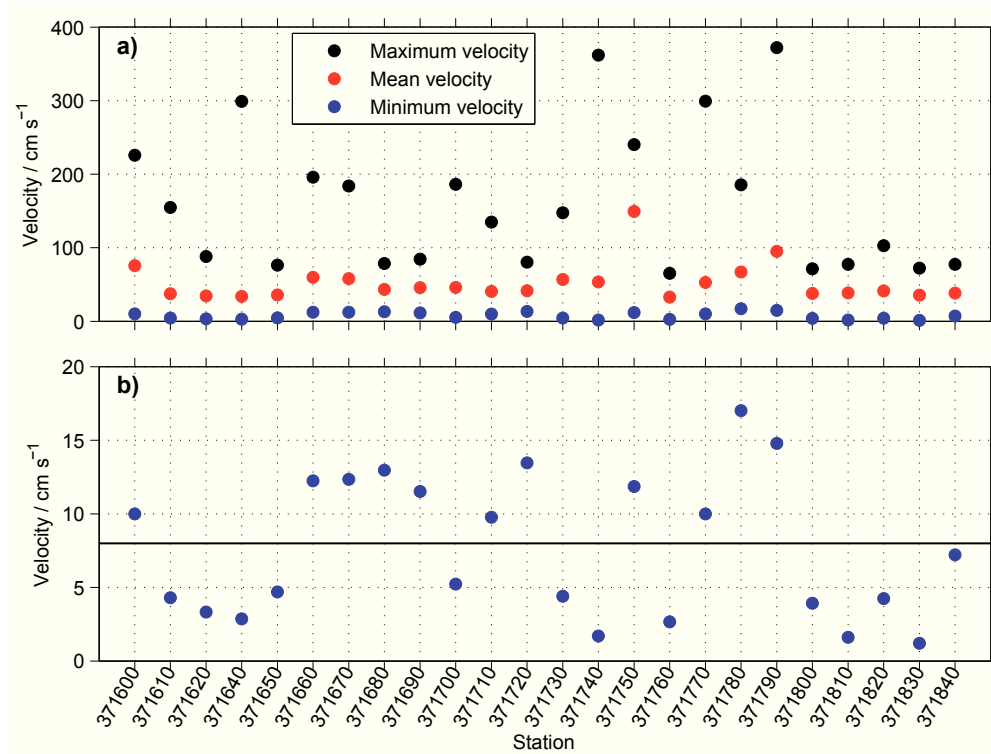


**Figure 5.9:** a) Maximum, mean and minimum near-bottom velocities for all stations. b) Minimum near-bottom velocities for all stations. The black horizontal line indicates the  $8 \text{ cm s}^{-1}$  velocities below which DBLs can become established.

The thickness of the DBL depends directly on the near-bottom current velocity: the stronger the currents the thinner is the DBL due to a higher bottom stress [Jørgensen and Des Marais, 1990; Tengberg *et al.*, 2004]. The calculated thicknesses of the DBLs lie between 0.19 and 1.05 mm for current velocities between  $7.2$  and  $1.2 \text{ cm s}^{-1}$  (Fig. 5.10). These thicknesses are consistent with those determined by Santschi *et al.* [e.g. 1983, 1991]; Jørgensen and Des Marais [e.g. 1990] and Kelly-Gerreyn *et al.* [2005] ranging between 0.1 to 1.2 mm. It should be noted that the calculation of the DBL by using

bottom-near current data (1 m above the seabed) is likely to underestimate the DBL thicknesses, as the direct bed shear velocity cannot be determined [Kelly-Gerreyn *et al.*, 2005] and may differ from those 1 m above.

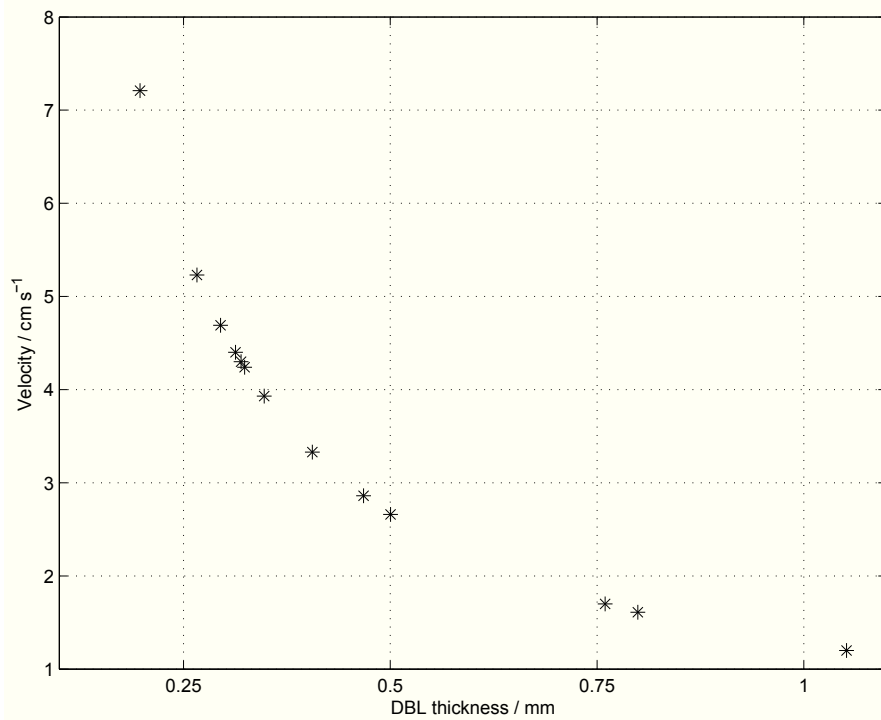


**Figure 5.10:** DBL thicknesses (mm) against the current velocities ( $\text{cm s}^{-1}$ ) for the stations with a minimum velocity below  $8 \text{ cm s}^{-1}$ .

Regionally, the stations where a DBL may occur are distributed over the entire study area (Fig. 5.11). Especially in the northern, the deeper middle and southern parts of the gulf DBLs are established. Greatest thicknesses are calculated for the southern and central part with values between 0.76 and 1.05 mm (Fig. 5.11). The highest mean DBL values are calculated for the BGCoZ (0.64 mm), followed by the SBGZ (0.49 mm) and the BGCoZ (0.41 mm, Fig. 5.12a).

In the BGCoZ most stations with a DBL are found (Fig. 5.12a). An only low mean thickness of around 0.31 mm is calculated for the QSZ. The division into tidal phases shows a highest mean DBL thickness of 0.57 mm for the ebb, followed by the slack water phase with 0.53 mm and the flood with 0.31 mm (Fig. 5.12b). The most and thickest DBLs are found for ebb indicating that during this phase the lowest current

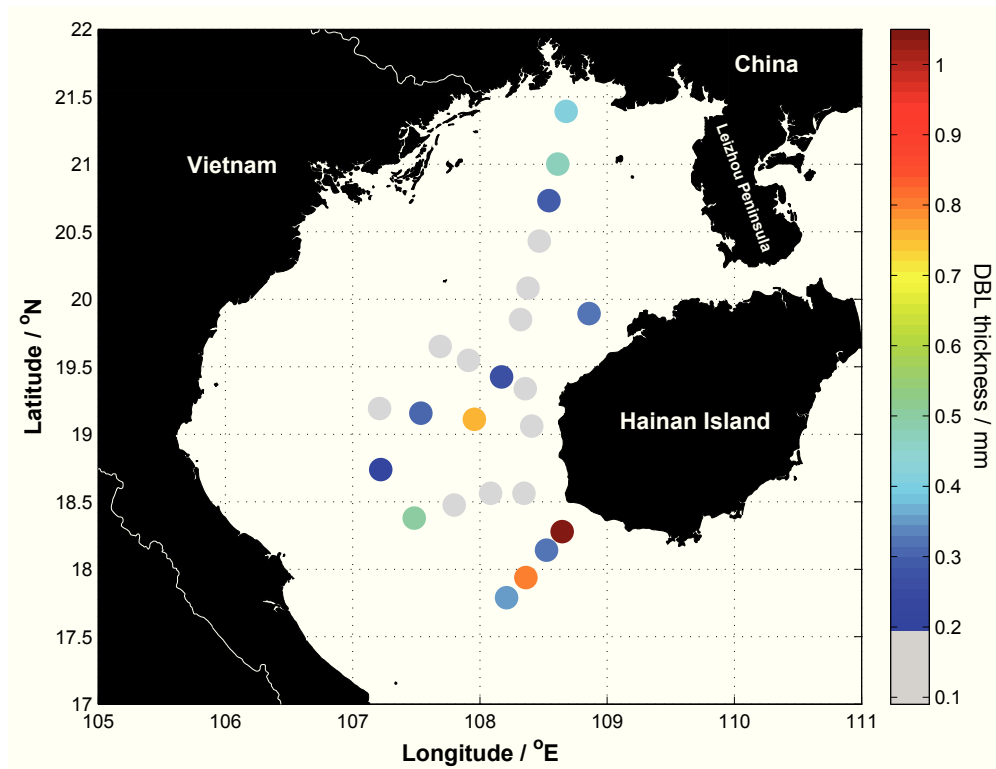


**Figure 5.11:** Spatial distribution of the calculated DBL thicknesses. The gray dots indicate stations at which the minimum current velocity exceeds  $8 \text{ cm s}^{-1}$  and hence no DBL has been calculated for.

velocities were measured during the sampling period. With a thickness of 0.76 mm during the slack water phase a strong DBL is found (Fig. 5.12b).

An unrestricted exchange of compounds, nutrients and gases over the sediment-water interface takes place while a DBL is absent, because this layer constitutes a barrier to mass transfer [Jørgensen and Des Marais, 1990]. In the Beibu Gulf this condition is given for most of the tidal cycle (56-76%) and for half of the sampled stations in all zones and for all tidal phases. As the 25 h currents were recorded during spring tide, which possibly leads to higher velocities compared to a neap tide, also velocities for a neap tide need to be investigated for a full understanding of the tides contribution on the DBL development.

Modeling results of Kelly-Gerreyn *et al.* [2005] showed lower oxygen fluxes across the sediment-water interface for simulations including a DBL (0.1-1 mm) compared to simulations without a DBL. Jørgensen and Des Marais [1990] found that with increas-

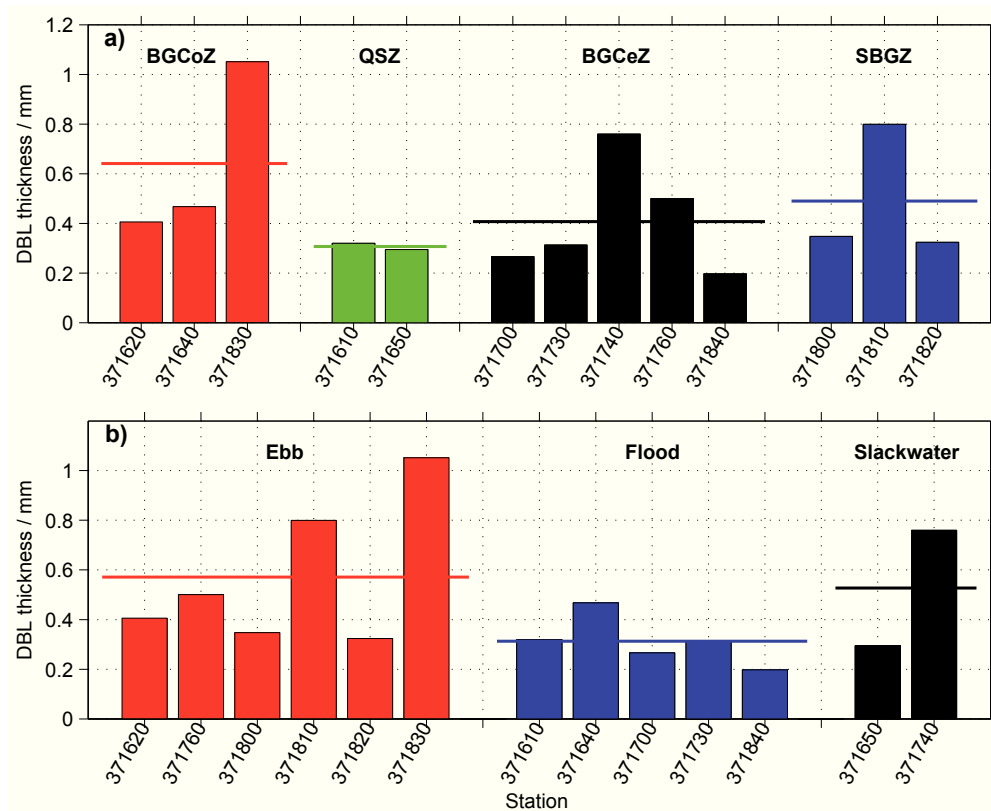


**Figure 5.12:** Calculated DBL thicknesses for stations a) in the Beibu Gulf Coastal Zone (BGCoZ), Qiongzhou Strait Zone (QSZ), Beibu Gulf Central Zone (BGCeZ) and Southern Beibu Gulf Zone (SBGZ) and b) during different tidal phases (ebb, flood, slack water). The horizontal lines indicate mean values for the respective groups.

ing flow velocities the oxygen concentration at sediment surface algal mats increase, as well as the oxygen penetration. For the Beibu Gulf this leads to the assumption that for 56-76% of the tidal currents a high oxygen flux across the sediment-water interface is possible and may lead to well aerated sediments. However, the oxygen uptake rate of aquatic sediments depends on the oxygen concentration of the overlying water and sediment stirring determined by the flow velocity *Jørgensen and Des Marais* [1990]. But not only the presence of a DBL influences fluxes across the sediment-water interface, also the thickness is of importance for chemical reactions and exchange processes. Thicker DBLs lead to a decrease in oxygen, ammonium, nitrate and sulphate fluxes across the sediment-water interface [*Kelly-Gerreyn et al.*, 2005]. The restricted oxygen fluxes reduce rates of organic carbon degradation, which implies that the DBL

contributes to the organic carbon preservation especially when the organic reactivity is high [Kelly-Gerreyn *et al.*, 2005]. High surface sediment pigment contents, indicating a high organic matter input, are found in the BGCoZ, the QSZ and the BGCoZ [Bauer *et al.*, in press]. Although the organic matter content is high in the BGCoZ, due to the high thickness of the mean DBL the oxygen fluxes are reduced and lead to a lower rate of organic carbon degradation in contrast to the QSZ, showing highest sediment pigment contents and thinnest DBLs. This coincides with the results by Xia *et al.* [in press] showing slightly lower TOC contents (zonally averaged) in the surface sediments of the BGCoZ, compared to the QSZ. Temporally, a thin mean DBL is found for the flood (Fig. 5.12), a thick one for the ebb, indicating that oxygen fluxes and hence organic carbon degradation are higher during flood compared to the ebb phase. It is still to be clarified whether the period a DBL establishes is sufficient for those processes. At this point, a combination of the obtained results with geochemical data for the Beibu Gulf is necessary for the understanding of organic matter degradation and induced element and material fluxes.

## 5.4 Conclusions

Sedimentological and geochemical processes are substantially influenced by the different current patterns within the Beibu Gulf. Tidal forcing is the main mechanism controlling sediment deposition, transport and erosion, as wind driven and geostrophic currents contribute less to the current velocities. Apparently, in the Beibu Gulf a near-bottom resuspension layer exists permanently, caused by currents strong enough leading to resuspension, small particles with a slow settling velocity and biogenic fluff.

For the mean and minimum currents, sediment transport and deposition, respectively, take place at most stations and is possible for all tidal phases, whereas, maximum current velocities leading to sediment resuspension occurring at stations within all zone and also for all tidal phases. On average the near-bottom currents of all zones are relatively similar during our observations.

In the Beibu Gulf the exchange across the sediment-water interface is possible for most of the tidal cycle as the currents are relatively strong and DBLs, restricting exchange processes, may establish only for 24 to 44% of the tidal currents and are overall suppressed. Hence, for a time span of 56-76% of a tidal cycle a direct benthic-pelagic

coupling may exist. Within the BGCoZ lowest organic carbon degradation took place within the sampling period compared to the other zones, as the mean DBL is thickest and thereby oxygen fluxes are reduced. In the QSZ, with the thinnest mean DBL, the most degradation of organic matter took place. Although in both zones the organic matter input is high, the degree of degradation within the sediment may differ. Also the different tidal phases may lead to a varying amount of organic carbon degradation.

For a better understanding of the geochemical processes within the Beibu Gulf the obtained results need to be compared to geochemical parameters of the surface sediments. Further, long-time measurements of tidal currents at different regions in the Beibu Gulf are necessary to obtain a more detailed picture of the tidal influence on sediment deposition, transport and resuspension as well as of the currents effect on the benthic-pelagic coupling.



## Conclusions and future perspectives

The present thesis investigated the hydrographical and biogeochemical conditions in the Beibu Gulf, SCS, a shelf region playing an important role for the near-coastal terrestrial material input and thus, as a transition zone between highly populated land masses and the SCS, fluxes of material and energy into the SCS northwestern areas. So far, only limited knowledge exists about the functioning of the ecosystem "Beibu Gulf". Hence, this work contributes to our understanding of the interaction between hydrography, water column biogeochemistry and sedimentology in the Beibu Gulf.

As a first step for the understanding of the hydrodynamical and sedimentological variability of the Beibu Gulf, hydrographical profiles, water and sediment samples has been taken during a cruise in September/October 2009 and analyzed in the interdisciplinary study in the third chapter of this thesis [*Bauer et al.*, in press]:

- For the sampling period in September/October 2009 regional differences in hydrographical properties has been distinguished. Hydrographically, different zones were defined which are influenced by riverine input and tidal mixing in the coastal areas (Beibu Gulf Coastal Zone), water mass transport from the South China coastal regions through Qiongzhou Strait (Qiongzhou Strait Zone and Beibu Gulf Central Zone) as well as SCS water influence in the south (Southern Beibu Gulf Zone).
- The influence of the different water masses due to the gulf's circulation pattern, driven by monsoon winds, tidal and residual currents and the effect of a typhoon is mirrored in the biogeochemical properties of the water column (Chlorophyll, nutrients and suspended particulate matter), grain size, distribution of plant pigments (chlorophyll *a* and phaeopigments) and foraminifera in the surface sediments within the different zones.
- The surface sediment plant pigment contents as well as the geochemical sediment

properties, depend on the depositional environment and follow the pattern of surface water productivity which is highest in the Beibu Gulf Coastal Zone and the Qiongzhou Strait Zone.

- Apatite-bound phosphorous is the dominant route of phosphorus removal from the pelagic to the benthic part of the ecosystem.

Marine primary production plays an important role in biogeochemical cycling within the water column as well as in the sediments and is crucial for the oceanic carbon fixation but only little is known about the oceanic and biological processes, including variations in spatial and temporal phytoplankton distribution for the Beibu Gulf [Tang *et al.*, 2003]. An established 1D physical-biological model along with *in-situ* measurements and satellite derived surface data has been used to investigate the connection between atmospheric forcing, water column structure and primary production in the central Beibu Gulf for an 11 year period in the fourth chapter [Bauer and Waniek, 2013]:

- During summer the central Beibu Gulf is thermally stratified due to high solar radiation and relatively weak winds during southwest monsoon which leads to a nutrient depletion and hence a low primary production in the surface layer and the development of a deep chlorophyll maximum in about 20-30 m depth, where euphotic depth and nutricline co-exist. A phytoplankton bloom establishes during winter when the strong northeast monsoon acts and the water column is deeply mixed, resulting in a nutrient supply from deeper waters which are then available for phytoplankton growth. The modeled phytoplankton bloom lasts on average for 6 months.
- The interannual variability in the meteorological forcing is generally low but nevertheless lead to a variability of about 2.5 months and around 1 month in autumn/winter for the timing of stratification breakdown and the establishment of a phytoplankton bloom, respectively.
- Strong wind events like typhoons are shown to enhance the primary production temporally short by up to 275% relative to the summer background chlorophyll concentration at the surface and play therefore an important role for the primary production in the central Beibu Gulf in summer and autumn during periods of low production. Further, these events are able to initiate a phytoplankton proliferation.

- In the central Beibu Gulf the tidal forcing is relatively weak, but despite that, contributes to nutrient supply into the thermocline and leads to a significant enhancement in strength (36%) and thickness (33%) of the deep chlorophyll maximum compared to a system without tidal forcing.

Currents influence not only sediment resuspension, transport and deposition but also the exchange between the seabed and the water column through the sediment-water interface. Current records, especially bottom near, has been analyzed to investigate the current patterns during the sampling period in September/October 2009 and their effects on sediment resuspension as well as the establishment of a diffusive boundary layer in the fifth chapter.

- Tidal forcing is the main mechanism controlling sedimentation patterns as well as material and energy exchange between the sediment and the water column.
- Current velocities contributing to sediment deposition, transport and resuspension are acting in all zones and during all tidal phases (ebb, flood, slack water) for the sampling period in September/October 2009.
- In general, the strength of the currents during most of the tidal cycle (56-76%) prevents the development of a diffusive boundary layer. Therefore, an exchange of compounds, nutrients and gases across the sediment-water interface is possible. Diffusive boundary layers may establish during all tidal phases and in all zones with varying thicknesses.

The obtained results give a first insight in the functioning of the system "Beibu Gulf" but show simultaneously that there is still need for further investigations to improve the understanding of processes acting in that region. As one of the next steps in the near future, the results obtained from the current records (chapter 5) should be combined with near-bottom water column properties and geochemical parameters also gathered during the FENDOU 5 cruise. Thereby, spatial and temporal (tidal phases) differences of the physical and chemical conditions contributing to element fluxes between the water column and the sediments could be investigated for the time of observation.

In this thesis mainly *in-situ* data of the FENDOU 5 cruise (September/October 2009) were analyzed, representing the conditions during the inter-monsoon phase. For an evaluation of the role the changing wind system plays for processes in the water column and

possibly at the seabed as well as the water mass exchange with the surrounding SCS waters, it is further necessary to analyze measured properties during other monsoon phases, for example data obtained during the SONNE cruise (December 2011) characterizing the winter northeast monsoon, and for the entire gulf including the Qiongzhou Strait.

Especially for an elucidation of the gulf's circulation pattern and the importance of tides in the different zones, stationary long-time measurements at selected stations are inevitable (e.g. moorings with current meters and turbidity sensors), which are unfortunately not available at present. Such data would also contribute to the understanding of sedimentation processes and the benthic-pelagic coupling. By the help of remote sensing time series conclusions may be drawn for transport processes, circulation patterns, surface near primary production and typhoon effects, but unfortunately the measurements of bio-optical properties depend on a clear sky. Especially during southwest monsoon the immense cloud cover prevents such measurements of necessary quality for the Beibu Gulf. Hence, an intense *in-situ* sampling is essential for investigating the Beibu Gulf.

## References

- Al-Raei, A., K. Bosselmann, M. Böttcher, B. Hespenheide, and F. Tauber (2009), Seasonal dynamics of microbial sulfate reduction in temperate intertidal surface sediments: Controls by temperature and organic matter, *Ocean Dynamics*, 59(2), 351–370.
- Alvarez, I., M. Gomez-Gesteira, M. deCastro, and E. M. Novoa (2008), Ekman transport along the Galician Coast (NW, Spain) calculated from QuikSCAT winds, *Journal of Marine Systems*, 72(1-4), 101–115.
- Angove, M., and R. Falvey (2010), 2010 Annual Tropical Cyclone Report, *Tech. rep.*, U.S. Naval Pacific Meteorology and Oceanography Center / Joint Typhoon Warning Center, pp. 93.
- Anschutz, P., S. Zhong, B. Sundby, A. Mucci, and C. Gobeil (1998), Burial efficiency of phosphorus and the geochemistry of iron in continental margin sediments, *Limnology and Oceanography*, 43(1), 53–64.
- Atangan, J., and A. Preble (2005), 2005 Annual Tropical Cyclone Report, *Tech. rep.*, U.S. Naval Pacific Meteorology and Oceanography Center / Joint Typhoon Warning Center, pp. 109.
- Babin, S., J. Carton, T. Dickey, and J. Wiggert (2004), Satellite evidence of hurricane-induced phytoplankton blooms in an oceanic desert, *Journal of Geophysical Research*, 109(C3), C03043.
- Bauer, A., and J. Waniek (2013), Factors affecting chlorophyll *a* concentration in the central Beibu Gulf, South China Sea, *Marine Ecology Progress Series*, 474, 67–88.
- Bauer, A., et al. (in press), Regional differences of hydrographical and sedimentological properties in Beibu Gulf, South China Sea, *Journal of Coastal Research, Special Issue 66*, doi:10.2112/SI\_66\_5.
- Bauer, S., G. Hitchcock, and D. Olson (1991), Influence of monsoonally-forced Ekman dynamics upon surface layer depth and plankton biomass distribution in the Arabian Sea, *Deep Sea Research Part I*, 38(5), 531–553.
- Bianchi, T., S. Findlay, and R. Dawson (1993), Organic matter sources in the water column and sediments of the Hudson River Estuary: The use of plant pigments as tracers, *Estuarine, Coastal and Shelf Science*, 36(4), 359–376.
- Bianchi, T., B. Johansson, and R. Elmgren (2000), Breakdown of phytoplankton pigments in Baltic sediments: Effects of anoxia and loss of deposit-feeding macrofauna, *Journal of Experimental Marine Biology and Ecology*, 251(2), 161–183.
- Boon, J. (2004), *Secrets of the Tide*, Horwood Publishing, Chichester, UK, pp. 212.
- Böttcher, M., et al. (2000), The biogeochemistry, stable isotope geochemistry, and microbial community structure of a temperate intertidal mudflat: An integrated study, *Continental Shelf Research*, 20(12), 1749–1769.

- Boyd, P., and S. Doney (2003), The impact of climate change and feedback processes on the ocean carbon cycle, in *Ocean Biogeochemistry*, edited by M. Fasham, pp. 157–193, Springer, Berlin, Germany.
- Braeckman, U., C. Van Colen, K. Soetaert, M. Vincx, and J. Vanaverbeke (2011), Contrasting macrobenthic activities differentially affect nematode density and diversity in a shallow subtidal marine sediment, *Marine Ecology Progress Series*, 422, 179–191.
- Brzezinski, M. (1985), The Si:C:N ratio of marine diatoms: Interspecific variability and the effect of some environmental variables, *Journal of Phycology*, 21(3), 347–357.
- Cai, S., Q. Huang, and X. Long (2003), Three-dimensional numerical model study of the residual current in the South China Sea, *Oceanologica Acta*, 26(5-6), 597–607.
- Chang, J., C. Chung, and G. Gong (1996), Influences of cyclones on chlorophyll a concentration and *Synechococcus* abundance in a subtropical western Pacific coastal ecosystem, *Marine Ecology Progress Series*, 140, 199–205.
- Chen, C., P. Li, M. Shi, J. Zuo, M. Chen, and H. Sun (2009), Numerical study of the tides and residual currents in the Qiongzhou Strait, *Chinese Journal of Oceanology and Limnology*, 27(4), 931–942.
- Chen, C.-T., K.-K. Liu, and R. MacDonald (2003), Continental margin exchanges, in *Ocean Biogeochemistry*, edited by M. Fasham, pp. 53–97, Springer, Berlin, Germany.
- Chen, Y., and D. Tang (2011), Remote sensing analysis of impact of typhoon on environment in the sea area south of Hainan Island, *Procedia Environmental Sciences*, 10, 1621–1629.
- Chung, C., G. Gong, and C. Hung (2012), Effect of Typhoon Morakot on microphytoplankton population dynamics in the subtropical Northwest Pacific, *Marine Ecology Progress Series*, 448, 39–49.
- Cooper, G., and R. Falvey (2008), 2008 Annual Tropical Cyclone Report, *Tech. rep.*, U.S. Naval Pacific Meteorology and Oceanography Center / Joint Typhoon Warning Center, pp. 116.
- Cooper, G., and R. Falvey (2009), 2009 Annual Tropical Cyclone Report, *Tech. rep.*, U.S. Naval Pacific Meteorology and Oceanography Center / Joint Typhoon Warning Center, pp. 109.
- Cullen, J., and R. Eppley (1981), Chlorophyll maximum layers of the Southern California Bight and possible mechanisms of their formation and maintenance, *Oceanologica Acta*, 4(1), 23–32.
- Dai, J., X. Zhang, D. Wang, C. Guo, R. Fang, and X. Wang (2011), Water quality change of Nanliu River in Guangxi Beibu Gulf Economic Zone, *International Conference on Remote Sensing, Environment and Transportation Engineering (RSETE)*, Nanjing, pp. 5629–5632.
- de Haas, H., T. van Weering, and H. de Stigter (2002), Organic carbon in shelf seas: Sinks or sources, processes and products, *Continental Shelf Research*, 22(5), 691–717.
- De Jonge, V., and M. Engelkes (1993), The role of mineral compounds and chemical conditions in the binding of phosphate in the Ems estuary, *Aquatic Ecology*, 27(2), 227–236.
- Dellwig, O., T. Leipe, C. März, M. Glockzin, F. Pollehne, B. Schnetger, E. Yakushev, M. Böttcher, and H.-J. Brumsack (2010), A new particulate Mn-Fe-P-shuttle at the redoxcline of anoxic basins, *Geochimica et Cosmochimica Acta*, 74(24), 7100–7115.

- Dickey, T. (1988), Recent advances and future directions in multi-disciplinary in situ oceanographic measurement systems, in *Toward a theory on biological-physical interactions in the world ocean*, edited by B. Rothschild, pp. 555–598, Kluwer Academic Publishers, Dordrecht, Netherlands.
- Doney, S., K. Lindsay, and J. Moore (2003), Global ocean carbon cycle modeling, in *Ocean Biogeochemistry*, edited by M. Fasham, pp. 217–238, Springer, Berlin, Germany.
- Einsele, W. (1938), Über chemische und kolloidchemische Vorgänge in Eisen-Phosphat-Systemen unter limnochemischen und limnogeologischen Gesichtspunkten, *Archiv für Hydrobiologie*, 33, 361–387.
- Emery, W., and R. Thomson (2001), *Data analysis methods in physical oceanography*, 2nd revised ed., Elsevier Science, Amsterdam, Netherlands, pp. 638.
- Enge, A., et al. (2011), Response of the benthic foraminiferal community to a simulated short-term phyto-detritus pulse in the abyssal North Pacific, *Marine Ecology Progress Series*, 438, 129–142.
- Fang, G., Y.-K. Kwok, K. Yu, and Y. Zhu (1999), Numerical simulation of principal tidal constituents in the South China Sea, Gulf of Tonkin and Gulf of Thailand, *Continental Shelf Research*, 19(7), 845–869.
- Fasham, M., T. Platt, B. Irwin, and K. Jones (1985), Factors affecting the spatial pattern of the deep chlorophyll maximum in the region of the Azores Front, *Progress In Oceanography*, 14, 129–165.
- Fogel, M., C. Aguilar, R. Cuhel, D. Hollander, J. Willey, and H. Paerl (1999), Biological and isotopic changes in coastal waters induced by Hurricane Gordon, *Limnology and Oceanography*, 44(6), 1359–1369.
- Folk, R. (1954), The distinction between grain size and mineral composition in sedimentary-rock nomenclature, *Journal of Geology*, 62(4), 344–359.
- Furze, P., and G. Engel (2002), 2002 Annual Tropical Cyclone Report, *Tech. rep.*, U.S. Naval Pacific Meteorology and Oceanography Center / Joint Typhoon Warning Center, pp. 393.
- Furze, P., and A. Preble (2003), 2003 Annual Tropical Cyclone Report, *Tech. rep.*, U.S. Naval Pacific Meteorology and Oceanography Center / Joint Typhoon Warning Center, pp. 827.
- Gago, J., X. Álvarez Salgado, M. Nieto-Cid, S. Brea, and S. Piedracoba (2005), Continental inputs of C, N, P and Si species to the Ria de Vigo (NW Spain), *Estuarine, Coastal and Shelf Science*, 65(1-2), 74–82.
- Gallagher, S., M. Wallace, C. Li, B. Kinna, J. Bye, K. Akimoto, and M. Torii (2009), Neogene history of the West Pacific Warm Pool, Kuroshio and Leeuwin currents, *Paleoceanography*, 24(1), PA1206.
- Gan, J., H. Li, E. Curchitser, and D. Haidvogel (2006), Modeling South China Sea circulation: Response to seasonal forcing regimes, *Journal of Geophysical Research*, 111, C06034.
- Gill, A. (1982), *Atmosphere-Ocean Dynamics, International Geophysics Series*, vol. 30, Academic Press, London, UK, pp. 662.
- Graf, G., and R. Rosenberg (1997), Bioresuspension and biodeposition: A review, *Journal of Marine Systems*, 11(3-4), 269–278.

- Grant, W., and O. Madsen (1986), The continental-shelf bottom boundary layer, *Annual Review of Fluid Mechanics*, 18, 265–305.
- Guillén, J., J. Jiménez, A. Palanques, V. Gracia, P. Puig, and A. Sánchez-Arcilla (2002), Sediment resuspension across a microtidal, low-energy inner shelf, *Continental Shelf Research*, 22(2), 305–325.
- Guinder, V., C. Popovich, and G. Perillo (2009), Particulate suspended matter concentrations in the Bahía Blanca Estuary, Argentina: Implication for the development of phytoplankton blooms, *Estuarine, Coastal and Shelf Science*, 85(1), 157–165.
- Guo, Y. (1994), Primary productivity and phytoplankton in China seas, in *Oceanology of China Seas*, vol. 1, edited by D. Zhou, Y.-B. Liang, and C.-K. Zeng, pp. 227–242, Kluwer Academic Publishers, Dordrecht, Germany.
- Haese, R., K. Wallmann, A. Dahmke, U. Kretzmann, P. Müller, and H. Schulz (1997), Iron species determination to investigate early diagenetic reactivity in marine sediments, *Geochimica et Cosmochimica Acta*, 61(1), 63–72.
- Halim, Y. (1991), The impact of human alterations of the hydrological cycle on ocean margins, in *Ocean Margin Processes in Global Change*, edited by R. Mantoura, J.-M. Martin, and R. Wollast, pp. 301–327, John Wiley & Sons, New York, USA.
- Hansen, H., and F. Koroleff (1999), Determination of nutrients, in *Methods of Seawater Analysis*, vol. 2, edited by K. Grasshoff, K. Kremling, and M. Ehrhardt, pp. 159–228, Wiley-VCH, Weinheim, Germany.
- He, Y., and L.-Y. Hu (2001), *Pliocene foraminifers from the Leizhou Peninsula of Guangdong, China*, Press of University of Science and Technology of China, Hefei, China, pp. 189 (in Chinese).
- Hemleben, C., M. Spindler, and O. Anderson (1989), *Modern planktonic foraminifera*, Springer, New York, USA, pp. 363.
- Hjulström, F. (1935), Studies of the morphological activity of rivers as illustrated by the River Fyris, *Bulletin of the Geological Institute of Uppsala*, 25, 221–527.
- Hoitink, A., and P. Hoekstra (2005), Observations of suspended sediment from ADCP and OBS measurements in a mud-dominated environment, *Coastal Engineering*, 52, 103–118.
- Holliday, N., J. Waniek, R. Davidson, D. Wilson, L. Brown, R. Sanders, R. Pollard, and J. Allen (2006), Large-scale physical controls on phytoplankton growth in the Irminger Sea Part I: Hydrographic zones, mixing and stratification, *Journal of Marine Systems*, 59(3-4), 201–218.
- Holmedal, L., and D. Myrhaug (2008), Tidal Boundary Layers, in *Proceedings of the ASME 27th International Conference on Offshore Mechanics and Arctic Engineering*, pp. 565–570, Estoril, Portugal.
- Howard, K., and J. Yoder (1997), Contribution of the subtropical oceans to global primary production, in *Space Remote Sensing of Subtropical Oceans, Proceedings of COSPAR Colloquium on Space Remote Sensing of Subtropical Oceans (SRSSO), COSPAR Colloquia Series*, vol. 8, edited by C.-T. Liu, pp. 157–167, Pergamon.
- Hu, J., H. Kawamura, and D. Tang (2003), Tidal front around the Hainan Island, northwest of the South China Sea, *Journal of Geophysical Research*, 108(C11), 1–9.



- Huang, B., Z. Jian, X. Cheng, and P. Wang (2003), Foraminiferal responses to upwelling variations in the South China Sea over the last 220 000 years, *Marine Micropaleontology*, 47(12), 1–15.
- Huang, Q.-Z., W.-Z. Wang, Y. Li, and C. Li (1994), Current characteristics of the South China Sea, in *Oceanology of China Seas*, vol. 1, edited by D. Zhou, Y.-B. Liang, and C.-K. Zeng, pp. 39–47, Kluwer Academic Publishers, Dordrecht, Netherlands.
- Huang, Y., Y. Li, H. Shao, and Y.-H. Li (2008), Seasonal variations of sea surface temperature, chlorophyll a and turbidity in Beibu Gulf, MODIS imagery study, *Journal of Xiamen University (Natural Science)*, 47(6), 856–863 (in Chinese).
- Hyacinthe, C., and P. Van Cappellen (2004), An authigenic iron phosphate phase in estuarine sediments: Composition, formation and chemical reactivity, *Marine Chemistry*, 91(1-4), 227–251.
- Jago, C., A. Bale, M. Green, M. Howarth, I. McCave, G. Millward, A. Morris, A. Rowden, and J. Williams (1993), Resuspension processes and seston dynamics, Southern North Sea, *Philosophical Transactions of the Royal Society of London A*, 343, 475–491.
- Jago, C., S. Jones, R. Latter, R. McCandliss, M. Hearn, and M. Howarth (2002), Resuspension of benthic fluff by tidal currents in deep stratified waters, northern North Sea, *Journal of Sea Research*, 48(4), 259–269.
- Jensen, H., and B. Thamdrup (1993), Iron-bound phosphorus in marine sediments as measured by bicarbonate-dithionite extraction, *Hydrobiologia*, 253, 47–59.
- JGOFS, P. (1994), JGOFS Protocols, Protocols for the Joint Global Ocean Flux Study (JGOFS) Core Measurement, 97-100.
- Jiang, X., Z. Zhong, and J. Jiang (2009), Upper ocean response of the South China Sea to Typhoon Krovanh (2003), *Dynamics of Atmospheres and Oceans*, 47(1-3), 165–175.
- Jørgensen, B. (1982), Mineralization of organic matter in the sea bed - the role of sulfate reduction, *Nature*, 296, 643–645.
- Jørgensen, B., and D. Des Marais (1990), The diffusive boundary layer of sediments - oxygen microgradients over a microbial mat, *Limnology and Oceanography*, 35, 1343–1355.
- Jørgensen, B., and S. Kasten (2006), Sulfur cycling and methane oxidation, in *Marine Geochemistry*, edited by H. Schulz and M. Zabel, pp. 271–309, Springer, Berlin, Germany.
- Jorissen, F., C. Fontanier, and E. Thomas (2007), Paleoceanographical proxies based on deep-sea benthic foraminiferal assemblage characteristics, in *Proxies in late cenozoic paleoceanography, Developments in Marine Geology*, vol. 1, edited by C. Hillaire-Marcel and A. De Vernal, pp. 263–325, Elsevier, Amsterdam, Netherlands.
- JTWC, J. T. W. C. (2000), 2000 Annual Tropical Cyclone Report, *Tech. rep.*, U.S. Naval Pacific Meteorology and Oceanography Center / Joint Typhoon Warning Center, pp. 399.
- JTWC, J. T. W. C. (2001), 2001 Annual Tropical Cyclone Report, *Tech. rep.*, U.S. Naval Pacific Meteorology and Oceanography Center / Joint Typhoon Warning Center, pp. 323.

- Kalnay, E., et al. (1996), The NCEP/NCAR 40-Year Reanalysis Project, *Bulletin of the American Meteorological Society*, 77(3), 437–471.
- Keil, R., D. Martlucan, F. Prahl, and J. Hedges (1994), Sorptive preservation of labile organic matter in marine sediments, *Nature*, 370, 549–552.
- Kelly-Gerreyn, B., D. Hydes, and J. Waniek (2005), Control of the diffusive boundary layer on benthic fluxes: A model study, *Marine Ecology Progress Series*, 292, 61–74.
- Kirk, J. (2011), *Light and photosynthesis in aquatic ecosystems*, 3rd ed., Cambridge University Press, Cambridge, pp. 649.
- Klein, P., and B. Coste (1984), Effects of wind-stress variability on nutrient transport into the mixed layer, *Deep Sea Research Part I*, 31(1), 21–37.
- Koroleff, F., and K. Kremling (1999), Determination of trace elements, in *Methods of Seawater Analysis*, edited by K. Grasshoff, K. Kremling, and M. Ehrhardt, pp. 340–342, Wiley-VHC, Weinheim, Germany.
- Kostka, J., and L. I.G.W. (1994), Partitioning and speciation of solid phase iron in saltmarsh sediments, *Geochimica et Cosmochimica Acta*, 58(7), 1701–1710.
- Krivtsov, V., M. Howard, and S. Jones (2009), Characterising observed patterns of suspended particulate matter and relationships with oceanographic and meteorological variables: Studies in Liverpool Bay, *Environmental Modelling & Software*, 24, 677–685.
- Kucera, M. (2007), Planktonic foraminifera as tracers of past oceanic environments, in *Proxies in late cenozoic paleoceanography*, *Developments in Marine Geology*, vol. 1, edited by C. Hillaire-Marcel and A. De Vernal, pp. 213–262, Elsevier, Amsterdam, Netherlands.
- Lauria, M., D. Purdie, and J. Sharples (1999), Contrasting phytoplankton distributions controlled by tidal turbulence in an estuary, *Journal of Marine Systems*, 21(1-4), 189–197.
- Leipe, T., F. Tauber, H. Vallius, J. Virtasalo, S. Uścińowicz, N. Kowalski, S. Hille, S. Lindgren, and T. Myllyvirta (2010), Particulate organic carbon (POC) in surface sediments of the Baltic Sea, *Geo-Marine Letters*, 31(3), 175–188.
- Li, C., J. Blanton, and C. Chen (2004), Mapping of tide and tidal flow fields along a tidal channel with vessel-based observations, *Journal of Geophysical Research*, 109(C4), C04002.
- Li, G., W. Liang, S. Liao, and G. Fang (1996), Climatic changes since Holocene along Guangxi coast, *Marine Geology & Quaternary Geology*, 16(3), 49–60.
- Lin, I. (2012), Typhoon-induced phytoplankton blooms and primary productivity increase in the western North Pacific subtropical ocean, *Journal of Geophysical Research*, 117(C3), C03039.
- Lin, I., W. Liu, C.-C. Wu, G. Wong, C. Hu, Z. Chen, W.-D. Liang, Y. Yang, and K.-K. Liu (2003), New evidence for enhanced ocean primary production triggered by tropical cyclone, *Geophysical Research Letters*, 30(13), 1718–1721.
- Liu, J., G. Li, M. Chen, and H. Hong (1992), The geomorphological and sedimentary characteristics in offshore of Guangxi Province, *Tropic Oceanology*, 11(1), 52–57.

- Liu, K., S. Chao, P. Shaw, G. Gong, C. Chen, and T. Tang (2002), Monsoon-forced chlorophyll distribution and primary production in the South China Sea: Observations and a numerical study, *Deep Sea Research Part I*, 49(8), 1387–1412.
- Liu, X., Z. Zhang, Y. Wu, Y. Huang, and Y. Zhang (2005), Distribution of sediment chloroplastic pigments in the Southern Yellow Sea, *Journal of Ocean University of China*, 4(2), 163–172.
- Liu, Z., X. Ning, and Y. Cai (1998), Distribution characteristics of size-fractionated chlorophyll a and productivity of phytoplankton in the Beibu Gulf, *Acta oceanologica sinica*, 20(1), 50–57 (in Chinese).
- Longhurst, A. (2007), *Ecological Geography of the Sea*, 2nd ed., Academic Press, San Diego, California, USA, pp. 542.
- Lü, X., F. Qiao, G. Wang, C. Xia, and Y. Yuan (2008), Upwelling off the west coast of Hainan Island in summer: Its detection and mechanisms, *Geophysical Research Letters*, 35(2), L02604.
- Lund-Hansen, L., M. Pejrl, J. Valeur, and A. Jensen (1993), Gross sedimentation rates in the North Sea-Baltic Sea transition: Effects of stratification, wind energy transfer, and resuspension, *Oceanologica Acta*, 16(3), 205–212.
- Mackensen, A., H. Grobe, G. Kuhn, and D. Fütterer (1990), Benthic foraminiferal assemblages from the eastern Weddell Sea between 68 and 73°S: Distribution, ecology and fossilization potential, *Marine Micropaleontology*, 16(3-4), 241–283.
- Madhupratap, M., M. Gauns, N. Ramaiah, S. Prasanna Kumar, P. Muraleedharan, S. de Sousa, S. Sardesai, and U. Muraleedharan (2003), Biogeochemistry of the Bay of Bengal: Physical, chemical and primary productivity characteristics of the central and western Bay of Bengal during summer monsoon 2001, *Deep Sea Research Part II*, 50(5), 881–896.
- Manh, D.-V., and T. Yanagi (1997), A three-dimensional numerical model of tide and tidal current in the Gulf of Tongking, *La Mer*, 35, 15–22.
- Manh, D.-V., and T. Yanagi (2000), A study on residual flow in the Gulf of Tongking, *Journal of Oceanography*, 56(1), 59–68.
- Mantoura, R., J.-M. Martin, and R. Wollast (1991), *Ocean Margin Processes in Global Change*, Report of the Dahlem Workshop on Ocean Margin Processes in Global Change, John Wiley & Sons, New York, USA, pp. 469.
- Mascarenhas Jr., A., R. Castro, C. Collins, and R. Durazo (2004), Seasonal variation of geostrophic velocity and heat flux at the entrance to the Gulf of California, Mexico, *Journal of Geophysical Research*, 109(C7), C07008.
- Mayer, L. (1994), Relationships between mineral surfaces and organic carbon concentrations in soils and sediments, *Chemical Geology*, 11, 347–363.
- McManus, I. (1988), Grain-size determination and interpretation, in *Techniques in Sedimentology*, edited by M. Tucker, pp. 63–85, Blackwell, Oxford, UK.
- Milliman, J. (1991), Flux and fate of fluvial sediment and water in coastal seas, in *Ocean Margin Processes in Global Change*, edited by R. Mantoura, J.-M. Martin, and R. Wollast, pp. 69–89, John Wiley & Sons, New York, USA.

- Milliman, J., and R. Meade (1983), Worldwide delivery of river sediment to the oceans, *Journal of Geology*, 91, 1–21.
- Morse, J. (1986), The surface chemistry of calcium carbonate minerals in natural waters: An overview, *Marine Chemistry*, 20(1), 91–112.
- Murray, J. (1991), *Ecology and palaeoecology of benthic foraminifera*, Wiley, New York, USA, pp. 397.
- Murray, J. (2006), *Ecology and applications of benthic foraminifera*, Cambridge University Press, Cambridge, UK, pp. 426.
- O'Hara, J., and R. Falvey (2006), 2006 Annual Tropical Cyclone Report, *Tech. rep.*, U.S. Naval Pacific Meteorology and Oceanography Center / Joint Typhoon Warning Center, pp. 98.
- O'Hara, J., and R. Falvey (2007), 2007 Annual Tropical Cyclone Report, *Tech. rep.*, U.S. Naval Pacific Meteorology and Oceanography Center / Joint Typhoon Warning Center, pp. 124.
- O'Kane, J., et al. (1991), What is the response of ocean margin systems to natural and anthropogenic perturbations?, in *Ocean Margin Processes in Global Change*, edited by R. Mantoura, J.-M. Martin, and R. Wollast, pp. 349–363, John Wiley & Sons, New York, USA.
- Pond, S., and G. Pickard (1983), *Introductory Dynamical Oceanography*, 2 ed., Pergamon Press, Oxford, England, pp. 329.
- Postma, H. (1988), Physical and chemical oceanographic aspects of continental shelves, in *Continental Shelves*, vol. 27, edited by H. Postma and J. Zijlstra, pp. 5–37, Elsevier, Amsterdam, Netherlands.
- Postma, H., and J. Zijlstra (1988), *Continental Shelves, Ecosystems of the World*, vol. 27, Elsevier, Amsterdam, Netherlands, pp. 421.
- Poulton, S., and R. Raiswell (2002), The low-temperature geochemical cycle of iron: From continental fluxes to marine sediment deposition, *American Journal of Science*, 302(9), 774–805.
- Price, J. (1981), Upper ocean response to a hurricane, *Journal of Physical Oceanography*, 11(2), 153–175.
- Repeta, D., and R. Gagosian (1987), Carotenoid diagenesis in recent marine sediments - I. The Peru continental shelf (15°S, 75°W), *Geochimica et Cosmochimica Acta*, 51(4), 1001–1009.
- Reynolds, C. (2006), *Ecology of phytoplankton*, Ecology, biodiversity and conservation, Cambridge University Press, New York, USA, pp. 535.
- Ridderinkhof, H. (1992), On the effects of variability in meteorological forcing on the vertical structure of a stratified watercolumn, *Continental Shelf Research*, 12(1), 25–36.
- Rock Color Chart, C. (1991), *Rock Color Charts*, Geological Society of America, Boulder, Colorado, USA, pp. 1–12.
- Ross, O. (2004), Algal motility in variable turbulence, PhD Thesis, University of Southampton, Southampton, UK.
- Ross, O. (2006), Particles in motion: How turbulence affects plankton sedimentation from an oceanic mixed layer, *Geophysical Research Letters*, 33(10), L10609.

- Ross, O., and J. Sharples (2007), Phytoplankton motility and the competition for nutrients in the thermocline, *Marine Ecology Progress Series*, 347, 21–38.
- Ross, O., and J. Sharples (2008), Swimming for survival: A role of phytoplankton motility in a stratified turbulent environment, *Journal of Marine Systems*, 70(3-4), 248–262.
- Ruttenberg, K., and R. Berner (1993), Authigenic apatite formation and burial in sediments from non-upwelling, continental margin environments, *Geochimica et Cosmochimica Acta*, 57(5), 991–1007.
- Santschi, P., P. Bower, U. Nyffeler, A. Azevedo, and W. Broecker (1983), Estimates of the resistance to chemical-transport posed by the deep-sea boundary-layer, *Limnology and Oceanography*, 28, 899–912.
- Santschi, P., R. Anderson, M. Fleisher, and W. Bowles (1991), Measurements of diffusive sublayer thicknesses in the ocean by alabaster dissolution, and their implications for the measurements of benthic fluxes, *Journal of Geophysical Research*, 96(C6), 10641–10657.
- Schmuker, B. (2000), The influence of shelf vicinity on the distribution of planktic foraminifera south of Puerto Rico, *Marine Geology*, 166(1-4), 125–143.
- Seeberg-Elverfeldt, J., M. Schlüter, T. Feseker, and M. Kölling (2005), Rhizon sampling of porewaters near the sediment-water interface of aquatic systems, *Limnology and Oceanography: Methods*, 3, 361–371.
- Seibold, E., and W. Berger (1996), *The Sea Floor*, 3rd ed., Springer, Berlin, Germany, pp. 358.
- Sharp, G. (1988), Fish populations and fisheries: Their perturbations, natural and man-induced, in *Continental Shelves*, vol. 27, edited by H. Postma and J. Zijlstra, pp. 155–202, Elsevier, Amsterdam, Netherlands.
- Sharples, J. (1999), Investigating the seasonal vertical structure of phytoplankton in shelf seas, *Marine Models*, 1(1-4), 3–38.
- Sharples, J. (2008), Potential impacts of the spring-neap tidal cycle on shelf sea primary production, *Journal of Plankton Research*, 30(2), 183–197.
- Sharples, J., and P. Tett (1994), Modelling the effect of physical variability on the midwater chlorophyll maximum, *Journal of Marine Research*, 52(2), 219–238.
- Sharples, J., M. Moore, T. Rippeth, P. Holligan, D. Hydes, N. Fisher, and J. Simpson (2001), Phytoplankton distribution and survival in the thermocline, *Limnology and Oceanography*, 46(3), 486–496.
- Sharples, J., O. Ross, B. Scott, S. Greenstreet, and H. Fraser (2006), Inter-annual variability in the timing of stratification and the spring bloom in the North-western North Sea, *Continental Shelf Research*, 26(6), 733–751.
- Shepard, F. (1954), Nomenclature based on sand-silt-clay ratios, *Journal of Sedimentary Petrology*, 24, 151–158.
- Shi, M., C. Chen, Q. Xu, H. Lin, G. Liu, H. Wang, F. Wang, and J. Yan (2002), The role of Qiongzhou Strait in the seasonal variation of the South China Sea circulation, *Journal of Physical Oceanography*, 32(1), 103–121.

- Shi, W., and M. Wang (2007), Observations of a Hurricane Katrina-induced phytoplankton bloom in the Gulf of Mexico, *Geophysical Research Letters*, 34(11), L11607.
- Shiah, F.-K., S.-W. Chung, S.-J. Kao, G.-C. Gong, and K.-K. Liu (2000), Biological and hydrographical responses to tropical cyclones (typhoons) in the continental shelf of the Taiwan Strait, *Continental Shelf Research*, 20(15), 2029–2044.
- Shields, M., and D. Hughes (2009), Large-scale variation in macrofaunal communities along the eastern Nordic Seas continental margin: A comparison of four stations with contrasting food supply, *Progress in Oceanography*, 82, 125–136.
- Simpson, J., W. Crawford, T. Rippeth, A. R. Campbell, and J. Cheok (1996), The vertical structure of turbulent dissipation in shelf seas, *Journal of Physical Oceanography*, 26(8), 1579–1590.
- Skyring, G. (1987), Sulfate reduction in coastal ecosystems, *Geomicrobiology Journal*, 5, 295–374.
- Smith, S. (1980), Wind stress and heat flux over the ocean in gale force winds, *Journal of Physical Oceanography*, 10(5), 709–726.
- Song, J. (2010), *Biogeochemical processes of biogenic elements in China marginal seas*, Advanced topics in science and technology in China, Springer / Zhejiang University Press, Hangzhou, China, pp. 662.
- SonTek/YSI, I. (2005), RiverSurveyor System Manual, pp. 176.
- Stookey, L. (1970), Two new spectrophotometric reagents for copper, *Talanta*, 17(7), 644–647.
- Strady, E., C. Pohl, E. Yakushev, S. Krüger, and U. Hennings (2008), PUMP-CTD-System for trace metal sampling with a high vertical resolution. A test in the Gotland Basin, Baltic Sea, *Chemosphere*, 70(7), 1309–1319.
- Su, G.-Q., and T.-X. Wang (1994), Basic characteristics of modern sedimentation in the South China Sea, in *Oceanology of China Seas*, vol. 1, edited by Z. D., Y.-B. Liang, and C.-K. Zeng, pp. 407–418, Kluwer Academic Publishers, Dordrecht, Netherlands.
- Su, J. (2004), Overview of the South China Sea circulation and its influence on the coastal physical oceanography outside the Pearl River Estuary, *Continental Shelf Research*, 24(16), 1745–1760.
- Su, Y.-S., and X.-C. Weng (1994), Water masses in China Seas, in *Oceanology of China Seas*, vol. 1, edited by D. Zhou, Y.-B. Liang, and C.-K. Zeng, pp. 3–16, Kluwer Academic Publishers, Dordrecht, Netherlands.
- Sun, M.-Y., and S. Wakeham (1999), Diagenesis of planktonic fatty acids and sterols in Long Island Sound sediments: Influences of a phytoplankton bloom and bottom water oxygen content, *Journal of Marine Research*, 57(2), 357–385.
- Sun, M.-Y., C. Lee, and R. Aller (1993), Anoxic and oxic degradation of <sup>14</sup>C-labeled chloropigments and a <sup>14</sup>C-labeled diatom in Long Island Sound sediments, *Limnology and Oceanography*, 38(7), 1438–1451.
- Sundborg, Å. (1956), The river Klarälven: A study of fluvial processes, *Geografiska Annaler*, 38(2), 125–237.

- Sverdrup, H. (1953), On conditions for the vernal blooming of phytoplankton, *ICES Journal of Marine Science*, 18(3), 287–295.
- Takahashi, M., and T. Hori (1984), Abundance of picophytoplankton in the subsurface chlorophyll maximum layer in subtropical and tropical waters, *Marine Biology*, 79(2), 177–186.
- Tanabe, S., K. Hori, Y. Saito, S. Haruyama, L. Doanh, Y. Sato, and S. Hiraide (2003a), Sedimentary facies and radiocarbon dates of the Nam Dinh-1 core from the Song Hong (Red River) delta, Vietnam, *Journal of Asian Earth Sciences*, 21(5), 503–513.
- Tanabe, S., K. Hori, Y. Saito, S. Haruyama, V. Vu, and A. Kitamura (2003b), Song Hong (Red River) delta evolution related to millennium-scale Holocene sea-level changes, *Quaternary Science Reviews*, 22, 2345–2361.
- Tang, D., H. Kawamura, M.-A. Lee, and T. Van Dien (2003), Seasonal and spatial distribution of chlorophyll-a concentrations and water conditions in the Gulf of Tonkin, South China Sea, *Remote Sensing of Environment*, 85(4), 475–483.
- Tengberg, A., E. Almroth, and P. Hall (2003), Resuspension and its effects on organic carbon recycling and nutrient exchange in coastal sediments: In situ measurements using new experimental technology, *Journal of Experimental Marine Biology and Ecology*, 285–286, 119–142.
- Tengberg, A., H. Stahl, G. Gust, V. Müller, U. Arning, H. Andersson, and P. O. J. Hall (2004), Intercalibration of benthic flux chambers I. Accuracy of flux measurements and influence of chamber hydrodynamics, *Progress In Oceanography*, 60(1), 1–28.
- Tett, P., D. Crisp, and G. Fogg (1981), Modelling phytoplankton production at shelf-sea fronts, *Philosophical Transactions of the Royal Society of London A*, 302(1472), 605–615.
- Tett, P., A. Edwards, and K. Jones (1986), A model for the growth of shelf-sea phytoplankton in summer, *Estuarine, Coastal and Shelf Science*, 23(5), 641–672.
- Thamdrup, B., H. Fossing, and B. Jørgensen (1994), Manganese, iron, and sulfur cycling in a coastal marine sediment, Aarhus Bay, Denmark, *Geochimica et Cosmochimica Acta*, 58, 5115–5129.
- van Maren, D., P. Hoekstra, and A. Hoitink (2004), Tidal flow asymmetry in the diurnal regime: Bed-load transport and morphologic changes around the Red River Delta, *Ocean Dynamics*, 54(3), 424–434.
- Varela, R., A. Cruzado, J. Tintore, and E. Garcia Ladona (1992), Modelling the deep-chlorophyll maximum: A coupled physical-biological approach, *Journal of Marine Research*, 50, 441–463.
- Velegrakis, A., S. Gao, R. Lafite, J. Dupont, M. Huault, L. Nash, and M. Collins (1997), Resuspension and advection processes affecting suspended particulate matter concentrations in the central English Channel, *Journal of Sea Research*, 38(1-2), 17–34.
- Walker, N., R. Leben, and S. Balasubramanian (2005), Hurricane-forced upwelling and chlorophyll a enhancement within cold-core cyclones in the Gulf of Mexico, *Geophysical Research Letters*, 32(18), L18610.
- Walsh, J. (1981), Shelf-sea ecosystems, in *Analysis of Marine Ecosystems*, edited by A. Longhurst, pp. 159–196, Academic Press, London, UK.

- Wang, P., and Q. Li (2009), *The South China Sea: Paleoceanography and sedimentology, Developments in Paleoenvironmental Research*, vol. 13, Springer, pp. 516.
- Wang, P., L. Zhang, Q. Zhao, Q. Min, Y. Bian, L. Zheng, X. Cheng, and R. Chen (1988), *Foraminifera and ostracoda in bottom sediments of the East China Sea*, Ocean Press, Beijing, China, pp. 438 (in Chinese).
- Waniek, J. (2003), The role of physical forcing in initiation of spring blooms in the northeast Atlantic, *Journal of Marine Systems*, 39(1-2), 57–82.
- Waniek, J., and N. Holliday (2006), Large-scale physical controls on phytoplankton growth in the Irminger Sea, Part II: Model study of the physical and meteorological preconditioning, *Journal of Marine Systems*, 59(3-4), 219–237.
- Wanielist, M., R. Kersten, and R. Eaglin (1997), Precipitation, in *Hydrology: Water quantity and quality control*, 2nd ed., p. 588, John Wiley and Sons, Inc., Toronto, Canada, pp. 588.
- Ward, B., and J. Waniek (2007), Phytoplankton growth conditions during autumn and winter in the Irminger Sea, North Atlantic, *Marine Ecology Progress Series*, 334, 47–61.
- Wei, G.-J., C.-Y. Huang, C.-C. Wang, M.-Y. Lee, and K.-Y. Wei (2006), High-resolution benthic foraminifer  $\delta^{13}\text{C}$  records in the South China Sea during the last 150 ka, *Marine Geology*, 232(3-4), 227–235.
- Werner, S., R. Beardsley, S. Lentz, D. Hebert, and N. Oakey (2003), Observations and modeling of the tidal bottom boundary layer on the southern flank of Georges Bank, *Journal of Geophysical Research*, 108(C11), 8005–8026.
- Williams, R., and M. Follows (2003), Physical transport of nutrients and the maintenance of biological production, in *Ocean Biogeochemistry*, edited by M. Fasham, Global Change - The IGBP Series (closed), pp. 19–51, Springer, Berlin, Germany.
- Wong, G., T.-L. Ku, M. Mulholland, C.-M. Tseng, and D.-P. Wang (2007), The Southeast Asian Time-series Study (SEATS) and the biogeochemistry of the South China Sea - An overview, *Deep Sea Research Part II*, 54(14-15), 1434–1447.
- Wu, D., Y. Wang, X. Lin, and J. Yang (2008), On the mechanism of the cyclonic circulation in the Gulf of Tonkin in the summer, *Journal of Geophysical Research*, 113, C09029.
- Wu, Y. (2008), The temporal and spatial patterns and size-fractionated structure of primary productivity in Beibu Gulf, M.Sc. Thesis, Xiamen University, Xiamen, China.
- Xia, Z., J. Waniek, and T. Leipe (in press), Anthropogenic fingerprint in Beibu Gulf (South China Sea) sediments, *Journal of Coastal Research, Special Issue* 66, doi:10.2112/SI\_66\_6.
- Xu, D., J. Long, J. Qian, and P. Xi (2008), The modern sedimentation rate and the distribution character of 7 cores in Hainan Island off shore, *Journal of Marine Sciences*, 26(13), 9–17.
- Yan, D. (2006), Fertilizer products, *Beibu Gulf Shipping*, 1, 1–13.
- Yoder, J., C. McClain, G. Feldman, and W. Esaias (1993), Annual cycles of phytoplankton chlorophyll concentrations in the global ocean: A satellite view, *Global Biogeochem. Cycles*, 7(1), 181–193.



- Yu, J., J. Jiang, D. Gong, S. Li, and Y. Xu (2011), Determining suspended sediment concentration and settling velocity from PC-ADP measurements in the Beibu Gulf, China, *Chinese Journal of Oceanology and Limnology*, 29(3), 691–701.
- Yuan, Y., H. Wei, L. Zhao, and Y. Cao (2009), Implications of intermittent turbulent bursts for sediment resuspension in a coastal bottom boundary layer: A field study in the western Yellow Sea, China, *Marine Geology*, 263(1-4), 87–96.
- Zheng, G., and D. Tang (2007), Offshore and nearshore chlorophyll increases induced by typhoon winds and subsequent terrestrial rainwater runoff, *Marine Ecology Progress Series*, 333, 61–74.
- Zheng, S.-Y., and Z.-X. Fu (1994), Foraminiferal faunal trends in China Seas, in *Oceanology of China Seas*, vol. 1, edited by D. Zhou, Y.-B. Liang, and C.-K. Zeng, pp. 255–274, Kluwer Academic Publishers, Dordrecht, Netherlands.
- Zu, T., J. Gan, and S. Erofeeva (2008), Numerical study of the tide and tidal dynamics in the South China Sea, *Deep Sea Research Part I*, 55(2), 137–154.

# List of Figures

1.1	Global shelf areas and mean surface chlorophyll- <i>a</i> concentrations. . . .	2
1.2	South China Sea and Beibu Gulf. . . . .	9
2.1	Sampling stations of FENDOU 5 and SONNE cruise. . . . .	14
2.2	Harmonic analysis of current data. . . . .	15
2.3	Model schema. . . . .	18
3.1	Beibu Gulf circulation pattern and cruise track. . . . .	22
3.2	Wind velocity vectors for the sampling period. . . . .	28
3.3	Vertical distribution of hydrographical parameters in the water column. .	29
3.4	Vertical distribution of biogeochemical parameters in the water column.	32
3.5	Grain size diagram. . . . .	35
3.6	Sediment pigment concentrations. . . . .	36
3.7	Foraminiferal distribution. . . . .	37
3.8	Pore water profiles. . . . .	38
3.9	Down-core variations of total organic carbon, reactive iron and phosphorous-bearing fractions. . . . .	39
3.10	T/S diagram of the four stations. . . . .	46
3.11	Proposed current pattern affecting the different zones during the sampling period. . . . .	47
3.12	Covariation of dissolved silica and phosphate in the pore waters. . . . .	57
4.1	Study area and sampling stations. . . . .	63
4.2	Mean meteorological forcing. . . . .	68
4.3	Simulated mean annual cycle. . . . .	71
4.4	Correlation between model and satellite SST data. . . . .	74
4.5	Simulated annual cycle for 2009. . . . .	75
4.6	Effect of typhoon KETSANA. . . . .	78
4.7	Tidal effect on the DCM. . . . .	80
4.8	Interannual comparison of the years 2000-2010. . . . .	81
4.9	Interannual variability of the modeled and remotely measured monthly mean surface chlorophyll concentrations. . . . .	84
S1	Meteorological forcing for the years 2000 to 2010 . . . . .	93
S2	Modeled and in-situ measured temperature, chlorophyll and DIN depth profiles . . . . .	95

5.1	ADP lines and stations for water sampling. . . . .	101
5.2	Validation of the tidal model. . . . .	103
5.3	Current u- and v-components measured in 15, 35 and 64 m depth. . . .	105
5.4	Harmonic analysis results of bottom currents. . . . .	106
5.5	Bottom north-south versus east-west velocity. . . . .	107
5.6	Near-bottom SPM concentrations. . . . .	109
5.7	Hjulström diagram. . . . .	110
5.8	Tidal cycle current velocities and calculated DBL thicknesses. . . . .	113
5.9	Maximum, mean and minimum near-bottom velocities for all stations. .	114
5.10	DBL thicknesses against the current velocities. . . . .	115
5.11	Spatial distribution of the calculated DBL thicknesses. . . . .	116
5.12	Calculated DBL thicknesses for the different zones and tidal phases. . .	117

## List of Tables

2.1	Harmonic constituents acting in the Beibu Gulf. . . . .	17
3.1	Mean values and standard deviations for hydrographical properties in surface and bottom layers of the different zones. . . . .	45
3.2	Mean values and standard deviations for biogeochemical properties in surface and bottom layers of the different zones. . . . .	49
4.1	Initialisation parameters for the model runs. . . . .	67
4.2	Relevant forcing parameters and calculated values for the modeled mean year and the years 2000 to 2010. . . . .	70
4.3	Wind events affected the primary production in the central Beibu Gulf. .	85
S1	Number of pixels from SeaWiFS. . . . .	96

## List of abbreviations

<b>ADP</b>	Acoustic Doppler Profiler
<b>BC</b>	Box corer
<b>BGCoZ</b>	Beibu Gulf Coastal Zone
<b>BGCeZ</b>	Beibu Gulf Central Zone
<b>CB</b>	algal chlorophyll biomass
<b>Chl<sub>sfc</sub></b>	Modeled surface chlorophyll concentration [ $\text{mg m}^{-3}$ ]
<b>CPE</b>	Chloroplastic Pigment Equivalents (sum of plant pigment contents)
<b>CTD</b>	Conductivity-Temperature-Depth-Sonde
<b>DBL</b>	Diffusive boundary layer
<b>DCM</b>	Deep chlorophyll maximum
<b>DIN</b>	Dissolved inorganic nitrogen
<b>DLRF</b>	Downward longwave radiation flux
<b>d.s.</b>	Dry sediment
<b>dT</b>	Dewpoint temperature
<b>dwt.</b>	Dry weight
<b>GC</b>	Gravity corer
<b>GMGS</b>	Guangzhou Marine Geological Survey, China
<b>IN</b>	Algal internal nutrients
<b>IOW</b>	Institut für Ostseeforschung Warnemünde
<b>Max</b>	Maximum
<b>Min</b>	Minimum
<b>MLD</b>	Mixed layer depth
<b>MODIS</b>	Moderate Resolution Imaging Spectroradiometer
<b>MUC</b>	Multi corer
<b>NCAR</b>	National Center for Atmospheric Research
<b>NCEP</b>	National Centers for Environmental Prediction
<b>P</b>	Sedimentary phosphorous

<b>P-Ap</b>	Apatite-bound phosphorus
<b>PAR</b>	Photosynthetic active radiation
<b>P-Fe</b>	Iron-bound phosphorous
<b>P-FeAl</b>	Iron-aluminum-bound phosphorous
<b>PP</b>	Primary production
<b>QSZ</b>	Qiongzhou Strait Zone
<b>RCM</b>	Recording Current meter
<b>RV</b>	Research vessel
<b>S</b>	Salinity
<b>SBGZ</b>	Southern Beibu Gulf Zone
<b>SCS</b>	South China Sea
<b>SeaWiFS</b>	SEA-viewing Wide Field of-view Sensor
<b>SOA</b>	South China Sea Branch of the State Oceanic Administration, China
<b>SPM</b>	Suspended particulate matter
<b>SST</b>	Sea surface temperature
<b>strat</b>	Stratification
<b>T</b>	Temperature [ $^{\circ}\text{C}$ ]
<b><math>T_{bot}</math></b>	Bottom temperature [ $^{\circ}\text{C}$ ]
<b>TD</b>	Tropical depression
<b>TMI</b>	Tropical Rainfall Measuring Mission Microwave Imager
<b>TOC</b>	Total organic carbon
<b>TS</b>	Tropical storm
<b><math>T_{sfc}</math></b>	Surface temperature [ $^{\circ}\text{C}$ ]
<b>TY</b>	Typhoon
<b>UK</b>	United Kingdom
<b>WE</b>	Strong wind events ( $>10 \text{ m s}^{-1}$ )
<b>WOCE UOT</b>	World Ocean Circulation Experiment Upper Ocean Thermal
<b>YSI</b>	YSI Inc.

## Specific contributions to the manuscripts

The contributions of the authors to the manuscripts are indicated in the following:

**Bauer, A.**, Radziejewska, T., Liang, K., Kowalski, N., Dellwig, O., Bosselmann, K., Stark, A., Xia, Z., Harff, J., Böttcher, M.E., Schulz-Bull, D.E. and Waniek, J.J. (in press): Regional differences of hydrographical and sedimentological properties in Beibu Gulf, South China Sea. *Journal of Coastal Research: Special Issue 66*, doi:10.2112/SI\_66\_5.

Specific contribution: A.B. carried out depth profiling and water sampling during the FENDOU 5 cruise, measuring of chlorophyll and SPM concentrations, data evaluation and interpretation as well as concept development and manuscript writing. Z.X. and K.L. carried out sediment sampling on FENDOU 5. Z.X. analyzed sediment parameters and contributed to results and discussion. T.R. and K.L. evaluated and interpreted data of sediment pigment concentrations and foraminifera, respectively. Both made contributions to the results and discussion. A.S. carried out sediment and pore water sampling for geochemical analysis during FENDOU 5. N.K., O.D., K.B. and M.E.B. analyzed geochemical parameters and contributed to results and discussion. J.J.W. initiated the work (project leader), carried out RCM measurements during FENDOU 5 and made contributions to the discussion. J.H. and D.S.-B. (project coordinator) contributed to the manuscript.

**Bauer, A.** and Waniek, J.J. (2013): Factors affecting chlorophyll *a* concentration in the central Beibu Gulf, South China Sea. *Marine Ecology Progress Series*: 474, 67-88.

Specific contribution: Analysis of *in-situ* data from the FENDOU 5 and SONNE cruise as well as derived from satellite measurements has been done by A.B., as well as model adjustment and interpretation of the modeling results. A.B. prepared the concept

of the paper and did the writing. J.J.W. made contributions to the manuscript.

**Bauer, A.,** Fründt, B. and Waniek, J.J. (Manuscript): Sediment resuspension patterns and the diffusive boundary layer in the Beibu Gulf, South China Sea.

Specific contribution: A.B. analyzed RCM and ADP current data as well as NCEP-derived wind data, made harmonic analysis and all calculations, gathered data for tidal heights from WXTide32 and measured SPM concentrations. Surface sediment data were provided by GMGS. Central idea for the tidal model came from A.B.; B.F. wrote the calculations routines. Data interpretation as well as concept development and manuscript writing has been carried out by A.B. J.J.W. initiated the work and made contributions to the manuscript.



## Danksagung

Zu allererst möchte ich mich bei meiner Doktor-Mutter PD Dr. habil. Joanna J. Waniek bedanken. Sie gab mir die Möglichkeit an diesem interessanten Projekt teilzunehmen und half mir, als Wissenschaftlerin, vor allem interdisziplinär, zu wachsen. Diese Arbeit entwickelte sich nicht nur durch meine Anstrengungen, auch ihre Anregungen haben erheblich zum Erfolg beigetragen. Danke für deine immerwährende Unterstützung und Geduld.

Außerdem möchte ich mich für die Möglichkeit zur Teilnahme an der FENDOU 5 Expedition bedanken. Diese Reise war eine unglaublich tolle Erfahrung und ich danke allen Fahrtteilnehmern, vor allem aber den chinesischen Projektpartnern (Xiong Liu, Zhangcun Yan, Kai Liang, uvm.) und Besatzungsmitgliedern, für die unvergessliche Zeit. Insbesondere sei dem Kapitän und seinen Offizieren gedankt, dass sie das Schiff und uns wohlbehalten durch einen Taifun gesteuert haben.

Ich danke meinem Thesis Komitee: PD Dr. habil. Joanna J. Waniek, Prof. Dr. Detlef Schulz-Bull, Dr. Herbert Siegel und Dr. Douglas Connelly für die Unterstützung und schnelle Hilfe, wenn es nötig war: Ihr hattet immer ein offenes Ohr für mich.

Für wissenschaftliche und auch sonstige Unterstützung bedanke ich mich bei: Dr. Teresa Radziejewska, Dr. Nicole Kowalski, Dr. Olaf Dellwig, Dr. Katja Bosselmann, Alexander Stark, Prof. Zhen Xia, Prof. Dr. Jan Harff, Prof. Dr. Michael Böttcher, Birgit Sadkowiak, Ines Hand, Annika Fiskal, Dr. Thomas Leipe, Dr. Kerstin Perner, Iris Stottmeister und Dr. Ralf Prien.

Ganz besonderer Dank gilt meinen "Büromitbewohnerinnen" Birte Fründt und Dr. Juliane Brust, für die vielen Gespräche, ihre Hilfe bei großen und kleinen Matlab-Sorgen und die entspannenden Mittagspausen. Die Zeit mit euch war super!

Desweiteren sei den Mitarbeitern des IOW, insbesondere der Sektion Meereschemie, für die schöne Zeit am Institut gedankt.

Mein größter Dank aber gilt meiner Familie, vor allem meinem Mario: Ohne eure ständige Unterstützung wäre diese Arbeit nicht möglich gewesen! Ihr wart immer für mich da und habt mich geduldig auch in stressigen Phasen ertragen. Vielen Dank dafür!

## **Eidesstattliche Erklärung**

Ich versichere hiermit an Eides statt, dass ich die vorliegende Arbeit selbstständig angefertigt und ohne fremde Hilfe verfasst habe, keine außer den von mir angegebenen Hilfsmitteln und Quellen dazu verwendet habe und die den benutzten Werken inhaltlich und wörtlich entnommenen Stellen als solche kenntlich gemacht habe.

---

Andrea Bauer

Rostock, den 30. August 2012